School of Chemical and Petroleum Engineering
Department of Chemical Engineering

Mathematical Modelling of Bio-oil/Char Slurry Steam Gasification in a Fluidized Bed Reactor

Mansoor Hassani Ghezelchi

This thesis is presented for the Degree of
Doctor of Philosophy
of
Curtin University

May 2018

DECLARATION

To the best of my knowledge and belief this thesis contains no material previously published by any other person except where due acknowledgment has been made.

This thesis contains no material which has been accepted for the award of any other degree or diploma in any university.

Signature: …  ……

Date: …..08/11/2018……..…….

ABSTRACT

Biomass is an important alternative to fossil fuels because of its significant advantages in overcoming the challenges of energy crisis and environmental issues. However, there are several key challenges associated with the utilisation of biomass including high costs of collection, storage and transport, high moisture content and low energy density. Therefore, a major challenge is to process biomass for improved fuel properties.

Pyrolysis is a promising technology to convert the biomass into high-energy-density fuels such as bio-oil and/or biochar. Biochar is of excellent grindability and can be pulverised into fines which can be mixed with bio-oil for producing bioslurry. Bioslurry fuels are suitable for stationary application including gasification for producing synthesis gas (CO, H_2), which is important intermediate product for subsequent power generation or synthesis of renewable chemicals. When bioslurry is used as feedstock for gasification; the physical and chemical complexity of bio-oil and bioslurry play important roles in gasification process. Bio-oil and bioslurry fuels are thermally unstable and experience polymerization which is responsible for many issues. Therefore, there are still significant research gaps in bio-oil/bioslurry gasification processes.

This PhD thesis reports a systematic study on steam gasification of bio-oil and bioslurry in fluidized bed reactor. Both experimental and mathematical simulation has been carried out. This thesis has firstly developed a mechanical method for measuring droplet mean diameter and size distribution. The method considers a practical algorithm for overlap minimization, the shape correction factor, the effective roundness, and evaporation correction factor. Characteristics of bio-oil/bioslurry sprays are reported for several nozzles, leading to development of empirical atomization correlations. Mathematical modelling has then been conducted for bio-oil steam gasification in a fluidized bed reactor, based on computational fluid dynamics (CFD) using ANSYS-Fluent. Further simulation was carried out for bioslurry steam gasification in a fluidized bed reactor. Details on the series of work are given below.

Firstly, a methodology of determining droplets size distribution of spray has been developed. The method is applicable for light and dense sprays by designing an aperture to reduce overlapping issue. Minimum distance of captured plate from nozzle (in experiments) and critical roundness (0.75 in image analysis) for minimising droplets overlapping to be below 5% of all droplets. This method also considers the fuel-dependent ratios of true drop size to impression size (correction factor). Evaporation of diesel and biodiesel at low temperatures is low because of low vapour pressure. The method has been validated via comparisons in the Sauter mean diameters measured for diesel, biodiesel and diesel/biodiesel blends (standard deviations: 0.7μm) and the analytical calculation, with average relative errors below 1.2%. The method was then applied for determining the Sauter mean diameters of bio-oil and bioslurry sprays.

Secondly, this study reports the spray characteristics of two fast pyrolysis bio-oils with different viscosities 7.53E-2 and 15.22E-2 Pa.s and a set of bioslurry samples at various biochar loading levels of 5, 10, 15 and 20 wt%. Two types of atomizers (impact atomizer and twin-fluid atomizer) were used. Experiments for the impact atomizers of various sizes were carried out at injection pressures of 2.07–4.96 MPa and feeding rates of 108-490 ml/min. At a constant pressure, the Sauter Mean Diameter (SMD) of bio-oil and bioslurry increases as the flow number increases while at a constant flow number, the SMD decreases rapidly with increasing pressure. The biochar loading level has a significant impact on the bioslurry atomization characteristics. An increase in biochar loading level results in a rapid increase in the SMD. Experiments using the twin-fluid atomizer (N_2 fed in the outer tube) were carried out at flow rates of 2–6 ml/min. It was found that spray using the twin-fluid atomizer is more efficient than the impact atomizer as it uses lower liquid flow rate. The SMD is mainly influenced by the liquid viscosity, Gas/Liquid ratio (GLR), and the biochar loading level. An increase in viscosity and biochar loading level leads to an increase in the SMD of spray while an increase in GLR leads to a reduction in the SMD. Correlations have also been developed for predicting the SMD for bio-oil and bioslurry atomization.

Thirdly, a three-dimensional CFD model has been developed for bio-oil gasification in a fluidized bed reactor. The model considers three-phase hydrodynamics, heat and mass transfer, bio-oil atomization, spray droplet vaporization and thermal decomposition in gas–solid flow. The model employs an Euler-Lagrange method, in which gas and solid flow are solved using the Eulerian method and the bio-oil droplets are tracked using the Lagrangian approach. Droplet trajectory is calculated via equation of motion using discrete phase model in the Lagrangian frame, taking into account its interactions with flow field by developing several user-defined functions (UDFs). The UDFs customize the Fluent solver for droplets heat and mass transfer and continuous phase source terms calculation. The injection characteristics are based on experimental data and simulated for generating the Rosin-Rammler distribution function under different injection conditions. The compositions of the synthesis gas have been predicted at various bed temperatures, steam-carbon molar ratios, methane equivalent gas hourly space velocity ($G_{C1}HSV$) of feed and the sizes of droplets injected into the gasifier. An increase in gasification temperature leads to an increase in the hydrogen and carbon yields from bio-oil droplets gasification, as results of enhanced thermal decomposition, water-gas shift and steam-methane reformation reactions. It is clearly demonstrated that droplet size significantly influences the droplet residence time and bio-oil conversion in the reactor.

Finally, CFD simulation of bioslurry (20% biochar loading level) gasification has been conducted, taking into account the catalytic effect of alkali and alkaline earth metallic (AAEM) species in biochar. After model validation with experimental data, sensitivity study was carried out for temperature, space velocity of feed, steam to carbon feeding ratio and biochar diameter in slurry on conversion and product gas compositions. It has been found that the size of biochar particles (10–45 μm) in bioslurry has insignificant effect on total bioslurry conversion to product gas yield due to very low reaction rate, which controlled the total conversion of feedstock to product gas. However, increases in gasification temperature and H_2O/C ratio leads to increases in the biochar steam reforming reaction rate then the hydrogen and carbon yields.

ACKNOWLEDGEMENTS

I gratefully acknowledge the Curtin University Postgraduate Scholarship (CUPS) and the Curtin Research Scholarship (CRS) which are provided by Curtin University. I also grateful to the partial support received from the Australian Research Council through its Discovery Projects Scheme.

I would like to gratefully acknowledge iVEC for allocating computing time on supercomputers under the iVEC Partner Merit Allocation Scheme at the iVEC's Pawsey Centre in Perth. In addition, the VTT (Finland) and another provider (who has chosen to remain anonymous) for supplying the fast pyrolysis bio-oil samples.

I would like to thank many individuals. The accomplishment of this work would not be possible without their kind technical and emotional support. In particular, I would like to acknowledge the following people.

To my supervisor, Professor Hongwei Wu, thank you for all you have done over the last four years, starting from my PhD application until its completion. I also deeply appreciate you for your invaluable advice, training, guidance, patience, inspiration, persistent support as well as devotion in supervision during the course of this research.

To our research group, Mr. Walter Ikealumba, Dr. Xiangpeng Gao, Dr. Yun Yu, Ms. Mingming Zhang, Mr. Sui Boon Liaw, Mr. Alan Burton, Mr. Muhammad Usman Rahim and for their help in various ways.

Finally my special thanks will go to my family for their support, encouragement and understanding during my PhD study. I also would like to express my appreciation to Ms. Karen Haynes, Mr. Jason Wright, Mr. Ross Hayes, as well as Ms. Roshank Doroushi for their laboratory assistance. Thanks also go to the staff from Department of Chemical Engineering.

LIST OF PUBLICATIONS

- **Mansoor Hassani Ghezelchi**, Hongwei Wu. Prediction of mean drop size of bio-oil and bioslurry by impact nozzle. *CHEMECA* 28 September - 1 October **2014,** Perth, Australia.

- Bioslurry as a Fuel. 7: Spray Characteristics of Bio-Oil and Bioslurry via Impact and Twin-Fluid Atomizers, **Mansoor Hassani Ghezelchi,** Manuel Garcia-Perez, and Hongwei Wu *Energy & Fuels* **2015***29* (12), 8058-8065

- Modelling of bio-oil steam gasification in a fluidized bed reactor, **Mansoor Hassani Ghezelchi,** Hongwei Wu, *Fuel*, **2018** *220*, 575-585

- **Mansoor Hassani Ghezelchi**, Hongwei Wu. Modelling of Bioslurry Steam Gasification in a Fluidized Bed Reactor. Currently preparing the manuscript for a journal paper.

TABLE OF CONTENTS

LIST OF FIGURES

LIST OF TABLES

CHAPTER 1 INTRODUCTION

1.1 Background

Fossil fuels, which account for more than 95% of the overall consumption in the automotive field, are the main source of energy being used[1] that will not be able to cope with the predicted increases in demand; mainly in terms of their sustainability.[2] Biomass is at least partially acknowledged as an interesting and economical alternative to fossil fuels because of several characteristics, including small carbon and energy footprints,[3-6] contribute net zero carbon emissions when used to produce hydrogen[7] and finally, the economical availability of biomass. For example, the mallee biomass production, the strategy used to manage and prevent salinity in Australia, has potential as aviation fuel and second-generation bioenergy feedstock.[3]

An alternative renewable energy source to environmentally harmful fossil fuels and the energy crisis, biomass can be used directly by combustion, gasification and pyrolysis. The commercial energy production of direct combustion is not economical[8] as well as ash-related issues[9] and formation/emission of fine inorganic particulate matter (PM).[10-12] On the other hand, there have been several researches about biomass gasification as renewable energy source for the hydrogen production.[13] However, the biomass is difficult to collect and store, and the energetic density of it is low, which leads to high transportation and store costs.

Using biomass pyrolysis with higher efficiency as renewable energy resource has been carried out in the past several years by many researchers. One key research outcome is to use bio-oil and biochar,[14-16] produced from distributed pyrolysis located in or near the biomass growth areas, as a fuel for synthesis gas production via steam gasification. The excellent grindability and desirable particle size of biochar[14] have enabled it be mixed with bio-oil to produce bioslurry, while direct use of biomass as a fuel addresses multiple disadvantages such as low energy density, high transportation cost, and poor grindability.[14]

Therefore, bio-oil and bioslurry are likely to be one of the key fuels for synthesis gas production which is an important intermediate product for many processes. Among variety of processes for the syngas generation from several types of feedstock, using

bio-oil and bioslurry steam gasification is recently increasing attention as renewable energy source for the syntactic gas production.[17, 18]

Bio-oil and bioslurry steam gasification inevitably encounters instability-related issues, largely due to the complexity of bio-oils. Among these issues, continuous and stable atomization of bio-oil and bioslurry into different type of reactors is an important consideration. Several experimental studies on steam gasification of bio-oil and/or bioslurry have been done to investigate product gas composition and yield due to some variables such as feedstock, reactor and bed material type, as well as operating conditions. Furthermore, prediction of the gas composition with equilibrium and its modified models has been done in the recent years.

Despite the progress made in the experiment field and modelling of syngas yield during steam gasification of bio-oil and bioslurry, there are still significant research gaps in this area. For example, mathematical modelling of bio-oil steam gasification, considering the mathematical representation of measured drop size distributions is essential to be developed for a system which is not at thermodynamic equilibrium under a given set of conditions. In this system, the hydrodynamic characteristics of the reactor, droplet trajectory and heat and mass transfer as well as the droplets size distribution may play an important role during gasification process. Yet such knowledge is essential to analyse a complex systems and design a production scale of gasification process by scaling up. While the previous studies were focused on equilibrium condition during bio-oil and bioslurry gasification, the contribution of many parameters such as droplets size distribution and reactor hydrodynamics on product gas distribution are unknown. Therefore, fundamental study on the injection ring of bio-oil and bioslurry and mathematical modelling of gasification process is important in case of better understanding of above complex system and developing practical application tools.

1.2 Scope and objectives

The present study aims to develop a mathematical model for steam gasification of bio-oil and bioslurry in fluidized bed reactor. The detailed objectives of this study are to:

(1) Develop and validate a modified mechanical method for measurement liquid fuels droplets size with advantages of simplicity, low cost, and visibility because the old version of mechanical method needs to be improved and update from disadvantage of several drawbacks.

(2) Examine the droplet size behaviour of bio-oil and bioslurry produced by impact and twin-fluid atomizer, aiming to provide useful data for the mathematical simulation part, using droplet size distribution function when feeding bio-oil or bioslurry into reactor.

(3) Develop mathematical modelling of bio-oil steam gasification in a fluidized bed reactor, using the Computational Fluid Dynamics (CFD) from ANSYS-Fluent with especial focus on droplet heat and mass transfer during vaporization and gasification of bio-oil.

(4) Reveal the significant roles of char in the mathematical modelling of bioslurry steam gasification in a fluidized bed reactor with essential consideration of Alkali and Alkaline Earth Metallic species on char reactivity and also its intraction between char and volatiles.

1.3 Thesis outline

This thesis is arranged in eight chapters (including this chapter). Figure 1-1 shows the thesis roadmap, including thesis structure as follows:

Chapter 1 introduces the background, scope and objectives of the present study.

Chapter 2 reviews the up to date literatures on the steam gasification of bio-oil and bioslurry, including experimental data and mathematical models, finally leading to the research gaps identification and objectives determination for this study.

Chapter 3 summarizes the methodology employed in this research to achieve the research objectives, accompanied by the explanations of the experimental methodology, analytical technique, and methodology of mathematical modelling.

Chapter 4 investigates the mechanical method of measuring liquid droplet size and then develops and modifies the effective parameters to overcome the disadvantages of method, therefore, validates with open literature data.

Chapter 5 assesses the droplet mean diameter and size distribution of bio-oil and bioslurry by impact and twin-fluid atomizer, especially, under conditions related to available experimental data on steam gasification of bio-oil and bioslurry in literatures for modelling application.

Chapter 6 presents the development steps of mathematical modelling of bio-oil steam gasification in a fluidized bed reactor by the CFD - Fluent, including bio-oil vaporisation model, gasification reactions with kinetic parameters, extracted from literatures and justified for the case study. Subsequently, several sensitivity analyses are conducted using the validated model.

Chapter 7 involves a further modelling approach to the model developed in Chapter 6 for slurry gasification system, considering the resultant char steam gasification during bio-oil steam gasification and its interaction on reaction rate; therefore, several sensitivity analyses are conducted using the validated model.

Chapter 8 concludes the present study and recommends future work.

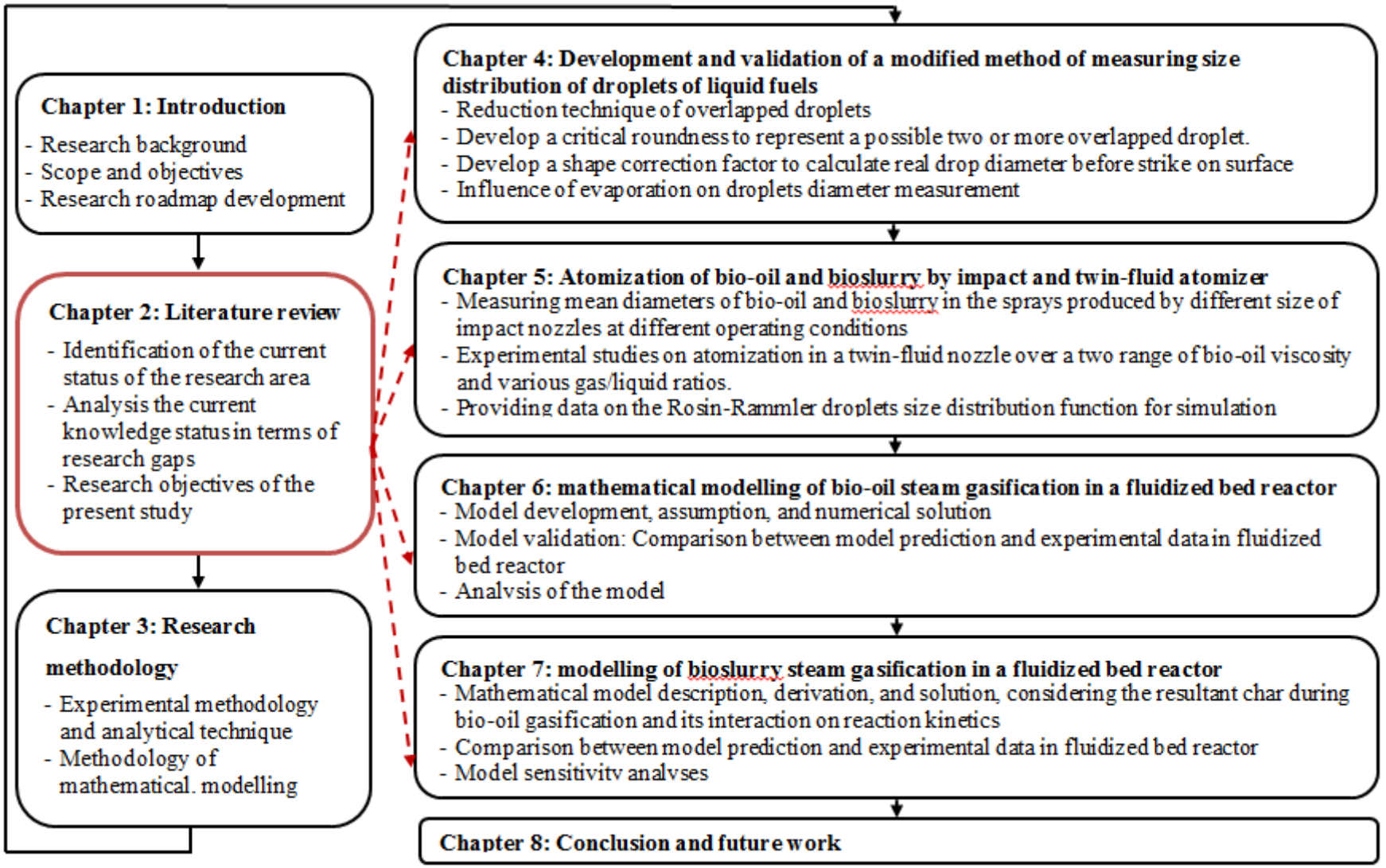

Figure 1- 1: Overall thesis roadmap

CHAPTER 2 LITERATURE REVIEW

2.1 Introduction

Bio-oil and/or bio-char are products from fast pyrolysis of biomass. It is becoming an increasingly important sustainable energy used to address the challenges of energy security, climate change, greenhouse gas emissions and economics of carbon price.[5, 14, 19-21] As compared with biomass, bio-oil and bioslurry (mix fine biochar into bio-oil) have higher energy density, for example, the volumetric energy density of bio-oil is roughly five times higher than biomass.[22] Also bio-oil and bioslurry are easier to be transported, processed, pressurized and stored. Using bio-oil as fuel for boilers, furnaces, diesel engines and gas turbines has been proved feasible, while gasification of bio-oil and bioslurry for synthesis gas which is an important intermediate product for many processes has also attracted considerable attention recently.[17, 18, 22, 23]

Recent research efforts have focused the experimental and equilibrium model of bio-oil and bioslurry gasification for synthesis gas production. This chapter aims to review the literature on experimental and modelling of bio-oil and bioslurry, identify the research gaps and outline the research objectives of this thesis. This chapter starts with reviewing the importance of measuring droplets size and its influence on different application, followed by the key issues related to the use of injection system and spray nozzle types. A brief review on bio-oil and bioslurry atomization related problems associated with the gasification of bio-oil and bioslurry in a reactor is also given. The importance of measuring of droplet mean diameter for different bio-oil and bioslurry with different level of char is then discussed, followed by details on the modelling of gasification of bio-oil and bioslurry. This chapter concludes with the key research gaps identified and the thesis scope.

2.2 Fuel spray characteristics

A spray is one type of two-phase flow. It involves a liquid as the dispersed or discrete phase in the form of droplets and a gas as the continuous phase.[24] Liquid streams injected into a gaseous environment tend to be unstable under a wide range of conditions. The Weber number is the dimensionless parameter that determines the ratio of the aerodynamic force to that of surface tension. At higher Weber numbers,

the aerodynamic force dominates, leading to distortion and disintegration. This process is called atomization.[24] Atomization typically results in liquid droplets with a characteristic dimension that is smaller than the original length scale associated with the stream. The mean drop size and the droplet size distribution are two important spray characteristics. Unfortunately, only empirical correlation is available for predicting mean drop sizes and drop size distributions. An excellent review of practical atomization systems is given by Lefebvre.[25]

2.2.1 Droplet size

2.2.1.1 Drop size measurement

There are two categories of methods developed for measuring spray droplet size distribution and average mean diameter.[25] One category is based on optical methods[26-29] such as light scattering techniques. These methods have respective advantages and disadvantages[30] and require the establishment of sophisticated and expensive optical systems. The other category of is the mechanical approach that deploys a suitable solid surface (such as glass) to allow droplets to strike on the surface. Images were then taken and analysed for droplet size distribution measurement. Therefore, the mechanical method has advantages of simplicity, low cost, visibility and reliability.

However, the mechanical method suffers from several drawbacks. Firstly, as permanently pressed, the droplets need to be corrected by a correction factor to obtain real diameters of the droplets.[31] Conventionally, a constant correction factor is used, e.g. 0.5 for clean glass surface.[25] This is a problem because the correction factor is known to be dependent on fluid properties (such as viscosity, surface tension etc) and droplet size.[25] Second, there are overlapping issues among droplets upon striking on the surface. Thirdly, the effect of potential evaporation on droplet size analysis is largely unknown. Lastly, the accuracy of droplets size analysis in past studies was largely limited by the low resolution of the photographs.

2.2.1.2 Mean Diameters

In many calculations of mass transfer and flow processes it is convenient to work only with mean or average diameters instead of the complete drop size distribution.

Mugele and Evans[32] suggested a list of mean diameters with their application. The most widely used is the Sauter Mean Diameter (SMD) D32, which is proportional to the ratio of the total liquid volume in a spray to the total droplet surface area in a spray.[24] This definition of mean drop size has special significance for heat and mass transfer applications, such as spray drying and the combustion of liquid fuel sprays.[25]

2.2.1.3 Droplet Size Distribution

In the absence of any fundamental mechanism or model on which to build a theory of drop size distributions, a number of functions have been proposed, based on either probability or purely empirical considerations, that allow the mathematical representation of measured drop size distributions.[24, 25, 33] Those in general uses include normal, log-normal, Nukiyama-Tanasawa, Rosin-Rammler and upper limit distribution.[25] The Rosin-Rammler distribution is frequently used for representing droplet size distribution in sprays. It is expressed in terms of the cumulative mass distribution.[34]

2.2.2 The main issue related to bio-oil and bioslurry injection system

Bio-oil and bioslurry as a higher energy density from fast pyrolysis of biomass can contribute significantly to synthesis gas production. However, the bio-oil and bioslurry injection into the high temperature reactor system has some important technical challenges related to high viscosity and the polymerization property of the bio-oil. Therefore, studies on the bio-oil steam gasification are less than model compounds of bio-oil, apparently because of quick solidification.[18]

During recent years, many researchers have been engaged in bio-oil and bioslurry application and its treatment and some of them reported issues related to proper injection of fuels into the reactor. The most commonly reported injection problem is due to high viscosity and the polymerization property of the bio-oil at high environment temperature.[18, 35] Wang et al.[36] employed a ripple nozzle injector and reported the issue related to the injection of bio-oil is due to a significant amount of residual solids, which often formed and block the feeding line and the rector while injection of bio-oil aqueous fraction was successful.

Sakaguchi[35] used a twin-fluid atomizer with inner and outer tube with surrounded cooling jacket to feed the bio-oil and bioslurry by atomizing gas (N_2) from the side of the fluidized bed reactor. It was recommended that more research is needed to achieve stabile injection for bio-oil and bioslurry. Marda et al.[37] investigated non-catalytic partial oxidation, while a mixture of bio-oil-methanol (50:50 wt%) was atomized from the top by an ultrasonic nozzle with flow rate between 0.1 and 10 ml/min. Latifi[18] developed the idea of syngas production from gasification of bio-oils in fluidized bed reactors with two types of twin-fluid atomizer with different ratio of the gas and liquid mass flow rate in the range of 0.5 to 2% (low ALR nozzle) and 50% (high ALR nozzle). The reason of using high ALR nozzle is to achieve perfect distribution and avoid agglomerates formation which typically formed in fluidized bed reactor.

2.3 Experimental results from gasification of bio-oil, and bioslurry.

Review of the published literatures indicates that various reactor setup such as fluidized bed and fixed bed with different bed materials based on non-catalytic and catalytic reforming are developed to gasify bio-oil model compounds, bio-oil aqueous fraction, whole bio-oil and bioslurry to syngas. Among this application the product gas composition and yield from gasification of bio-oil and bioslurry depends on bio-oil types, reactor type and size, and operating conditions such as gasification temperature, space velocity of feed and steam to carbon molar ratio (S/C) as well as the bed material type and mass. This section will mainly focus on doing surveys on gasification of bio-oil aqueous fraction, bio-oil and bioslurry which has been conducted, extensively, in previous published literatures as summarised in Table 2-1.

Table 2- 1: Literature review on gasification of bio-oil aqueous fraction, bio-oil and bioslurry

Feed material	Flow rate	Reactor	Bed Material	Temperature °C	Molar ratio of steam to carbon(S/C) or gas flow rate	Injection type	Hydrogen yields or bio-oil conversion	Reference
Bio-oil aqueous fraction $CH_{1.5\text{-}1.9}O_{0.6\text{-}0.8}$	G_{C1}HSV in the range of 760 to1230 h^{-1}	Fixed bed (1.65 cm I.D. and 42.6 cm length)	100 g of a commercial, nickel-based catalyst (Particle size 2.4-4.0 mm).	600-700	S/C = 5-35	Triple nozzle injector(using nitrogen and mixed with superheated steam in nozzle)	Hydrogen yield of 85% of the stoichiometric value	Wang *et al.*, 1998[36]
Bio-oil aqueous fraction $CH_{1.34}O_{0.81}$	G_{C1}HSV in the range of 62300 to126000 h^{-1}	Dual-bed quartz fixed bed	commercial catalysts(G-91, ICI 46-1, ICI 46-4, and C11-NK), and the Ni/Al_2O_3 reference catalysts mixed with quartz chips	825 and 875	S/C = 4.92-11	needle injector	Hydrogen yield of Max. close to 83.8% of the stoichiometric potential	Garcia *et al.* 2000[38]
Bio-oil aqueous fraction $CH_{1.25}O_{0.55}$	GHSV in the range of 700 to1000 h^{-1}	fluidized bed reactor	200-250 gof C11-NK, a commercial nickel based naphtha reforming catalyst	800 - 850	S/C = 7-9	N/A	Hydrogen yield of Up to max of 88% of the stoichiometric value	Czernik*et al.* 2002[39]

Biomass-derived oil with elemental composition of C = 43.6%, H = 8%, N = 0.5%, and O =47.9%	4.5 to 5.5 g/h	Fixed bed (12.7 mm I.D. and 500 mm long)	non-catalytic	650 - 800	Nitrogen Flow Rate: 18-54 mL/min	N/A	Maximum conversion of 83 wt% of bio-oil achieved	Panigrahi*et al.* 2002[40]
Biomass-derived oil with elemental composition of C = 43.6%, H = 8%, N = 0.5%, and O =47.9%	5g/h	Fixed bed (12.7 mm I.D. and 500 mm long)	non-catalytic	800°C	Nitrogen Flow Rate:12 to 30 (STP) as a carrier gas used with H_2, CO_2,or steam	N/A	The conversion decreased from 75 to 68 wt% with addition of CO_2 by 40% in nitrogen gas, The conversion unaffected with addition of H_2 by 40% in nitrogen gas. However, conversion varied from 67 to 81 wt% during the steam gasification.	Panigrahi*et al.* 2003[41]
Bio-oil aqueous fraction $CH_{2.48}O_{0.94}$	G_{C1}HSV in the range of 300 to 600 h^{-1}	Fixed bed reactor (12.52 mm I.D. and 712 mm long)	Industrial Ni-based catalyst (C11-NK)	600-900	S/C = 8.2	Twin fluid atomizer (N_2 used as an injection agent gas)	Hydrogen yield around 60% because of the high extent of coking	Kechagiopoulos*e t al.*[42]
Bio-oil $CH_{2.3}O_{1.04}N_{0.01}$	5 ml/h	A double envelop reactor	Ni/Al_2O_3 and $Ni–K/La_2O_3–Al_2O_3$ catalysts	700	S/C = 2.5 and 10	syringe pump (droplet by droplet)	Maximum hydrogen productivity was 18bysequential cracking, versus 20and37 mmolH_2 / g bio-oil by steam reforming at H_2O/C ratios of2.5 and 10, respectively	Davidian*et al.*[43]
Bio-oil (36.5% carbon, 8.4% hydrogen, and 55.0% oxygen)	G_{C1}HSV in 920 h^{-1}	Fluidized bed reactor	Four NREL-prepared catalysts with various amounts of nickel	850	S/C = 5.8	N/A	Hydrogen yield in the range of 70 to 80% of the stoichiometric potential	Czernik*et al.*[44]

Bio-oil aqueous fraction (The average composition of bio-oil was $CH_{2.3}O_{1.04}N_{0.01}$)	GHSV=4880–16570 h^{-1}	Fixed bed micro-reactor.	Structured Ru / MgO / Al_2O_3 catalysts	700–800	S/C = 7.2	Used a nozzle but detail not reported	The conversion is complete, while selectivity towards H_2 production is 100% over the entire temperature range investigated	Basagiannis and Verykios[45]
The volatile organic components ($CH_{2.70}O_{0.50}$_0.79 H_2O) of the crude bio-oil ($CH_{2.33}O_{0.95}$_0.56 H_2O)	GC1HSV =10000 h^{-1}	Fixed bed micro reactor	C12A7-O_, C12A7-O_/M (M = non-noble metals), and M/g-Al_2O_3 catalysts	250–750	S/C = 1.5, 4.0 and 9.0	N/A	The yield of hydrogen of 80% was obtained under the optimum steam reforming condition	Wang *et al.*[46]
Beech wood oil (C = 30.4-37.7%, H = 7.6-7.9%, and O = 54.4-61.7%) and pine wood pyrolysis oil (C = 30.4-37.7%, H = 7.6-7.9%, and O = 54.4-61.7%)	0.2- 2.5 kg/h	Fluidized bed reactor with diameter of108 mm and 72 cm height	Sand and Three different types of nickel-alumina catalysts	523-914	S/C = 1- 3.3	Gas-assisted atomizer using nitrogen as the atomizing gas	Carbon to gas conversion up to 87% with sand bed and up to 91% with catalyst bed while the H_2 yield were about 15 and 45% respectively	Van Rossum*et al.*[23]

Four different liquid feedstock(Pyrolysis Oils and Sugar Stream) used	0.2-2.5 kg/h	Staged reactors for evaporation and reforming(an inert fluidized bed and a catalytic fixed bed)	Inert bed and two type catalysts (K23 and K46)	430-830	S/C = 1 – 2.7	Gas-assisted atomizer using nitrogen as the atomizing gas	A mix of fixed and fluidized bed reactors as a gasifier and evaporator utilised to increase the gas product yield. Desirable gas product achieved by shifting the function of reactors, bed material, different S/C, temperature and bio-oil.	Van Rossum *et al.* [47]
Bio-oil with Ultimate analysis of C =45.8%, H =6.9%, and O =47.3%	GHSV=1800-14400h^{-1}	Two stage fixed bed reactor	Dolomite catalyst for primary stage and nickel-based catalyst (Ni/MgO) for second stage	700-900	S/C = 1 – 16	N/A	High temperature (>850°C) and high S/C (>12) are necessary for efficient conversion of bio-oil to desirable gas product in the first stage and also 100% conversion of CH_4 is obtained under the conditions of S/CH_4 no less than 2 and temperature no less than800°C in second stage.	Wu *et al.* [48]
The bio-oil ($CH_{1.32}O_{0.46}$ 0.23 H_2O) was mixed with methanol (50 wt%)	0.1-10 ml/min	A vertical quartz reactor (32 cm long and inside diameter of 1.1 cm)	Non-catalytic partial oxidation	625 - 850	O/C = 0.7 - 1.6	ultrasonic nozzle	The bio-oil carbon to gas conversion is typically between 85% and 95% for optimal conditions. However, high yields of CO (50 -70% of the maximum possible) and low yields of hydrogen (25% of the maximum possible) from the bio-oil have been observed.	Mardaet *al.* [37]

Bio-oil and Bioslurry (80 wt% bio-oil / 20 wt% char)	Methane equivalent gas hourly space velocity ($G_{C1}HSV$) value between 210 and 400 h^{-1}	Fluidized bed reactor	Sand or Ni-based catalyst	720–850	2.0–7.5	Twin fluid atomizer (N_2 used as an injection agent gas)	The carbon conversion for bio-oil was higher than bioslurry. The differences reduced from 24% to14% by increasing temperature from the range of 725–755°C to 803–815°C. Greater yields of H_2 and lesser yields of CO and hydrocarbons were found when catalyst was used.	Sakaguchi*et al.* [35]
Bio-oil with Ultimate analysis of C = 56.64%, H = 7.968%, and O = 33.064%	Weight hourly space velocity (WHSV)between 0.2 and 0.8h^{-1}	Fluidized bed reactor700 mm in height and 50 mm in diameter	Nickel-based catalyst NiO / MgO (7.2 wt% NiO)	500-800°C	8-20	Nozzle with mix of steam and bio-oil	The optimum conditions on hydrogen production were obtained at 700°C, S/C =17, and WHSV = 0.4 h^{-1}. Also reported that the main reason for fresh catalyst deactivation is due to the NiO grain sintered on the supporter surface and the carbon deposition is not the main reason	Xu*et al.*[7]
Bio-oil $CH_{1.688}O_{0.438}$	The liquid hourly space velocity (LHSV) : 0.8 – 2.5 and 0.2 -1.5 h-1for fixed and fluidized bed respectively	Fixed bed and Fluidized bed reactors	Self-made Ni/MgO-La_2O_3-Al_2O_3 catalyst	Fixed bed reactor under 650–950°C and a fluidized bed reactor under500–800°C	Fixed bed reactor: 8 - 20 Fluidized bed reactor: between 3 and ≅14.3	Jet nozzle: The bio-oil and steam were mixed through a nozzle and then fed into the reactor from the bottom	For the fluidized bed reactor, maximum hydrogen yield was 75.88% which was 7% higher than that of the fixed bed and also, the temperature required for efficient H_2 production from the fluidized bed was 100°C lower	Lan*et al.*[49]

Bio-oil aqueous fraction $CH_{2.39}O_{0.71}$	$G_{C1}HSV$ values of around 11,800 h^{-1}	Quartz fluidized bed reactor	Ni-Al catalysts modified with Ca or Mg	650°C	7.6	Quartz coaxial injection nozzle	The results showed the carbon conversion of around 80% in one step at 650°Cdue to the best performance of the magnesium modified catalyst	Medrano*et al.*[50]
Bio-oil $CH_{1.87}O_{0.754}$	Mass flow rate of bio-oil to mass of catalyst (W_bHSV): 9-26 h^{-1}	Fixed bed catalytic reactor	Nickel/alumina (Ni/Al2O3) supported	650-955	1-8	High-pressure syringe pump	The yield of hydrogen up to 73% with catalyst test (14.1% Ni), and the carbon conversion was up to 79% under: S/C=5, W_bHSV = 13 h^{-1} and T=950°C.	Seyedeyn-Azad*et al.*[51]
Fresh hardwood bio-oil ($CH_{2.071}O_{0.920}N_{0.005}$), three years aged hardwood bio-oil ($CH_{2.624}O_{1.121}N_{0.007}$), and birch wood bio-oil($CH_{4.326}O_{1.827}N_{0.019}$)	Residence time of 10-30s	Jiggle bed reactor where the solid particles are fluidized in a ceramic crucible by vibration	Silica sand was the bed material for non-catalytic and two catalysts with almost similar elements, but major differences of Nickel, calcium and lanthanum	700 - 800	-	Drummond capillary tubes with 4µl volume were used to inject precise amount of the bio-oil to the reactor	Since in the absence of excess steam the maximum carbon conversion achieved for the hard wood bio-oil and the birch wood bio-oil was 64% and 72%, respectively. Also higher hydrogen yields resulted due to higher water content of birch wood bio-oil.	Latifi[18]

2.3.1 Bio-oil type

Various biomass pyrolysis technologies are developed to improve biomass fuel properties. Among these technologies, thermal conversion by fast pyrolysis is a common method/technology to convert the biomass into high-energy-density fuels such as bio-oil[19, 20, 52, 53] and/or biochar.[14, 15, 54] Fast pyrolysis converts up to 75%[55] of biomass, including energy content to a bio-oil which is suitable for furthermore upgrading to synthesis gas by thermal gasification. However, the impact of biomass type, process conditions and recovery techniques on bio-oil yield and quality, on gasification would result in different gaseous product and conversion, under similar operating conditions. Therefore, the proximate and ultimate analysis of bio-oil and char is critical considerations that affect process operations and efficiency of gasification.

Elemental analysis (water free oil basis) of typical bio-oil[56] gives quantitative concentrations of C, H, O, N, and ash content at 55-58, 5.5-7.0, 35-40, 0-0.2, 0-0.2 wt% respectively. In addition, water content in bio-oils reported between 20 and 30 wt%. Additional consideration is contents of inorganic species (e.g. Al, Fe, P, Mn), alkali, and alkaline earth metals (e.g. Ca, K, Mg, Na), in the feedstock which is important during the gasification owing to catalyse the thermal degradation. The authors[55, 57-62] postulated that the gasification of bio-oil and/or char, including alkali, and alkaline earth metals (e.g. Ca, K, Mg, Na) is mainly important and responsible for interactions between char and volatiles.

Bio-oil is thermally unstable under the polymerization condition which make it more viscous fuel at temperature higher than 80°C.[63] Despite the progress made in the syngas yield during steam gasification of crude bio-oil recently, there are still significant issues, largely due to the complexities of bio-oil and gasification process. Therefore, a simpler model component mainly acetic acid[64-68] and aqueous phase of bio-oil,[36, 38, 39, 42] extracted by water was used by many researchers for experimental studies.

2.3.2 Reactor setup and bed material

Many authors have reported different setups of fixed bed and fluidized bed reactors for bio-oil aqueous fraction, including whole bio-oil and bioslurry as reported in Table 2-1. Czernik et al.[39] used the fixed bed reactor that was originally designed for steam reforming of natural gas and reported the issue was related to carbon deposits in the upper layer of the catalyst and in the reactor freeboard. In addition, the rate of coke formation in the fixed bed reactor is high while for fluidized bed reactor depends on enhancing contact with the catalyst surface.[42, 49]

Fluidized bed reactors have been shown to be more efficient in terms of hydrodynamics.[69, 70] Hydrodynamics plays an important role on the reactor performance and transport phenomena in binary systems such as heat and mass transfer in multiphase flow. Fluidized bed reactors with higher efficiency resulted in lower coke deposition due to a better contact of catalysts surface and feedstock. Employing two reactors in series to increase the bio-oil conversion and the hydrogen yield have been done by some researchers. In this way two fixed bed reactor[48] or a combination of fixed and fluidized bed reactors[47] where proposed with a higher efficiency.

As identified by the above literature review, there are various bed materials bass on non-catalytic (e.g. sand) and catalysts (commercial or synthesized catalysts[23, 38, 43, 44, 71]) and have been employed, with different optimization of the catalyst mixtures and metal promoters (Mg, Co, La and Ca) to maximize feed conversion and hydrogen yield[50, 67, 72] on steam gasification of bio-oil. However, these studies also dedicated to the formation/deposition of coke on catalysts surface and deactivation of the catalyst, especially, with nickel based catalysts during the steam gasification of bio-oil. The deposition of coke during steam gasification of bio-oil depends on the composition of the catalyst[71, 73, 74] and also composition of the feedstock.[17, 42]

2.3.3 The effects of operating parameters, and reactor type on the syngas yield and bio-oil conversion

The physical and the chemical complexity of fast pyrolysis bio-oils play an important role of steam gasification into the syngas (H_2+CO), CO_2, CH_4, and C_2^+ productions. Another important consideration is that the diversity of bio-oil resources results in

considerable variability in its composition with over 300 compounds[75] and properties. This variability makes it difficult to summarize data on syngas yield composition and bio-oil conversion, as function of feedstock and operating conditions that are available in the literature. However, an overall consideration can be done to evaluate how the operating parameters (temperature, feedstock flow rate, and H_2O /C ratio), reactor type and bed materials affect the bio-oil conversion and/or syngas yields.

Temperature of the gasification reactor is found to have significant on the bio-oil conversion and syngas yields produced from steam gasification of bio-oil.[23, 42, 46-48, 51] Increasing temperature increases hydrogen yield and carbon conversion due to endothermic reaction of thermal cracking of bio-oil. Kechagiopoulos et al.[42] examined various temperatures between 650 -900°C on non-catalytic gasification of aqueous phase of bio-oil with a constant methane equivalent gas hourly space velocity ($G_{C1}HSV$) of 500 h^{-1} and reported, the conversion of bio-oil to gaseous products (CO, CO_2, CH_4, C_2H_6) increase from 12% at 650°C to 60% at 850°C, while the coke formation reduced from 20% at 650°C to 12% at temperature above 800°C. They also outlined the effect of temperature on aqueous phase of bio-oil conversion and hydrogen yield in the presence of the commercial catalysts (Süd-Chemie C11-NK), with a fixed bed reactor.

- The maximum total conversion of bio-oil was reported 80% with non-catalytic bed, while it was 100% in the presence of the catalysts.

- The hydrogen yields observed maximum 60% at temperature about 850°C due to higher coke deposition on catalysts surface, while it was obtained about 90% with thermodynamic calculation.

- Basis on experimental results the hydrogen yield was considered not to be from thermal decomposition of bio-oil, as it was very low in non-catalytic bed.

- The ratio of H_2/CO reduced with increasing temperature between 600 – 850°C, while the ratio of CO/ CO_2 increased.

- Carbon formation due to thermal decomposition of the unstable oxygenates with catalysts reaction is a major issue during gasification even if the aqueous fraction is used.

- Minimization of carbon formation is possible if bio-oil has direct and immediate contact with catalysts surface, therefore it was predicted, the fluidized bed rector with a proper injecting system is more efficient than fixed bed rector.

- The test had been done with two different GC1HSV at 300 and 600 $h^{-1}$and postulated that there was not a notable influence on hydrogen yield.

- The H2O /C ratio of 8.2 was kept constant in all experiments at the original water content of the bio-oil aqueous fraction, therefore, the effect of H2O /C was not considered in their experiments.

In a different bench-scale reactor Sakaguchi[35] produced syngas from gasification of bio-oil and bioslurry in fluidized bed reactor under catalytic and non-catalytic conditions. Upon the review of this study, the main qualitative and quantitative outlines are drawn as follows:

- Differences in the process configuration (fixed bed reactor versus fluidized bed reactor and catalytic bed versus non-catalytic bed) and temperature seem to be more important factors which can influence the total conversion of bio-oil and product gas yields. The author reports that, while temperature appeared to have significant effect on carbon conversion of bio-oil, which led to high conversion at high temperature, the products gas yields from non-catalytic and catalytic bed had very different elemental composition. This was expected because the steam gasification and water-gas shift reactions in the presence of the catalysts had significant effect on gas yields (larger H_2 and CO_2, as well as, smaller hydrocarbon yields).

- The carbon conversion of bioslurry was reported less than that of bio-oil, probably because of more carbon content in bioslurry and less reaction rate of slurry char steam gasification. The carbon conversion differences decreased from 24% at 725 – 755°C to 14% at 803 – 815°C under H2O / C ≈ 5.5,

$G_{C1}HSV \approx 340\ h^{-1}$. Consequently, the residual carbon of steam gasification, of bioslurry is not mainly from the originally contained char at high temperature.

- The hydrogen and carbon yield (total carbon conversion to gas) increased with increasing temperature under non catalysts condition, while with catalysts effect there was no clear relationship between the carbon and hydrogen yield.

- Basis on experimental results on steam conversion, water was mostly involved in steam gasification under catalytic conditions with steam conversion over 15% at temperature of 803°C, while thermal decomposition is the main reaction under non-catalysts condition because of steam conversion of approximately 2% at 836°C.

- The test had been performed with at three different $G_{C1}HSV$ values between 210 – 400 h^{-1}, T ≈ 790°C, H_2O /C ≈ 5.5, and postulated that it does not clearly affect the product gas yield and composition.

- The effect of the steam to carbon ratio on the hydrogen and carbon yields at three different H_2O /C between 2.7– 7.5, T ≈ 800°C and $G_{C1}HSV$ ≈ 320 h-1 shows there is not a notable influence on product gas yield and composition.

2.4 Thermodynamics-based model studies of bio-oil and bioslurry gasification

Equilibrium models, which take into account only thermodynamic limitations, are increasingly being used to describe complex multidisciplinary of bio-oil and its model compounds to permanent gases by thermal gasification. Full conversion of bio-oil and its model component and also maximum yield of syngas can be predicted by equilibrium model at temperatures above 700°C.[65, 76] However, even at high temperatures, product prediction was not in close agreement with experimental observation.[37, 40, 42, 67, 77, 78] Therefore, upper bounds for the efficiency of converting bio-oil and its model compounds into products gas can be predicted by equilibrium model while for non-equilibrium processes, it requires more general concepts such

as, hydrodynamics, heat and mass transfer, chemical kinetics, residence time and even particle size distribution.

2.4.1 Equilibrium model

Many authors have reported on the modelling of gasification of carbonaceous feedstock, especially the equilibrium. Equilibrium models,[79] including stoichiometric and non-stoichiometric, have been employed by several researchers to predict product gas composition from a gasifier with a range of carbonaceous feedstock. In stoichiometric approach,[80-83] the reactants composition changed according to the stoichiometry of chemical reactions. In addition, the gas-phase is assumed to be at equilibrium (e.g. water-gas shift reaction) at the local temperature and gas composition. In this model mass and energy balances are combined with equilibrium relationships to calculate species in the produced gas.

However, this model may not be applicable for a complex system, where reaction mechanism is not fully clear, the molecular formulation of feed is unknown and/or a large number of reactions and species are involve in the gasification system. A more general method for solving these complicated problems is the direct minimization of the Gibbs function of the system (non-stoichiometric approach) which is achieved at equilibrium. In this model, the system with C, H, O, N and S, obtained from ultimate analysis data was simplified to 42 gaseous species and two solid species.[35, 84, 85] The model was solved, using the RAND algorithm.[86-88]

2.4.2 Kinetic modified equilibrium model

Equilibrium modelling can also be considered with a kinetics modification due to kinetic limitation of the system, which is far from fully equilibrium. This modification has led to the development of more accurate and reliable models that some investigators have reported, on kinetic modified equilibrium model. As mentioned before carbon conversion and hydrocarbon yields in the real gasification system are included in experimental studies while in the equilibrium calculation they are not considered. Therefore, if unconverted carbon and hydrocarbons which can be obtained from experimental studies be initially withdrawn and then after the equilibrium calculation the hydrocarbons be included to the product composition, the

modified products gas composition are in good agreement with experimental results and it is called kinetic modified equilibrium model.

Li et al.[85] modified the equilibrium method kinetically for partially oxidation of biomass steam gasification to synthesis gas in a circulating fluidized bed reactor by considering methane (hydrocarbon) in outlet gas. More recently, the non-stoichiometric approach was also applied to modelling bio-oil and bioslurry gasification in fluidized bed reactor reported by Sakaguchi.[35] The amount of unconverted carbon and hydrocarbons, determined experimentally from the actual gasification system was considered in the calculation.

2.5 Conclusions and research gaps

The approach to the identification and analysis of above literature review are drawn as follows:

- Fast pyrolysis is a well-known technology to produce bio-oil and biochar from biomass. Biochar as a solid fuel with good grindability and high energy density is suitable for direct mixing with bio-oil to obtain bioslurry. Therefore, bio-oil and bioslurry can be updated to produce syngas product.

- Bio-oil has a much higher energy density than the raw biomass and can be used as a replacement for numerous applications where natural gas or liquid hydrocarbons are used to produce syngas by steam gasification system.

- The effects of operating parameters (e.g. feed flow rate, temperature, H_2O /C), reactor types (fixed bed and/or fluidized bed reactors), and bed materials (catalysts and/or sand) on the syngas yield and carbon conversion from bio-oil and bioslurry steam reforming have been investigated by many researches. Temperature, flow pattern, and bed materials have significant effects on carbon conversion and product gas distribution.

- One important challenge during bio-oil or bioslurry catalytic gasification is the catalysts deactivation due to carbon formation on the catalysts surface, which is shown to reduce catalysts efficiency.

- The bio-oil and bioslurry injection into the high temperature reactor system has some important technical challenges related to high viscosity and the polymerization property of the bio-oil.

- Several injection types were employed for bio-oil model component, bio-oil aqueous fraction, bio-oil and bioslurry in the steam gasification system; however data related to droplets size measurement have been not investigated, especially, for bio-oil and bioslurry.

- Thermodynamic base model of bio-oil and bioslurry have been investigated by several researchers to predict product gas composition in the steam gasification system.

- Steam gasification of coal or related solid feedstock (sources of carbon) is a matured technology for synthesis gas production (e.g. CO, H_2), upgraded in Fischer–Tropsch plants to liquid hydrocarbon.[89]

Summary of above previous studies on the steam gasification of bio-oil model component, bio-oil aqueous fraction, bio-oil and bioslurry indicates that:

- The spray characteristics must be considered in designing a proper atomizer ring for bio-oil and bioslurry injection system but little consideration has been given on this aspect so far.

- The contribution of drops diameter on steam gasification system is not yet studies.

- Current studies of mathematical modelling of bio-oil and bioslurry steam gasification are limited to equilibrium models, while mathematical modelling, considering the hydrodynamic characteristics of the reactor, droplet trajectory with heat and mass transfer, droplets size distribution, is yet to be studied.

- Current understanding on effect of Alkali and Alkaline Earth Metallic species on intraction between char and volatiles based on a limited number of expermental data and the contribution of this effects on kinetics parameters of biochar remain unknown.

- Up to now the kinetics and reaction mechanism during steam bio-oil gasification is still largely unclear.

Therefore, further studies will be required in order to improve and develop the fundamental understandings of bio-oil and bioslurry steam gasification, including:

1. Measuring mean diameter and droplet size distribution is the key objective of hydrodynamic simulation. While the optical based methods such as light scattering techniques requires the establishment of sophisticated and expensive optical systems, the mechanical method has advantages of simplicity, low cost, and visibility. However, this method needs to be improved and updated from disadvantage of several drawbacks.

2. Developing a proper atomizer ring for continuous atomization of bio-oil and bioslurry. This requires a systematic experimental study on different type of atomizer to provide better results (mean diameters and/or droplet size distribution) and continuous and stable feeding system.

3. Accordingly, much research effort has been undertaken to address the steam gasification of bio-oil model component, bio-oil aqueous fraction, bio-oil, and bioslurry in different type of reactors. However, the majority of these works are experimental studies with especial attention to bed materials. Little modelling work on equilibrium condition have been done due to the complex nature of the feedstock, while there is no work on a simulation where hydrodynamics, heat and mass transfer, chemical kinetics, residence time and even particle size distribution may play an important role, particularly when conducted in a fluidized bed reactor. Such simulation is an important tool and has led to quantitative and better understanding of this complex operation.

4. Several experiments on effects of Alkali and Alkaline Earth Metallic species on char reactivity in steam gasification system and also its intraction between char and volatiles have been done. Furthermore, the kineticks paramteres of steam gasification of slurry char has been done. Therefore, based on above experimental data, simulations can help to identify the contribution of catalysts effect of AAME on kinetics parameters of steam reforming of slurry char during bioslurry gasification.

5. Kinetic studies of the steam reforming reactions and establishment of reaction mechanisms is needed to provide a fundamental underestanding on the mechanisms and kinetics of steam reforming of bio-oil to syngas which should be considered in simulation.

6. Althoughthe Alkali and Alkaline Earth Metallic species are known to catalyzethe seam gasification of slurry char, more research need to elucidate the reaction mechanisms an kinetics during slurry char gasification.Such work is required to provide kinetics parameters for further simulation and modelling works.

7. Kinetic studies of the steam reforming reactions of bio-oil with varied chemical composition and physical attribute in the precence of different catalysts, espically, commercial cataysts will require to develope a robust process of gsification. However, little work has been done on this aspect so far.

2.6 Research objectives of the present study

The above literature review has identified the several research gaps in the research field. Although several research gaps have been noted, some of them will be done to fill research gaps during limited PhD program time. Therefore, this study will focus on the mathematical modelling of bio-oil and bioslurry steam gasification in a fluidized bed reactor. The main research objectives of this study are:

- Developing the mechanical method for measuring droplet size distribution and mean diameter. In these way four parameters, including a practical algorithm for overlap minimization, the shape correction factor, the effective roundness, and evaporation correction factor will be considered.

- Examining several nozzles for bio-oil and bioslurry atomization, in order to provide the data related to the spray characteristics which are useful in mathematical simulation.

- Mathematical modelling of bio-oil steam gasification in a fluidized bed reactor, using the Computational Fluid Dynamics (CFD) simulation software from ANSYS-Fluent. This method will be used to generate flow simulation

with three phases and their interactions by writhing user define function code in Fluent.

- Mathematical modelling of bioslurry steam gasification in a fluidized bed reactor, using CFD Fluent.

CHAPTER 3 RESEARCH METHODOLOGY

3.1 Introduction

Material in this chapter describes how thesis objectives, outlined in previous chapter, will be achieved via the methodology employed in this study. This chapter also provides the details of experimental and analytical technique as well as simulation methodology.

3.2 Experimental methodology and simulation approach

Several fuels employed in this study, i.e. two types of bio-oil, biochar, diesel, and biodiesel (rapeseed oil, methyl ester). A series of systematic experiments were then carried out, including:

- Preparing four blends of biodiesel and diesel at various blending ratios (based on volume) in closed containers with magnetic stirrer to produce homogenous mixtures.

- Pyrolysis of pine wood (biomass) in fluidized bed reactor to produce biochar, and then mixed with bio-oil to produce bioslurry with different loading levels for further experiments.

- Atomization of prepared fuels by different type and size of nozzles at several operation conditions to produce size distributions of droplets, captured on glass slide for further measurement and analysis.

- Photography of droplets, using extreme close-up technique by a full frame digital camera under well controlled conditions of light source.

- Analyses of the images via a series of developed techniques in this study such as shape correction factor and critical roundness, etc.

- Transfer the droplet size data in the form of Rosin-Rammler distribution function (a cumulative frequency distribution) to determine mathematical function for droplet size in sprays.

- Single droplet of bio-oil model vaporization and gasification by Fluent Discrete Phase Model (DPM).

- Overall performance of a fluidized bed steam gasification reactor in terms of modelling product quality and outputs with a good approximation of the hydrodynamics at the macro-scale for bio-oil and bioslurry, using Computational Fluid Dynamics (CFD).

In this study, the reproducibility of experiments and analyses has been done to access the quality of the research results. Figure 3-1 shows a flow chart for the overall methodology developed in this study as discussed in the following sections.

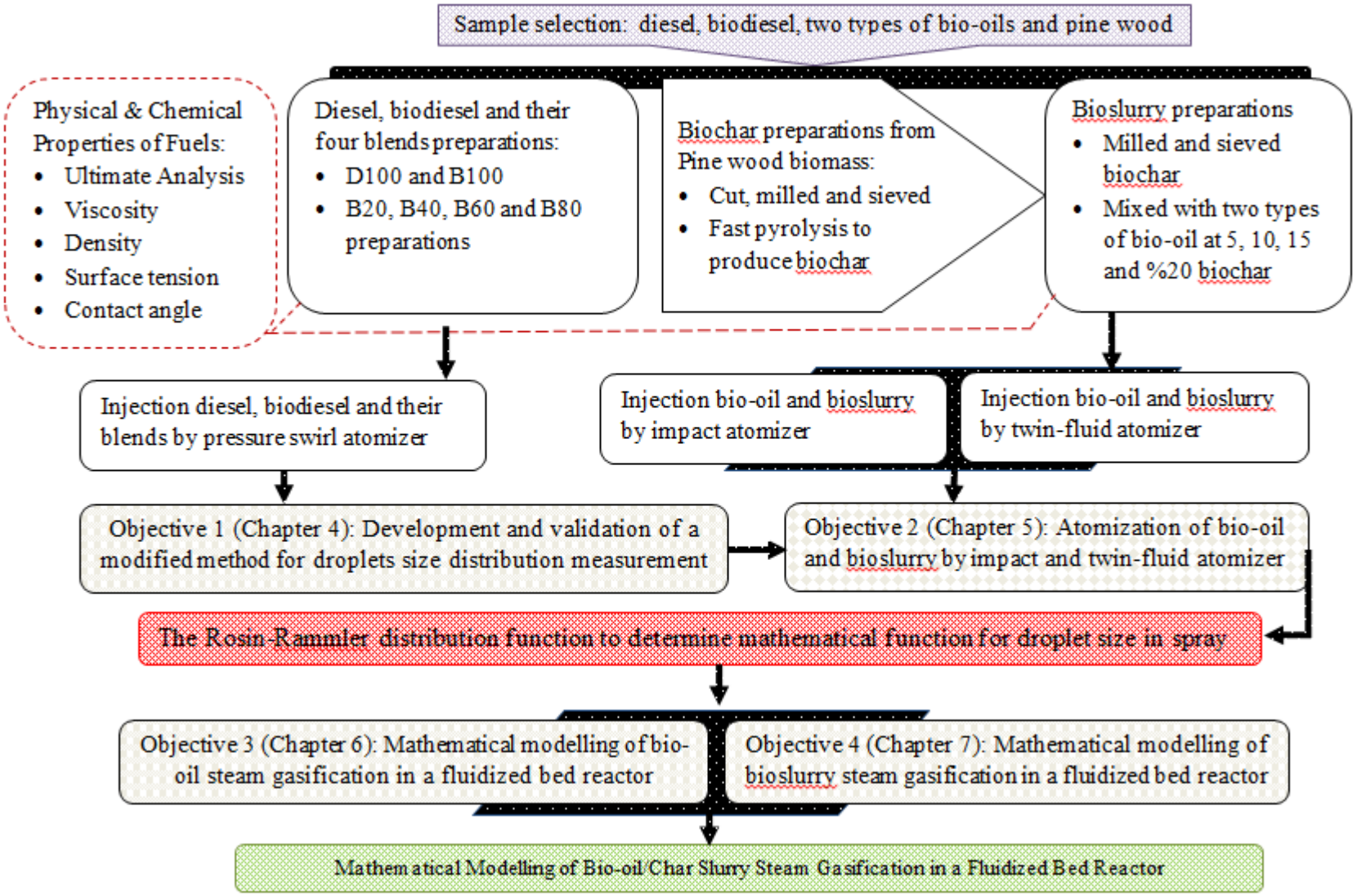

Figure 3- 1: Research methodology

3.2.1 Experiment on droplet mean diameter and size distribution of diesel, biodiesel and their blends

As discussed in Section 2.6 of Chapter 2, a key issue that needs to be addressed is the development of a proper method for bio-oil and bioslurry droplet measurement in the absence of light scattering technique which is too expensive. This is particularly important to ensure that the measurement of droplet size distribution and/or mean diameter of bio-oil and bioslurry will be relatively accurate, with acceptable systematic and random errors. Therefore, the mechanical method (see Section 3.3.2) with advantages of simplicity, low cost, visibility and reliability was employed. However, different effective parameters were developed or modified to reduce or eliminate several disadvantages of the method. In this thesis a series of experiments were carried out on diesel, biodiesel and their blends (sample preparations, see Section 3.3.1), considering the extensive data available on literatures for droplet mean diameter and size distribution in case of method validation. The new developed mechanical method which is also applicable for measuring all type of liquid fuels at ambient temperature and pressure was then developed in Chapter 4 and employed in the studies on mean drop size and drop size distribution of bio-oil and bioslurry as will be discussed in the next section.

3.2.2 Experiment on droplet mean diameter of bio-oil/ bio-slurry sprays under various atomization conditions.

In line with the research objectives, outlined in Section 2.6 of Chapter 2, the second part of this study aims at investigating bio-oil and bioslurry droplet measurement by conducting a series of systematic experiments. Firstly, eight bioslurry samples prepared from suspending of fine biochar particles into two types of bio-oil with different loading level of biochar (see Section 3.3.1.2) at room temperature. Secondly, to investigate the different type of atomizer behaviour and characteristics, the raw bio-oil and bioslurry samples were atomized by two different nozzle designs, followed by measuring and analysis, using the method developed in Chapter 4. Furthermore, the effect of operating conditions and liquid properties were investigated on the variation of droplet size with detailed results and discussion in Chapter 5.

3.2.3 Three dimensional Computational Fluid Dynamics (CFD) modelling of flow, mass transfer and reactions for steam gasification of bio-oil in fluidized bed reactor

The results in Chapter 5 were employed to transfer particle size data into discrete sizes ranges (e.g. the number of droplets between 30 and 40 μm) when sieve analysis was used, such result, were considered in the determination of mathematical function for droplet size in sprays. Thus, in Chapter 6 the cumulative frequency of mass distribution curve with the Rosin-Rammler format employed to determine the drop size distribution when bio-oil is delivered into the reactor through the fuel injector. In this chapter the ANSYS FLUENT CFD software was employed, which can provide in-depth analysis of bio-oil steam gasification in fluidized bed reactor. The model takes into account the reactions, mass and heat transfer, hydrodynamics as well as thermal decomposition of the feed droplets and interactions of the three phases. In this model, the gas and solid flow fields will be determined by the Eulerian method and the droplet flow field will be examined by Lagrangian. The results of this work are presented in Chapter 6.

3.2.4 Three dimensional modelling and simulation of bioslurry steam reforming in fluidized bed reactor, using CFD

Chapter 6 provide details of how the cumulative frequency of mass distribution curve with the Rosin-Rammler format obtains from experimental measurement of particle size distribution. Thus, the result was used to transfer bioslurry particle size data into the Rosin-Rammler expression as detailed in Chapter 7. In this chapter, three-dimensional Computational Fluid Dynamics (CFD) technique was also developed to investigate the impact of the biochar thermal decomposition on product gas composition during steam gasification of bioslurry. During gasification, several parallel and consecutive reactions take place that lead to the conversion of bioslurry into gaseous products. The heterogeneous reactions include bio-oil gasification and char conversion (char reacts with steam to produce CO and H_2) with its interaction on reaction rate by hooking a User Defined Function (UDF) to ANSYS FLUENT. In case of modelling particle transport in CFD simulation, the gas and solid bed material flow fields was determined by the Eulerian method and the bio-oil droplets and bio-char particles were examined by Lagrangian approach.

3.3 Experimental

3.3.1 Sample preparations

3.3.1.1 Diesel, biodiesel and their blends for experiments

Automotive diesel fuel and biodiesel (rapeseed oil, methyl ester) were purchased from commercial suppliers in Western Australia for experiments in this study. Four blends of biodiesel and diesel was then prepared at various blending ratios (based on volume) in closed containers with magnetic stirrer to produce homogenous mixtures. Therefore, a total of 6 liquid fuel samples were used in the experiments, denoted as D100, B20, B40, B60, B80 and B100. Here, B20 refers to mixture of 20% vol biodiesel and 80% vol diesel while D100 and B100 refer to diesel and biodiesel fuels, respectively. After sample preparation, one of the most common determinations is the ultimate analyses of the prepared sample which is summarized in Table 3-1.

3.3.1.2 Fast pyrolysis bio-oil, biochar and bioslurry samples

This study considered two fast pyrolysis bio-oil samples ("bio-oil A" and "bio-oil B"), both of which were produced from pine wood and provided by commercial suppliers. A local pine wood sample was sourced for the production of biochar from fast pyrolysis in a laboratory-scale fluidized bed reactor at 500℃. The detailed descriptions of the procedure for biochar production can be found elsewhere.[90] The ultimate analyses of bio-oil A, bio-oil B, and biochar are summarized in Table 3-1. After the grinding of the biochar, a set of bioslurry samples were prepared via suspending the fine biochar particles into the bio-oil samples at a series of biochar loading levels of 5, 10, 15 and 20 wt%. The fine biochar sample after grinding has a Sauter Mean Diameter of 18.446 μm (measured by Mastersizer 2000). Depend on type of bio-oil used and the level of biochar loaded, the bioslurry samples are denoted as either "bioslurry Axx" or "bioslurry Bxx" which A or B stands for bio-oil A or B used and xx (%) stands for the levels of biochar loading in the bioslurry.

Table 3- 1: Ultimate Analysis fuels used in this study (wt%)

Fuel	C	H	N	S	O [a]
Diesel	86.32	13.68	0	0	0
B 20	84.6	13.12	0.01	<0.01	1.94
B 40	82.71	13.4	0.02	<0.01	4.06
B 60	80.91	13.14	0.03	0.01	5.91
B 80	78.94	12.78	0.03	0.01	8.24
Biodiesel	76.89	12.35	0.05	0.01	10.7
Bio-oil A	42.66	7.69	0.19	0.02	49.43
Bio-oil B	40.64	8.41	0.28	0.01	50.66
Biochar	85.03	3.34	0.3	0.03	11.3

"a" Oxygen calculated by differences

3.3.2 Experimental setup

3.3.2.1 A spray setup for pressure-swirl and Impact atomizers

An atomization setup was developed to investigate the spray characteristics, as illustrated in Figure 3-2. The system consists of a liquid fuel feeding system, an atomizer, a droplet enclosure, and camera setup. Two types of atomizers are considered in this study: one is an impact atomizer and the other is a twin-fluid atomizer. For experiments using impact atomizers which require higher flow rates than twin-fluid atomizers, the fuel feeding system includes a two-litre reservoir, a magnetic mixer, a variable speed cavity pump and a flow meter with pulse output. Spray experiments were conducted at feeding rates of 108–490 ml/min for impact atomizers (model "PJ10", "PJ12", and "PJ15" with orifice diameter of 254, 305, and 381 μm), considering operating limits such as pump pressure and flow rate, to achieve fully developed spray. For experiments using twin-fluid atomizers, the fuel feeding system is replaced with a syringe pump. In addition, the aircap body (Paasche Model VLB) with VLA-3 aircap has been assembled to build the twin – fluid atomizer, in which liquid fuel is injected down the centre line of the tubing

along with nitrogen gas in outlet as illustrated in Figure 3-3. The gas and the liquid are required to be delivered separately and close to the tip of the injection nozzle with carefully-controlled flows to ensure proper atomization at feeding rates of 2-6 ml/min.

A droplet enclosure (60 × 60 × 60 cm) was designed with an aperture (10 × 20 cm) on the top to capture spray droplets. The liquid is atomized and the spray passes through the aperture (open/close via a shutter) into the enclosure, then settle on the collection glass slide on the bottom. Photography of the droplets were taken using a 20.2 MP full frame digital camera (Canon EOS 6D Digital SLR Camera) with Tamron SP AF 90mm f/2.8 Di Macro Lens. The surface area of glass collection plate was divided into 49 (7×7) square areas, with each single area being close to sensor size of camera (35.8 × 23.9 mm) for taking high-resolution images.

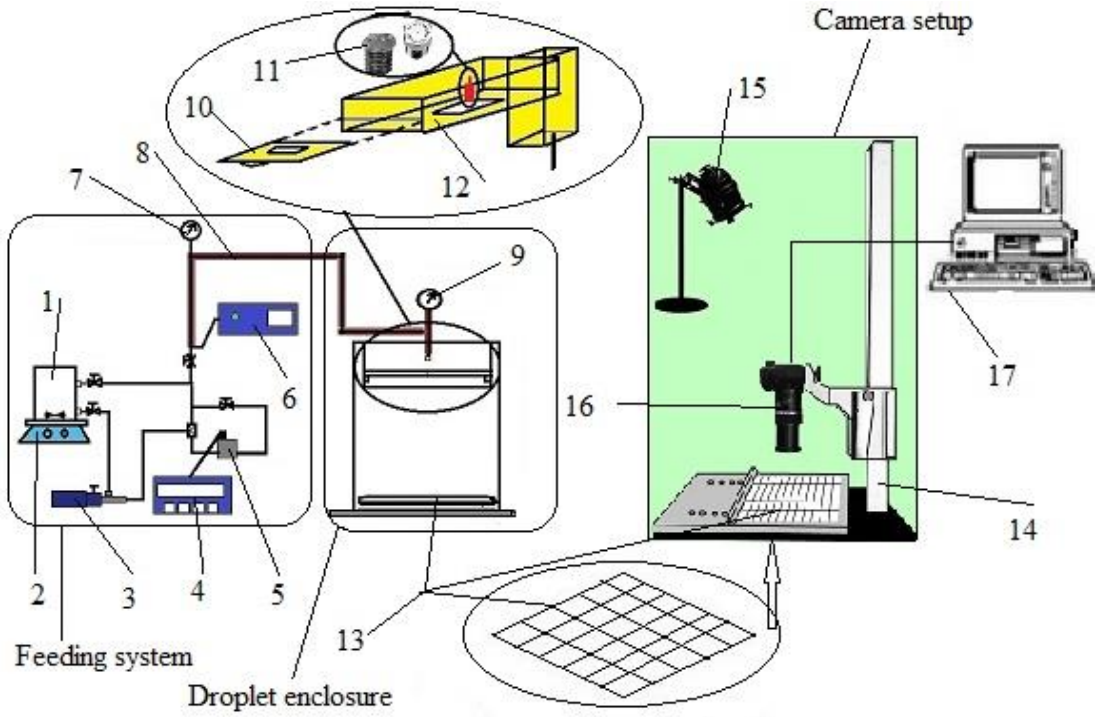

Figure 3- 2: Schematic diagram of experimental setup: (1) 2-litre reservoir, (2) Magnetic stirrer, (3) Cavity pump, (4) Flow monitor, (5) Flow meter (Gear), (6) Temperature controller, (7) Pressure gage, (8) Heating tape, (9) Thermometer, (10) Shutter, (11) Nozzle, (12) Aperture, (13) Droplet glass slide, (14) Camera stand, (15) Light source, and (16) High-resolution digital camera, (17) Computer with graphics software.

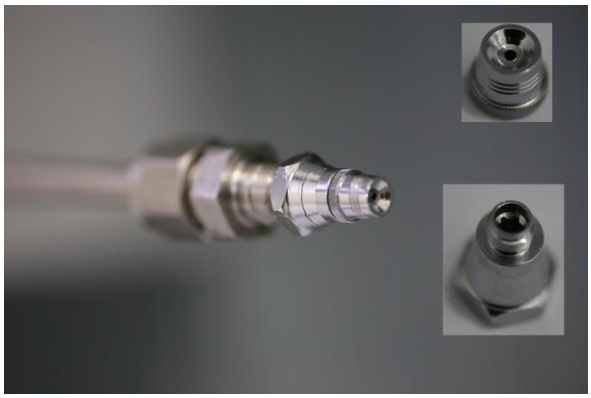

Figure 3- 3: VLB air cap body and VLA-3 air cap assembled with 1/4 and 1/8 inch outer and inner tube

3.3.3 Method for droplets sampling and size analysis

An experimental method was developed for measuring droplet diameter, as shown in Figure 3-4. The method includes two steps: droplet sampling and droplet size analysis. The droplet sampling step ensures the collection of representative droplets with collection efficiency (calibration). This is achieved via the determination of the minimum distance from the atomizer exit to the glass slide for minimized droplets overlapping. The second step is droplet size analysis which is essentially based on image analysis. Three key considerations have been incorporated. The first is the introduction of critical roundness. This enables the image analysis process to eliminate possible overlapped droplets which have roundness below the critical roundness. The second is the correction for the shape of droplets on the glass slide in order to find the real droplets diameters. The shape correction factor depends on the contact angle of the droplet on the glass slide, which is determined by wettability, density, surface tension, dynamic and kinematic viscosity of the liquid. The third and last is the correction factor for evaporation which consider the evaporation effect during drops travelling period from nozzle exit to glass slide. Moreover, Chapter 4 provides more details for developing new parameters on the mechanical method in case of photography technique, set up calibration, critical roundness, shape correction factor, and evaporation correction to measure spray drops diameters.

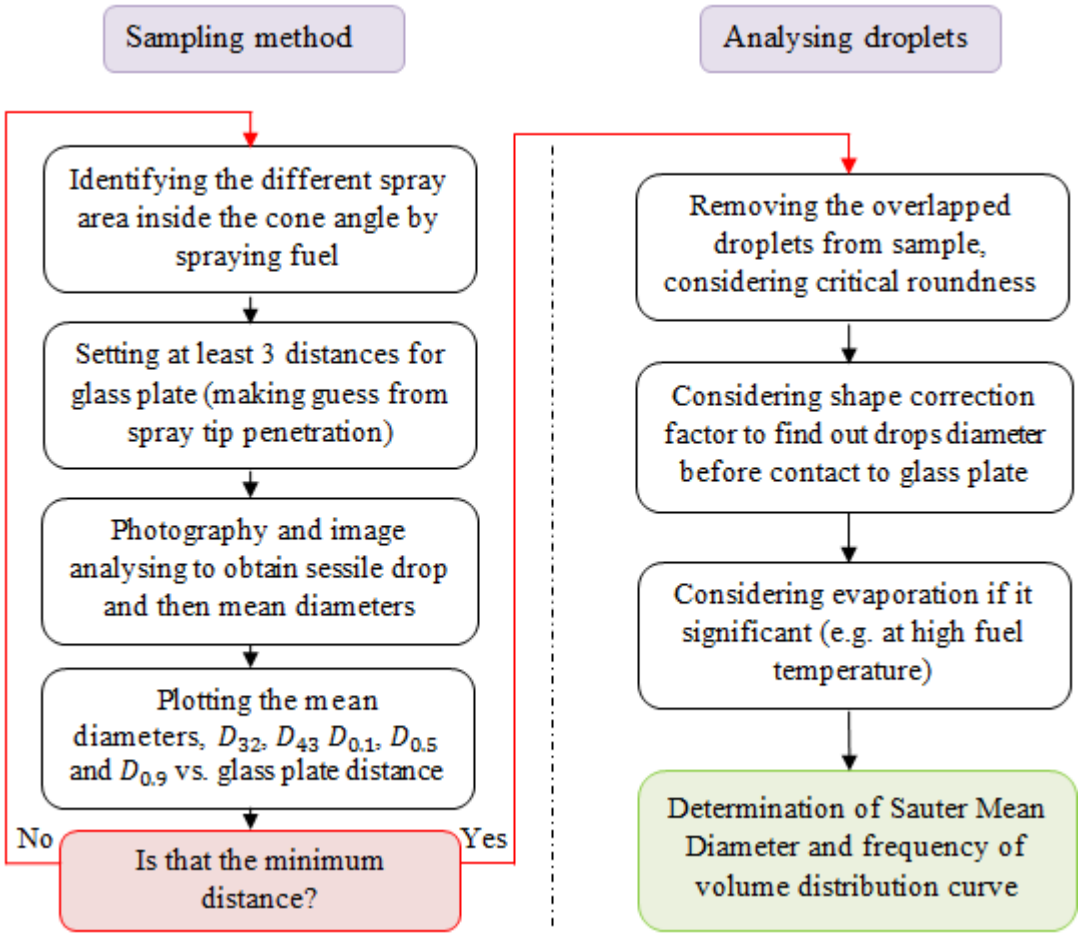

Figure 3- 4: Methodology flow chart for measuring drop size

3.3.3.1 Sampling of droplets

In this study a simple and high collection efficiency sampling method was developed to collect a representative droplet sample and also reduce overlapped droplets on glass slide before any further analysis for real droplet diameter estimation. First, a cluster sample of droplets had been taken by identifying the different spray areas inside the cone angle, formed by two straight lines drawn from the nozzle exit. A sample of these areas should be chosen along the spray radial distance at the specific axial position from the atomizer tip; because the concentration and mean diameter of droplets in the central line of spray was noted to be significantly higher than exit line area. Therefore, all droplets in those spray areas selected, would be included in the sample by moving the glass slide in the spray radial distance.

Next, in this sampling method the distance of glass slide from nozzle exit plays a significant role to increase the collection efficiency. The coalesced droplets are more likely to appear when the distance is less than the minimum amount and depends on

drops range of interest, the results might be affected by overestimation. As discussed in detailed in Chapter 4 several experiments have been done to find out what is the minimum distance of glass slide form nozzle exit where further increase in distance from nozzle will not affect the results significantly.

3.3.3.2 Direct optical image of sessile fuel drops

Recent developments in digital cameras have opened new possibilities to use high sensitivity full frame sensor packed with high megapixels included micro lens to capture high quality direct optical images. The acquired images were then analysed using image processing software (Digimizer) for determining Sauter Mean Diameter (SMD) of the droplets. Figure 3-5 shows the raw image of the droplets of bio-oil or bioslurry spray on the glass slide and the respective sharp edge image before analysis.

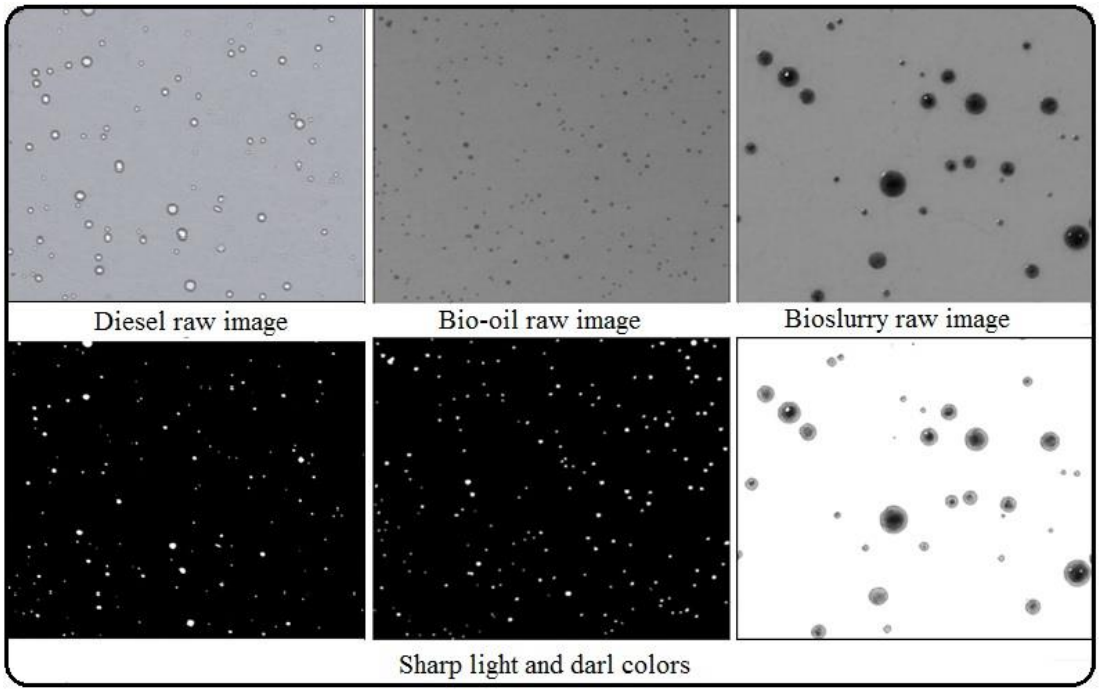

Figure 3- 5: Sample images with same camera depth of field, taken from group of droplets collected on glass slide for diesel, bio-oil and bioslurry. The droplet images were taken from injection of diesel fuel by pressure swirl atomizer while an impact atomizer was employed for spray bio-oil and bioslurry.

3.3.3.3 Development of a method for estimating droplet diameter before contact the glass slide

Although, finding the minimum distance of nozzle exit from glass slide will help to increase collection efficiency in terms of reducing the overlapped drops, numerous overlapped drops may still exist in the collected drops, which need to be removed. The area and roundness of objects during image analyses was considered to obtain the sphere diameter of drops and critical roundness. Value of roundness close to one indicates a perfect circular of drop which can be recognized as single droplet. However, as the roundness decreases, the noncircular form of the drops might be due to drops overlapping. In addition, the critical roundness has been defined in Chapter 4 to eliminate overlapped drops during analysing. In this way droplet with roundness less than critical, are eliminated from the calculation.

Finally, the sessile drop diameters should be corrected by considering shape and evaporation correction factors. Drop diameter on the glass slide is larger than drop before contact, and depends on fuel properties and drops receiver material, there are different shape correction factors. In addition to shape correction factor, the evaporation correction has been done to consider evaporation effect during drop travelling period from nozzle exit to glass slide. The details of these correction factors are discussed in Chapter 4.

3.4 Instruments and analytical techniques

3.4.1 Ultimate analysis (CHNS/O)

Ultimate analysis of fuels was determined using the PerkinElmer 2400 Series II CHNS/O Elemental Analyser that uses a combustion method to convert the sample elements to gases (CO_2, H_2O, and N_2). For analysis, the solid samples were wrapped in tin foil and liquid samples filled in tin capsule. In terms of calibration, accurately weighed samples of a known standard, are first analysed to calibrate the analyser. A calibration curve was generated to calculate the contents of unknown samples. Total carbon, hydrogen, nitrogen and sulphur contents were determined while the oxygen content was calculated by the difference from the C, H, N, and S contents of the samples.

3.4.2 Particle size distribution of char

Particle size distribution of biochar was obtained, using light scattering technique of Malvern Instrument (Mastersizer 2000). The results displayed by instrument include the histogram graph, undersize plot, oversize plot, and the frequency curve. However, it was transferred to the Rosin-Rammler distribution function to determine a mathematical function for droplet size in sprays.

3.4.3 Quantification of fuels surface tension

The surface tension of the liquid fuel samples was measured using a tensiometer (Model: Sigma 701, KSV Instruments Ltd). The method of measuring is based on the Wilhelmy technique by using a one millimetre platinum rod, immersed into the sample and then pulled out with the maximum force measurement at different temperatures with ranges from 20℃ to 80℃, by intervals of 20℃. A water bath was used to incubate samples in water maintained at a constant temperature. Calibration of instrument has been achieved by comparison to a known standard quantity (e.g. distillate water) to determine if the equipment is measuring surface tension accurately.

3.4.4 Quantification of fuels density

Digital density meter (Model: DMA4500, Anton Paar) was used to measure fuels density at different temperature between 20 and 80℃ with 10℃ intervals.

3.4.5 Quantification of fuel viscosity

Viscosity measurement of liquid fuels of this study were performed in a rotational rheometer (Model: HAAKE MARS II, Thermo Scientific), using conical sensor (C35/4° Ti) at room temperature. The All measurements were carried out applying different temperatures with range from about 20℃ to 80℃ by intervals of 10℃. All viscosity measurements were performed three times per temperature for each material.

3.4.6 Quantification of fuel contact angle

The contact angle of different liquid fuels was measured using a KSV Contact Angle Meter (Model: CAM 101, Camera: Imaging source DMK21F04, Software: KSV CAM Software v 3.81). For 5 data point at room temperature of small and large samples on glass slide, the average contact angle for left and right of sessile droplet was measured and reported.

3.5 Simulation

3.5.1 Computational fluid dynamics (CFD)

As a part of this study, the Computational fluid dynamics (CFD) as a powerful and cost-effective engineering tool was employed to model bio-oil and bioslurry gasifier system involving a fluidized bed flow, droplet heat and mass transfer and associated phenomena such as chemical reactions by means of computer – based simulation. Pre-processor, Solver and Post processor are usually the main elements of all CFD code.

3.5.1.1 Pre-processor

The pre-processing stage involves the preparation of data entry such as materials information into the CFD program for use in subsequent numerical calculations by the solver. Pre-processing is generally described as defining the model and includes the following user activities.

- **Geometry:** It describes the physical bound and size of the objective, aimed to be analysed. In this study the geometry of fluidized bed reactor was performed with the same dimension (height of 0.8m and inner diameter of 0.0779m), reported by Masakazu S. et al.,[35] related to their efforts on experimental study of bio-oil and bioslurry gasification.

- **Computational grid or mesh:** It is discrete performance of a geometry where surface area or volume of the computational domain is divided into polygonal (in 2D) or polyhedral (in 3D) with tessellation pattern to crate uniform or ununiformed cells. Mesh generation is a key feature responsible for the solution accuracy, rate of convergence-and computing time (CPU

time). Solution accuracy increase by refining the mesh at certain areas (increasing the number of cells per unit area) in order to improve mesh quality. Increasing the mesh quality also lead to a faster convergence rate as well as capturing possible phenomena such as boundary layer separation that may occur in fluid flow. However, the CPU time cost increases as the mesh is refined. Thus, the optimal mesh needs to be obtained by comparison between the desired solution accuracy and the suitable computation time.

- **Physical and chemical models:** Selection of physical and chemical phenomena depends on case study which may include, for example, the equations of motion, energy, turbulence model and species conservation as well as homogeneous and heterogeneous chemical reactions in single or multiphase flow. The multiphase flow can also be divided to Volume of Fluid (VOF), Mixture and Eulerian, models. Discrete Phase Model (DPM) is another option of CFD tools with particles tracking and its interactions in a flow field. However, in many studies the standard features of CFD code is not applicable, therefore, the user-defined function (UDF) which can be written in C programming language, customise and enhance the standard features of the code. Chapter 6 and 7 include the detail of physical and chemical models, employed in this study.

- **Material properties, boundary and initial conditions:** Specifying and checking material properties, boundary and initial conditions is an important part of problem definition. Figure 3-6 shows the sketch of the calculated fluidized bed gasifier and its boundary conditions in this thesis. At the inlet, gas velocity and temperature were specified. At the outlet, the total pressure at the exit was assumed to be atmospheric. At the wall, the normal component of the fluid velocity was set to be zero (no-slip wall condition) and the outer wall also was heated to maintain a constant temperature. For transient problems, the initial conditions are also defined. In this simulation the sands (with average diameter of 0.0002m) in the bed were packed initially with the volume fraction of 0.595 while the maximum packing is 0.63. Initially, the bed solid velocity was set to zero and the height of the bed settled considered 0.13m.

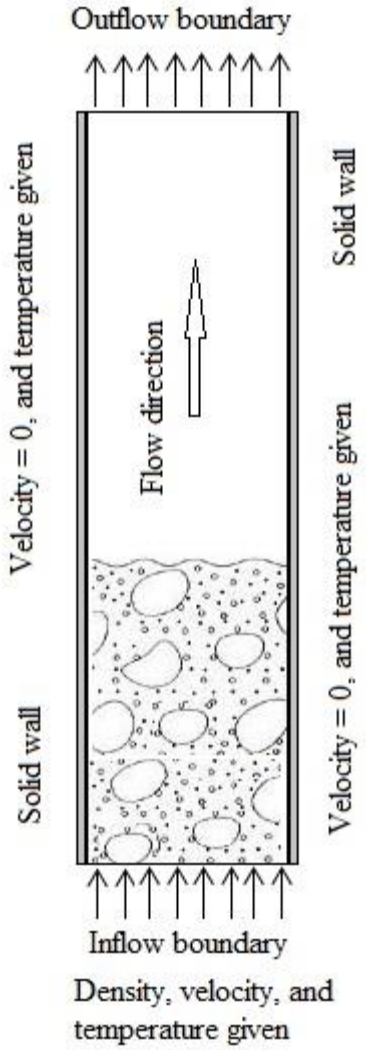

Figure 3- 6: Boundary conditions for the internal fluidized bed reactor

3.5.1.2 CFD solver

A numerical technique for solving the equations represent conservation of continuity, momentum, and energy as well as other transport equations based on the finite volume method which is a common approach used in commercially available CFD codes, including CFX, FLUENT, PHOENICS and STAR-CD. In this approach, instead of solving the continuous partial differential equations the governing equations are integrated over all the finite control volumes of the solution domain. The resulted equations convert to a system of algebraic equations (discretization) to apply iterative solution methods with successive approximations.

3.5.1.3 Post-processor

Post-processing supports the most commercial CFD codes with high performance capabilities of large and complex models through the numerous visualization and reporting tools. Some of its main features;

- Display geometry and mesh structure
- Display of contour plots, iso-surface, streamline, cut planes and victor plots.
- Display particle track
- Functionality such as performance of Maximum and minimum flow variables and its locations
- Model manipulation such as rotation and translation
- Dynamic result display by animation tool

3.5.2 Mathematical modelling of bio-oil and bioslurry steam gasification in fluidized bed reactor, using the ANSYS FLUENT CFD software

3.5.2.1 Hydrodynamics of gas-solid fluidized bed

The gas-solid Fluidized bed usually consists of a vertical cylinder containing a bed of granular material where gas is introduced in the bottom (suspends the solid particles) of cylinder as indicated in Figure 3-6. Hydrodynamics plays an important role in transferring phenomena taking place in fluidized bed reactor such as heat and mass transfer.[69, 70] Computational fluid dynamics (CFD) using Eulerian-Eulerian or Eulerian-Lagrangian approaches are key techniques used to describe the details of gas-solid hydrodynamics.[91]

In this thesis modelling hydrodynamics with unsteady state behaviour of a gas–solid fluidized bed reactor has been done by applying CFD Fluent code, considering Eulerian-Eulerian multiphase flow approach with relatively low computational cost which was revealed as a suitable model approach for fluidized bed reactor.[92, 93] In this approach the continuity and momentum equations apply for both phases with the equation of particles granular temperature. The Syamlal–O'Brien drag model

employed for gas-solid flow pattern in fluidized bed reactor as it can reasonably predict the hydrodynamic behaviour of gas-solid fluidized bed.[70]

3.5.2.2 Droplet trajectories, heat and mass transfer

The gas-solid flow fields in fluidized bed gasification reactor determined by applying the Eulerian - Eulerian approach (see Section 3.5.2.1) and the droplet flow field was examined by Eulerian - Lagrangian approach in which the fluid phase (the gas –solid flow) is treated as continuous and fuel droplets as discrete phase. Therefore, the droplet trajectory was considered through the use of discrete phase model (DPM) including interaction with the continuous phase in terms of momentum, heat and mass transfer.

ANSYS FLUENT use a combination of several laws (laws 1-7) for different particle type (Mass less, Inert, Droplet, Combusting, and Multicomponent) to model the heat and mass transfer between continuous and discrete phases. However, the above particle types cannot fit the modelling of bio-oil and bioslurry gasification in this study. Several customized codes (User-Defined Function) were developed to model heat and mass transfer as well as reaction rate due to interaction of droplets with continuous phase. The detail discussion is given in Chapter 6 and 7.

3.5.2.3 Droplet injection

As mentioned in previous section, the particle type and size distribution are applicable in the DPM model to recognize the discrete character of the particle phase in modelling flow. ANSYS FLUENT provide several types of injections (e.g. The Plain-Orifice Atomizer and The Effervescent Atomizer Model) with different defined classes of particle size distribution (e.g. uniform and the Rosin-Rammler distribution function). The Rosin-Rammler distribution function was considered in this study to determine mathematical function for droplet size in sprays. Chapter 5 to 7 provide more detail with results to present drop size distribution in terms of the cumulative frequency of mass distribution curve with the Rosin-Rammler format.

3.5.2.4 Turbulent model

The prediction of gas–particle turbulent flow is an essential part of fluidized bed reactor. ANSYS FLUENT provides a number of turbulent models (e.g. Spalart-

Allmaras model, $k-\varepsilon$ models, $k-\omega$ models, Reynolds stress models (RSM)) for different classes of problems. In the reactor system of this study the standard $k-\varepsilon$ model was employed with solving two separate transport equations to simulate mean flow characteristics for gas-solid turbulent flow. In this model two transport variable should be determined, i.e. the turbulent kinetic energy (k) and the turbulent dissipation (ε). Therefore, the turbulent velocity and length scales can be determined by solving the two separate transport equations with detail discussion reported in Chapter 6.

3.5.2.5 Model validation

For validation of the models developed in this work, a set of the experimental data of Masakazu S. et al.[35] under different operating conditions was used to compare the residuals from the model predictions and experimental data by graphical analysis of residuals. In addition, different types of plots provided information on the adequacy of different aspects of the model, i.e., the sensitivity studies of model parameters such as reactor temperature was studied to compare the overall trend of simulation results with experimental data, published in the literatures.

3.6 Summary

Diesel and biodiesel and their blends were selected as typical fuels to develop a measurement technique concerning droplets size, sprayed with pressure-swirl micro whirl atomizer. Bio-oil and bioslurry samples were then atomized using different types and sizes of nozzle to investigate the mean diameter and droplet size distribution at several operating conditions. The droplet size information of bio-oil and bioslurry were transferred to the Rosin-Rammler distribution function to determine mathematical function for droplet size in spray. The mathematical drop-size was employed for simulation part (see Section 3.5.2.3) where Lagrangian approach was used to simulate the bio-oil and bioslurry droplets injected in a fluidized bed reactor for syngas products via steam gasification using CFD Fluent code. The interaction of droplets and flow field (gas and bed material) as well as reaction rate of homogeneous and heterogeneous was considered by writing several UDF code. The fundamental understandings on the mathematical modelling of bio-oil and bioslurry steam gasification in a fluidized bed reactor were then achieved.

CHAPTER 4: DEVELOPMENT AND VALIDATION OF A MODIFIED METHOD FOR DROPLETS SIZE DISTRIBUTION MEASUREMENT†

4.1 Introduction

Substantial research efforts are being made to advance the technologies for the production, storage, transportation and utilization of liquid biofuels,[94, 95] including bioethanol,[96] biodiesel[97-99] and biofuels derived from biomass pyrolysis and refining [19-21]. Spray and atomization characteristics of liquid fuels are important considerations for the applications (such as combustion) of these fuels. Particularly, the determination of droplet size distribution and average mean diameter of a spray is essential.

There are two categories of methods developed for measuring spray droplet size distribution and average mean diameter.[25] One category is based on optical methods[26-29] such as light scattering techniques. These methods have respective advantages and disadvantages[30] and require the establishment of sophisticated and expensive optical systems. The other category of is the mechanical approach that deploys a suitable solid surface (such as glass) to allow droplets strike on surface. Images were then taken and analysed for droplet size measurement. Therefore, the mechanical method has advantages of simplicity, low cost, visibility and reliability. However, the mechanical method suffers from several drawbacks. Firstly, as permanently pressed, the droplets need to be corrected by a correction factor to obtain real diameters of the droplets.[31] Conventionally, a constant correction factor is used, e.g. 0.5 for clean glass slide.[25] This is a problem because the correction factor is known to be dependent on fluid properties (such as viscosity, surface tension etc.) and droplet size.[25] Second, there are overlapping issues among droplets upon striking on the surface. Thirdly, the effect of potential evaporation on droplet size analysis is

largely unknown. Lastly, the accuracy of droplets size analysis in past studies was largely limited by the low resolution of the photographs.

This study has developed an improved mechanical method for measuring the droplet size of the sprays of liquid fuels and the method has been validated using diesel, biodiesel and their blends. The novelties of method are four fold: i) adoption of a flexible correction factor for a droplet based on its fluid properties and size; ii) design of the spray to minimize droplets overlapping; iii) deployment of high-resolution camera which enables the analyses submicron droplets photographed on glass slide and iv) estimation of the effect of droplet evaporation.

4.2 Development of the Method for Measuring Droplets Size

4.2.1 Minimisation of droplets overlapping in measuring droplets size

In the present work to reduce drop overlapping and also increase the collection efficiency, a series of experimental investigation have been done for different fuels at different temperature to find out the minimum distance of receiver (glass slide) from nozzle exit where more increasing in distance from nozzle won't be resulted in considerable change of spray characteristics.

A series of images captured at different distance between 105 and 220 mm by 25 mm intervals from spray nozzle exit at different temperatures at 20, 30 and 40℃. The raw images clearly indicate that the merging of many overlapping fuel droplets deposited on the receiver reduces by increasing distance. It shows after distance of 105-125 mm depend on fuel temperature, the change of reduction drops diameter can’t be observed by visual inspection, therefore, beyond this observation, image analysing has been done to find out where is the minimum distance of glass slide from nozzle exit to minimize coalesced droplets.

Figure 4-1 shows the mean diameters of diesel fuel at different temperature resulted from at least 50,000 drops analysing in each distance including all overlapped drops which make larger drop size range and bigger mean diameter. Depend on the drops range of interest and its application the most common choices for mean diameter are D_{32} and D_{43} while for representative diameter are $D_{0.1}$, $D_{0.5}$ and $D_{0.9}$. As it is clear from Figure 4-1 the coalesced droplets less influenced on droplets mean diameters

from distance above 155-175mm at temperatures of 40 and 20℃ respectively. Therefore, to reduce overlapping issue all experiment has been done at 20 cm distance of glass slide from nozzle exit.

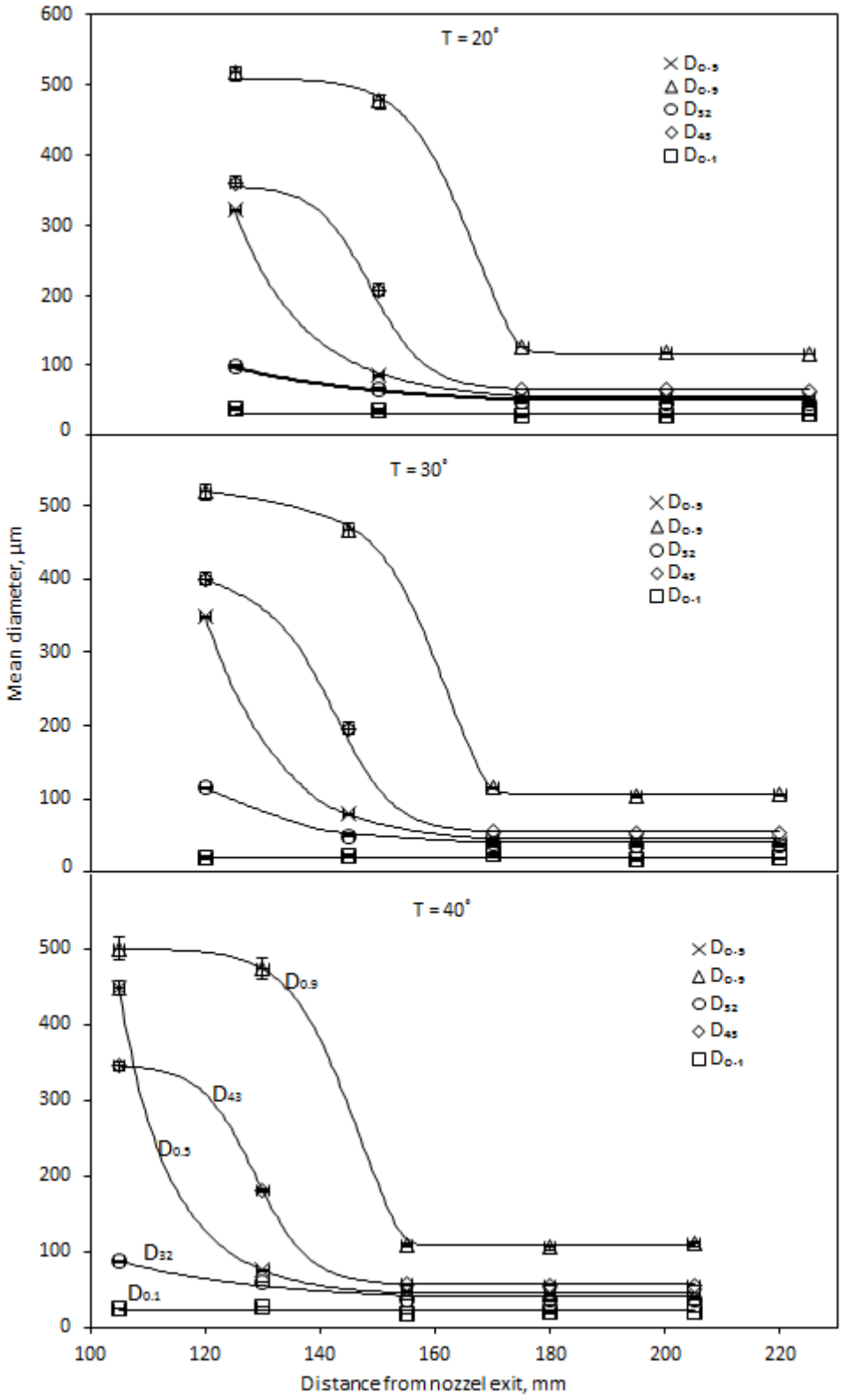

Figure 4- 1: Comparisons of several mean diameters at different distance of nozzle exit for pressure swirl atomizer with the cone angle of 70˚

The other strategy to minimizing droplet overlapping is to determine whether droplets in image analysis should be considered to be individual droplets or overlapped droplets. To qualify overlapped drops, visual inspections have been done for many spray tests to find out what parameter should be considered to evaluate individual and overlapped drops. A series of photography were made for droplets collected on glass slide for any given set of physical conditions and extensive study has been done on roundness of droplets for both single and overlapped drop to find out critical roundness which more reduction arises from overlapping problem.

Therefore, to determine the critical roundness, two methods employed as shown in Figures 4-2 and 4-3. The first one as indicated in Figure 4-2 the critical roundness less than 0.75 considered to be more likely from overlapping problem. Two different drops joint together and made a clear bond while roundness of 0.75 or above indicates individual droplet. The second method to quantify the critical roundness was shown in Figure 4-3. This figure shows the SMD reduce slightly until reach to 0.75 and then reduce sharply by increasing the degree of roundness. In this way the percentage of drops excluded from calculation increased sharply by considering the roundness larger than 0.75 which make considerable error from elimination of large parts of droplet in calculation. Therefore, with above considerations all data represented in this paper, include analysing of drops with roundness above 0.75. The result shows over 96% of total droplets lies above 0.75.

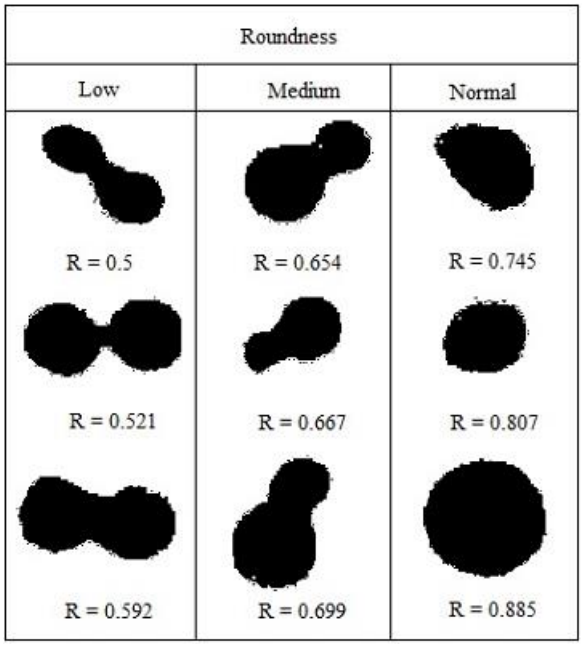

Figure 4- 2: Roundness of Biodiesel fuel for different shape of droplet

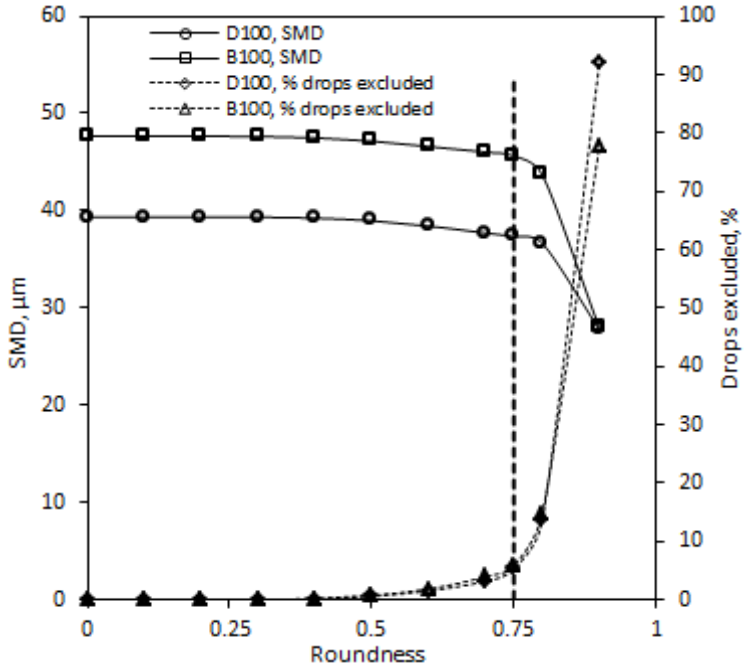

Figure 4- 3: Critical roundness of biodiesel and diesel fuel

4.2.2 Correction for the shapes of droplets

Estimating shape correction factor is important to find out real diameter of drops before settle on the surface of the glass slide. The shape correction factor depends on fuels properties and nature of solid, make different contact angle. Measuring the

contact angle of different fuels and the developing the sessile drop technique to find out the shape correction factor have been done in this study.

The effective correction factor formula ($f = r/a$) defined to estimate drops diameter before contact the glass slide by using sessile drop technique as illustrated in Figure 4-4. The problem of the sessile drop, that is a drop of liquid at rest on a horizontal surface with the effect of gravity being balanced by surface tension, is classical, and numerical solutions are known for more than a century.[100] A variety of methods have been used in order to obtain the shape of sessile drops which fit the experimental data. Briefly three approaches that have been discussed in literatures are:

- Assume that the drop has the shape of a spherical cap
- Numerically integrating the Laplace–Young equation, using axisymmetric drop shape analysis (ADSA) method (see Figure 4-4, a)
- Model approximation of contact angle, that discussed by Jeffrey S. Allen

When drop is small enough the spherical cap approach may be a good approximation. However, the spherical cap is valid when gravitational effect is neglected. Furthermore, the negligible gravitational influence on the surface shape occurs when $\beta \ll 1$ as shown in Table 4-1. As summarized in this table, the analytical solution for calculating contact angles from sessile drops developed by Jeffrey S. Allen[101] is valid for any Bond number, i.e., any drop size. However, it is valid when the contact angle is less than 30°.

To estimate the shape correction factor related to sessile drop characteristics, the equations of contact angle by Jeffrey S. Allen[101] rearranged to obtain the radius of the contact angle and then substitute in the effective correction factor formula as proposed in this study and summarized in Table 4-2 in different parameter ranges.

The same contact angle for different size of drops of same liquid, placed on the same solid surface (glass) is main approximation of this study. The accuracy of this assumption back to work of Amir fazli et al.[102] which examined the accuracy of $ADSA-TA$ algorithm (Axisymmetric Drop Shape Analysis-Two-Drops) and conclude that it is a viable technique to measure surface tension and contact angle for

wetting ($\theta < 90°$) as well as non-wetting ($\theta > 90°$) liquids which based on the same contact angle.

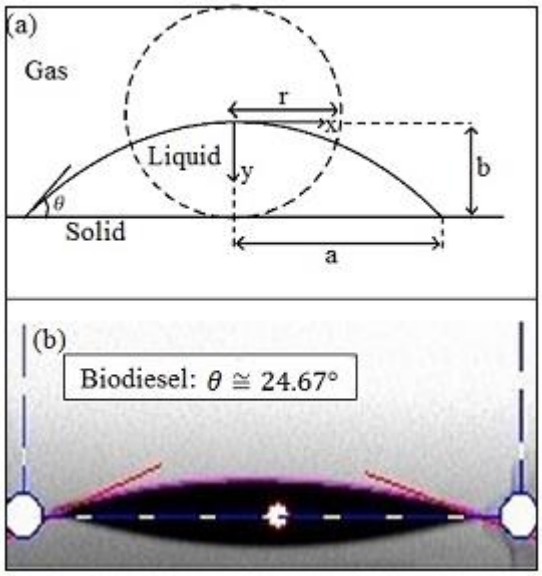

Figure 4- 4: **a)** Schematic of an axisymmetric drop on a wetting substrate($\theta < 90°$), where a is the radius of the contact line, b is the height of the drop and θ is the contact angle of the liquid drop at the three phases contact line. **b)** A sample of measuring contact angle

Fuels properties and drop contact angle for different type of fuels need to be measured as explained above in case of shape correction factor calculation. The results of density, surface tension, dynamic and kinematic viscosity presented in Table 4-3 and Figure 4-5 respectively. The comparison has been done for fuel properties from diesel to biodiesel and their blends as well.

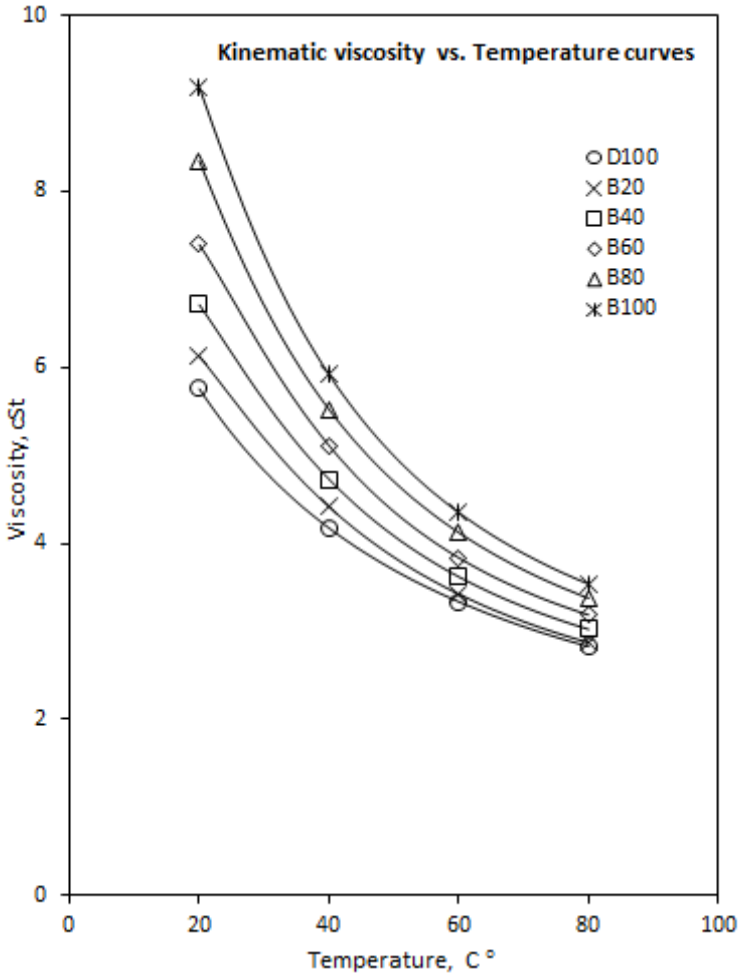

Figure 4- 5: Kinematic viscosity of fuels at different temperature

The result of contact angle for different type of fuels is presented in Table 4-4. In this study all models listed in Table 4-1 are valid because the contact angles of all fuels are less than 30°. The radius of contact lines calculated with assuming that the modified bond number ($\beta = a/\sqrt{\sigma/((\rho_l - \rho_v)g)}$ is equal to one to find out what is the maximum of drop contact line radius if model case number I be applicable. The maximum radius of contact line measured in every test are far less from maximum predicted above, therefore, the correction factor of all fuels calculated with model case number I and the result presented in Table 4-4.

Table 4- 1: Model approximations of contact angle[101] at small and large β and Spherical cap solution where modified bond number, β is defined as: $\beta \equiv a/Lc$ and capillary length, L_c defined as: $L_c = \sqrt{\sigma/(\rho_L - \rho_v)g}$

Parameter range	Static contact angle	Accuracy	Dimensionless shape factor Ω
θ<30◦ and β< 1	$\theta \approx \tan\theta \cong \frac{4V}{\pi a^3}$	At $\beta = 1$, the error is approximately 4%. But when β = 0.5, the error has decreased to 1% and the error is less than 0.1% for β = 0.1	$\Omega \cong 4$
$\theta < 30°$ and $\beta > 4$	$\theta \approx \tan\theta \cong \frac{V}{\pi a^2 Lc}(\frac{\beta}{\beta - 3/2})$	At $\beta = 4$, the error is approximately 5.02%. But when β = 6, the error has decreased to 1.67% and the error is less than 0.5% for β = 10. Therefore, the Ω approximation becomes sufficiently accurate at $\beta = 4$.	$\Omega \cong \frac{\beta^2}{\beta - 1.5}$
$\theta < 30°$ and $\beta > 25$	$\theta \approx \tan\theta \cong \frac{V}{\pi a^2 Lc}$	The maximum error is 5.94% when $\beta = 25$. Therefore, the Ω = βapproximation only becomes sufficiently accurate when $\beta > 25$.	$\Omega \cong \beta$
When volume of the drop is small and $\beta \ll 1$	$\frac{b}{a} = \frac{1 - \cos\theta}{\sin\theta}$	The shape of a sessile drop may be assumed to be that of a spherical cap (SC) when gravitational effects may be neglected. Shanahan [103]reports that when $\beta^2 \gg 1$ the spherical cap shape becomes inaccurate.	$\Omega_{SC} = \frac{3\ \sin^4\theta}{\cos^4\theta - 3\cos^2\theta + 2\cos\theta}$

Table 4- 2:Model approximate of drop correction factor when θ < 30◦ at different value of modified bond number $f = \frac{r}{a}$,V = $\left(\frac{4}{3}\right)\pi r^3$ and$f = \frac{\sqrt[3]{3V/(4\pi)}}{a}$

Case number	Radius of wetted area on substrate[101, 102]	Parameter range	functional relationship	Proposed Correction factor
I	$a \cong \sqrt[3]{4V/(\pi\theta)}$	θ<30◦ and β< 1	$f = f(\theta)$ $\theta = \theta(V, a)$	$f \cong \sqrt[3]{3\theta/16}$
II	$a \cong \sqrt{\beta V/(\pi\theta L_C(\beta - 3/2))}$	$\theta < 30°$and $\beta > 4$	$f = f(\theta, V, L_C)$ $\theta = \theta(V, a, L_C)$	$f \cong \frac{\sqrt[3]{3V/(4\pi)}}{\sqrt{\beta V/(\pi\theta L_C(\beta - 3/2))}}$
III	$a \cong \sqrt{V/\pi\theta L_C}$	$\theta < 30°$and $\beta > 25$	$f = f(\theta, V, L_C)$ $\theta = \theta(V, a, L_C)$	$f \cong \frac{\sqrt[3]{3V/(4\pi)}}{\sqrt{V/\pi\theta L_C}}$
IV	$a = \frac{b \sin\theta}{1 - \cos\theta}$	When volume of the drop is small and $\beta \ll 1$	$f = f(\theta, V, b)$ $\theta = \theta(a, b)$	$f = \frac{(1 - cos\,\theta)\sqrt[3]{3V/(4\pi)}}{b\,sin\,\theta}$

Table 4- 3: Density, surface tension and dynamic viscosity of different type of fuels

	Characteristic of fuels at different temperature, ℃													
	Density (kg/m³)			Surface tension (mN/m)			Dynamic viscosity (cP)							
Fuels	20	30	40	20	30	40	20	25	30	40	50	60	70	80
Diesel	0.821	0.816	0.812	26.07	25.65	25.23	4.71	4.28	3.82	3.39	2.95	2.67	2.39	2.22
B20	0.835	0.829	0.822	24.48	23.93	23.38	5.1	4.65	4.19	3.63	3.17	2.77	2.53	2.29
B40	0.842	0.838	0.835	25.75	25.08	24.42	5.64	5.09	4.64	3.95	3.4	2.98	2.66	2.45
B60	0.855	0.851	0.847	26.70	25.97	25.24	6.31	5.68	5.11	4.33	3.65	3.2	2.85	2.62
B80	0.864	0.858	0.853	29.40	28.60	27.79	7.19	6.37	5.67	4.71	4	3.48	3.09	2.8
Biodiesel	0.876	0.871	0.865	32.36	31.35	30.34	8.02	7.04	6.25	5.12	4.32	3.72	3.21	2.98

Table 4- 4: Calculation of correction factor using the model approximate of drop correction factor

	Contact angle at different temperature of 20,30,and 40 ℃, $(\theta°)$			Correction factor where $\beta < 1\ or a < a_m$, (f)			Maximum drop contact lines radius where $\beta = 1$, $(a_m, \mu m)$		
Fuel	20	30	40	20	30	40	20	30	40
Diesel	21.06	20.83	20.59	0.41	0.408	0.407	1800.6	1791.1	1781.5
B20	20.17	19.86	19.56	0.404	0.402	0.4	1729.6	1717	1704.1
B40	20.88	20.51	20.13	0.409	0.406	0.404	1767.2	1747.6	1727.7
B60	21.42	21.01	20.59	0.412	0.41	0.407	1785.4	1764.9	1744
B80	22.92	22.47	22.02	0.422	0.419	0.416	1864.1	1844.1	1823.6
Biodiesel	24.58	24.01	23.45	0.432	0.428	0.425	1941.8	1917.2	1892

4.2.3 Corrections for evaporation

The evaporation process of a spherically symmetric droplet could be generally described by using D^2-law[34] ($D^2 = {D_0}^2 - \lambda t$) which explains droplet size depletion against time. Rearrangement of the D^2-law leads to the formula (${D_0}^2 = D^2 + \lambda t$) for finding the initial drop diameter of fuels over time *t*, where λ is

$$\lambda = \frac{4Sh\rho_c D_v}{\rho_d}(\omega_{A,s} - \omega_{A,\infty}) \tag{4.1}$$

The calculation λ in Equation 4.1 depends on reliable estimation of Sherwood number. In this way, one commonly used empirical result is the Ranz - Marshall Correlation[104] (Equation 4.2) that corrects the spherically symmetric vaporization rate with relative velocity of droplets in surrounding gas.

$$Sh = 2 + 0.6\ {Re_r}^{0.5} Sc^{0.33} \tag{4.2}$$

In above equations $\omega_{A,s}$ and $\omega_{A,\infty}$ are mass fraction of species A at droplet surface and free stream respectively. D_v and ν also are diffusion coefficient, and kinematic viscosity of the mixture at the film conditions. In addition, Re_r, Sh and Sc are famous dimensionless groups known as relative Reynolds number, Sherwood number and Schmidt numbers. The diffusion coefficient of fuel in air (D_v) in Equation 4.1 can be predicted by using the semi empirical correlation of Fuller et al.[105] (Equation 4.3).

$$D_v = \frac{10^{-7} T^{7/4}}{P[{(\sum v)_A}^{1/3} + {(\sum v)_B}^{1/3}]^2} \sqrt{\frac{1}{M_A} + \frac{1}{M_B}} \tag{4.3}$$

Where D_v, T, P, M_A and M_B are in m^2/sec, $°K$, total pressure in atmospheres and Molecular weight of the binary system A+B respectively. In addition, $(\sum v)_A$ and $(\sum v)_B$ are molecules diffusion volumes which can be calculated from atomic diffusion volumes.

The next variable in Equation 4.1 is the mass fraction of species A at droplet surface ($\omega_{A,s}$), dependent on the vapor pressure or equilibrium vapour pressure of fuels and hence on the fuel temperature. The Figure 4-6 shows that the vapour pressure of diesel[106] and biodiesel[107] fuels which remains very low near room temperature and

increased up to critical temperature. For biodiesel/diesel blends the Raoult's law which assumes ideal solution used to predict the fuel vapour pressure of mixtures. Biodiesel have less vapour pressure than diesel fuel,[108] therefore, at low temperatures the reduction of drop diameter due the evaporation is minor.

The above explanation introduced in case of calculation of λ in the D^2-law. In this equation the time travelling of droplets should be estimated as well. Measuring drops time travelling depends on the size-velocity of droplets to find out real time travelling for different particle size. However, this study limited to this measurement and the spray tip penetration over time used instead to find out average velocity. In this case the FASTCAM high speed camera with 6000 frame per second employed to capture the average time travelling of fuels from nozzle exit to glass slide which located at 20 cm distance from nozzle exit. The average time travelling for different fuels estimated between 0.0185 (see Figure 4-7) and 0.0197 sec from diesel to biodiesel.

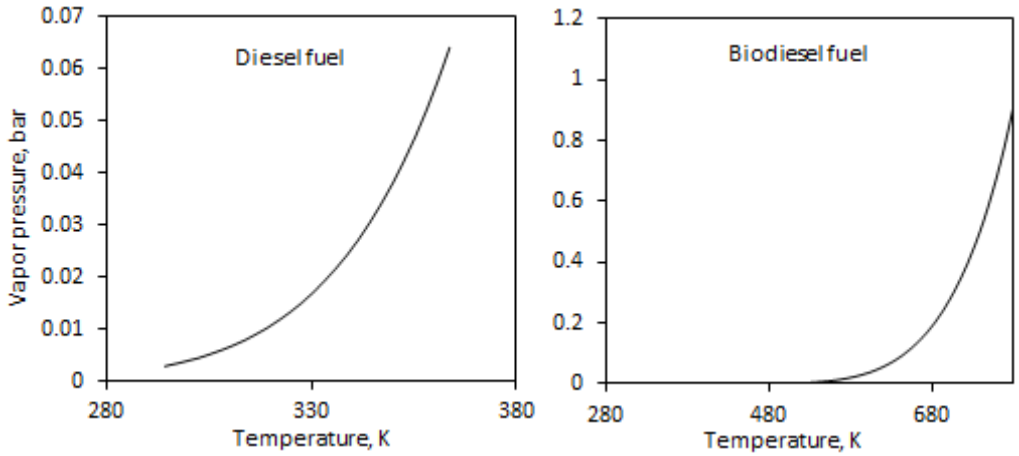

Figure 4- 6: Vapor pressure of diesel and biodiesel fuels at different temperatures

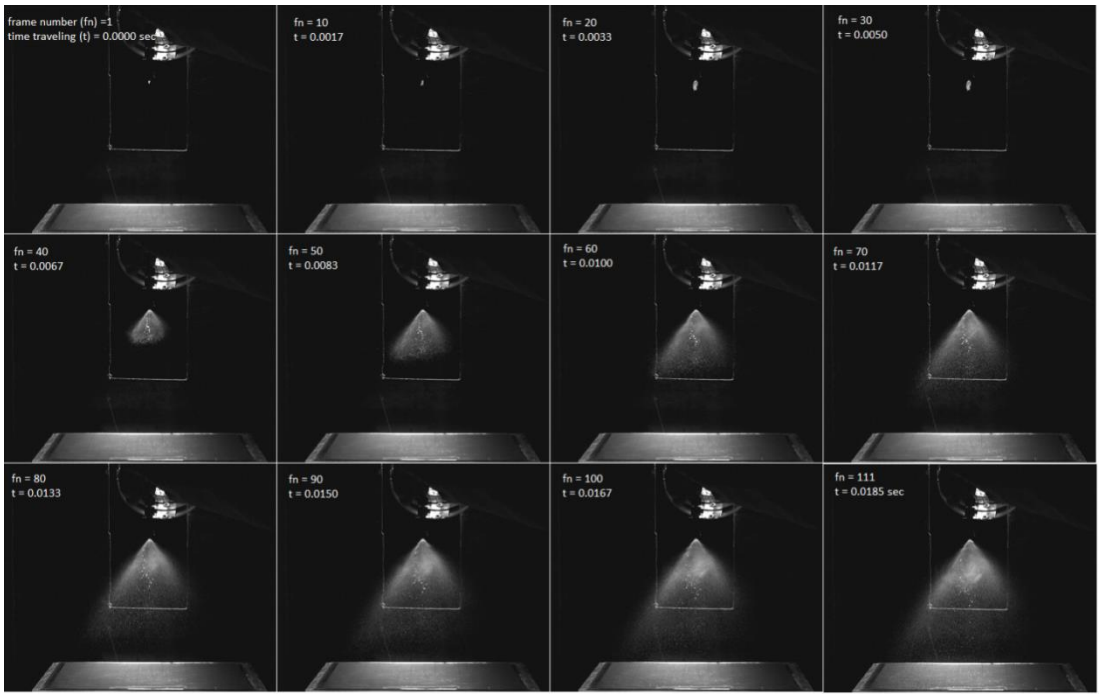

Figure 4- 7: 12 samples out of 111 frames captured for atomisation of diesel fuel at room temperature by pressure swirl atomizer, using the FASTCAM high speed camera with 6000 frame per second

The initial diameters of individual droplets predicted by estimating both, the average time travelling and λ in D^2-lawand then calculating the SMD which will be discussed in the following section. The result shows the SMD increased between 0.42 and 0.74 percent for diesel fuel from 20 to 40℃. Although the temperature of fuels in this study is low between 20 and 40℃, the attention need for liquid at higher temperature to prevent the error of measuring drops diameter.

4.3 Validation of the Method for Measuring Droplets Size

4.3.1 Analytical calculation

The next step after refining droplets is presentation of drop mean diameter. The most widely used measure of interest drops mean diameter in evaporation and combustion application is Sauter Mean Diameter (SMD or D_{32}). Many correlations depend on different condition and atomizers have been developed to calculate the SMD as an extensive value to describe the quality of atomization.

Therefore, comparisons between the SMD of biodiesel-blended diesel fuels are made between experimental results in this study and the well-known published correlation[109] for a pressure-swirl atomizer. The published[109] given below are based on extensive measurements (using Malvern particle size analyser) on different nozzle sizes and spray cone angles for wide range of liquid properties.

$$\mathrm{SMD} = 4.52\left(\frac{\sigma\,\mu_l^2}{\rho_a \Delta P_l^2}\right)^{0.25}(\mathrm{t}\,\cos\theta)^{0.25} + 0.39\left(\frac{\sigma\,\rho_l}{\rho_a \Delta P_l}\right)^{0.25}(\mathrm{t}\,\cos\theta)^{0.75} \qquad (4.4)$$

Suyari and Lefebvre[110] recommend the following correlation for calculation of film thickness in final orifice.

$$\mathrm{t} = 2.7\left[\frac{\mathrm{d_o FN}\mu_l}{(\Delta P_l \rho_l)^{0.5}}\right]^{0.25} \qquad (4.5)$$

where FN is flow number (unit: $\mathrm{m^2}$) and$\mathrm{FN} = \dot{m}/(\Delta P_l \rho_l)^{0.5}$, SMD, σ, μ_L, ρ_a, ΔP_l, t, θ, denote spray Sauter Mean Diameter, surface tension, liquid dynamic viscosity, injection pressure differential across nozzle, film thickness in final orifice, and spray cone half angle in μm, $\mathrm{kg/s^2}$, $\mathrm{kg/m.\,s}$, $\mathrm{kg/m^3}$, Pa, m,and degrees respectively. The physical quantifies, ρ_l, $\mathrm{d_o}$, and $\dot{m}$, are liquid density, discharge orifice diameter, and flow rate in $\mathrm{kg/m^3}$, m, and kg/s, respectively.Equation 4.5 encompassed within the ranges of viscosity $1 < \mu_L < 18$ and surface tension $0.027 < \sigma < 0.0734$ in (cS) and ($\mathrm{kg/s^2}$) respectively.

Experiments were conducted at room temperature (20℃) and atmospheric pressure as an ambient condition. The injection pressure, the orifice size and fuel flow rate, were, 10 bar, 0.825 mm and 250-300cm^3/min respectively. Also three different fuel temperatures of 20, 30 and 40℃ were chosen and result reported.

4.3.2 Comparison analytical calculation with experimental result

Figure 4-8 presents the SMD of diesel, biodiesel and their four blends at different temperature of 20, 30, and 40℃. In this figure the diesel and biodiesel have the smallest (34.99 μm) and the largest (45.6 μm) estimated SMD at 40℃ and 20℃ respectively. Accordingly, the SMD increased by increasing the biodiesel in blend due to changing the fuel properties. In this figure estimation of SMD divided into three categories. One category is based on analytical calculation as discussed in

previous section. The other category is based on experimental result, considered critical roundness; evaporation correction and also different shape correction factor depend on different fuel properties at different temperature which developed in this work. The last category is based on experimental result with no correction for overlapped drops (the critical roundness) and evaporation. In addition in this category the shape correction factor considered equal to 0.5 for glass materials.[25]

In Figure 4-8, if the critical roundness for overlapped drops, the correction shape factor and the evaporation correction for different type of fuels considered in calculation (second category) , the SMD from experimental method become more close to analytical calculation (first category). Therefore, the experimental results with different standard deviation of SMD between 0.3 and 1.1μm are in a good agreement with analytical calculation with average relative error at 1.16%.

In comparison as Figure 4-9 shows, if overlapped drops which is controlled by critical roundness (equal to 0.75) and correction factor of 0.5 considered in calculation with non-evaporation condition (third category) the average relative error increase to 13.81% which might be not acceptable. Therefore, the result shows the developing of shape correction factor, critical roundness and evaporation correction are essential to be considered when mechanical method employs for drops size measurement, particularly when this method aimed to be used for high different type of fuels.

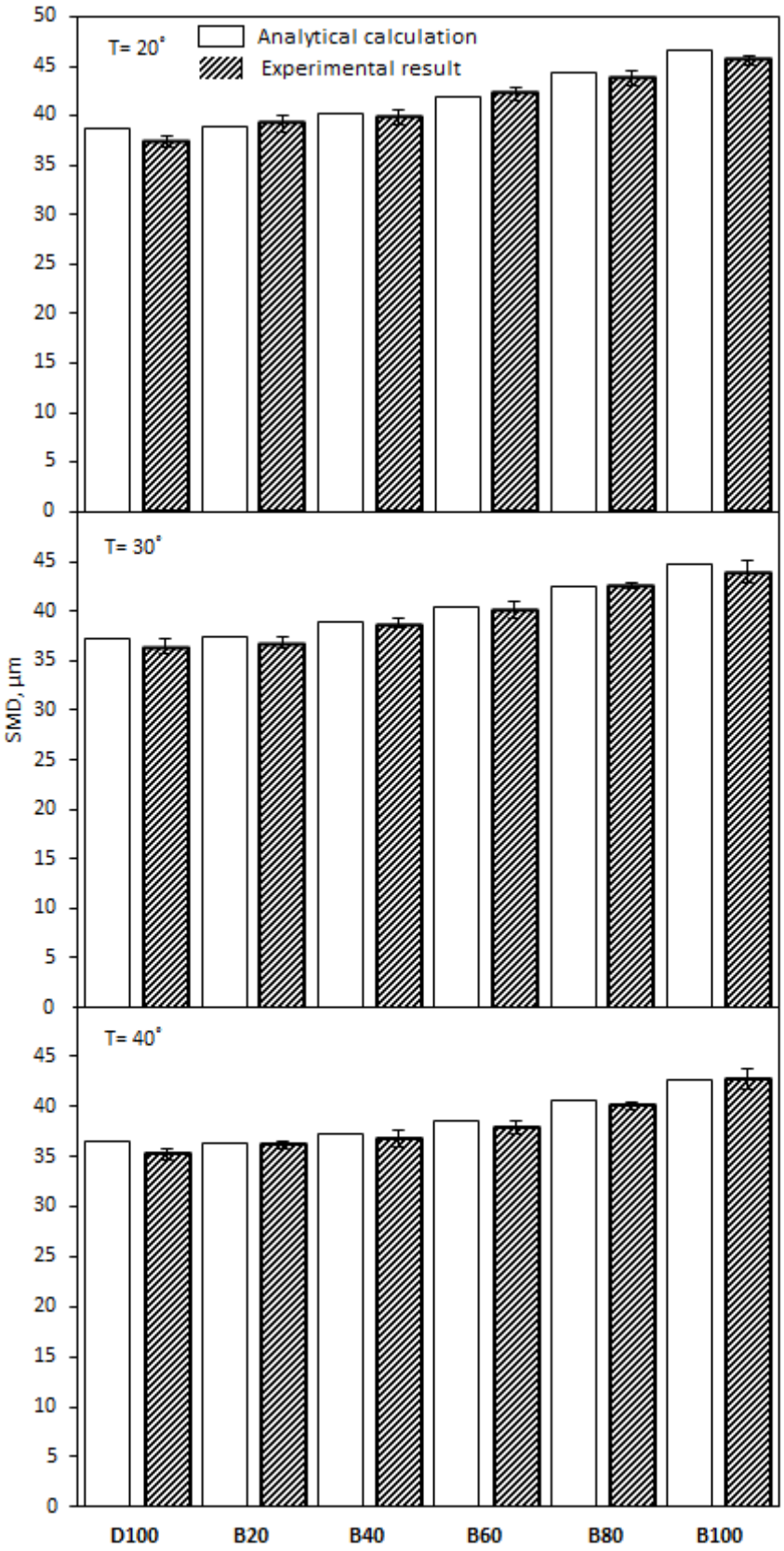

Figure 4- 8: Comparison of SMD, using analytical calculation and experimental results for diesel, biodiesel and their blends at different temperature

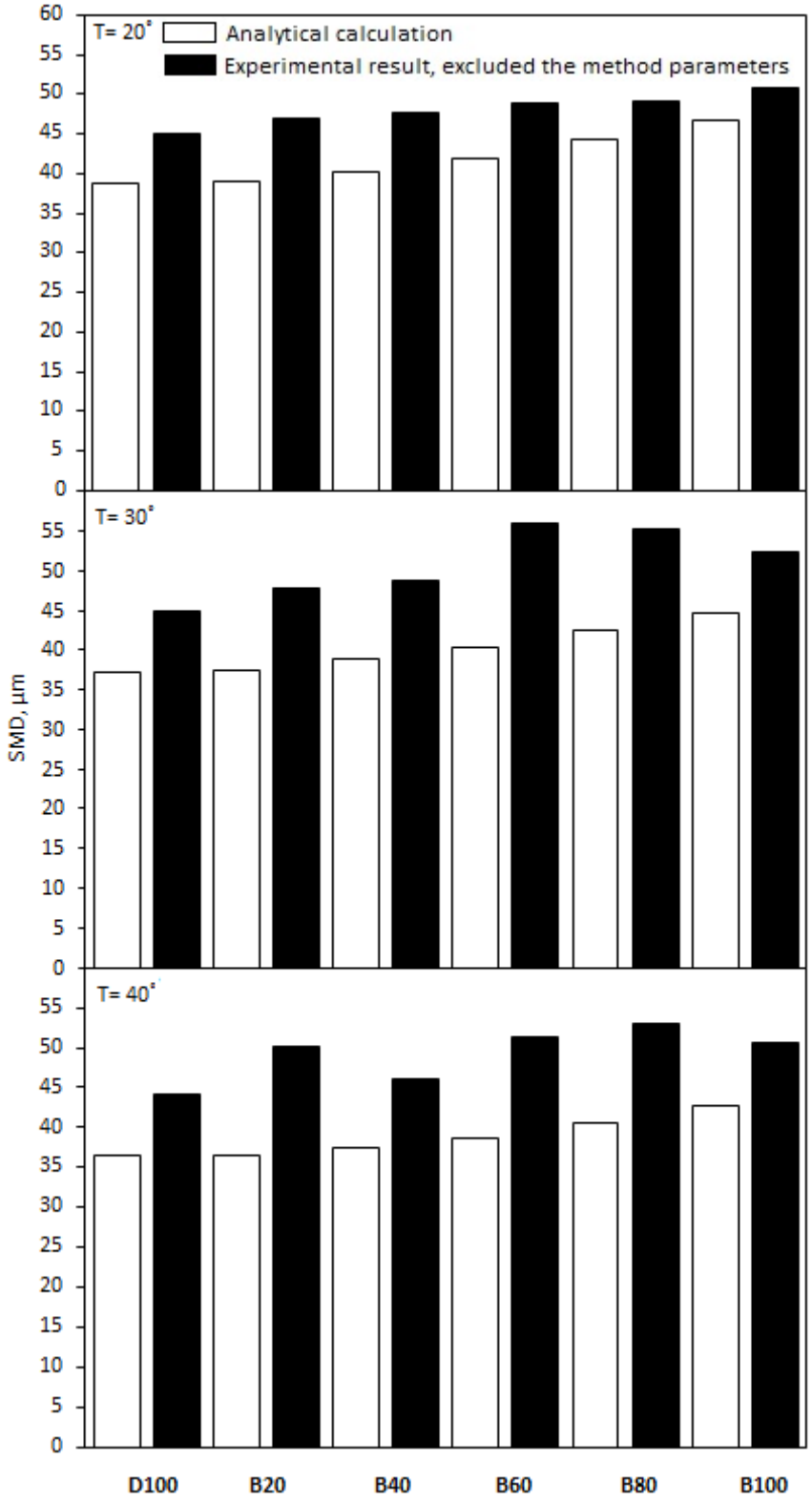

Figure 4- 9: Comparison of SMD, using analytical calculation and experimental results (excluded overlapped droplets, critical roundness, shape correction factor, and droplet evaporation) for diesel, biodiesel and their blends at different temperature

4.4 Droplet size distribution of diesel, biodiesel and their four blends

In addition to the Sauter Mean Diameter the frequency of volume distribution curve for different type of fuels presented to have comparison of different data scattering on classified distribution curve. Frequency and cumulative frequency of ordinate values of drops in several alternative ways (such as drop volume, mass, number and surface) may be used to plot distribution curve depend on their application. Frequency distribution curve is useful to present how affect different conditions of experiment on size distribution while cumulative frequency distribution is useful tools of determining mathematical distribution function for further application such as simulation. Therefore, in this work the frequency of volume distribution curve employed to have comparison of drop size distribution for different fuels.

The overall drop size distribution of D100, B20, B40, B60, B80 and B100 plotted, using frequency of volume distribution curve as shown in Figure 4-9 at temperature of 20℃. It's clear that the droplet size distribution transfers to the right side of graph where the spray accumulated with larger drops by increasing the blending ratio from B20 to B100

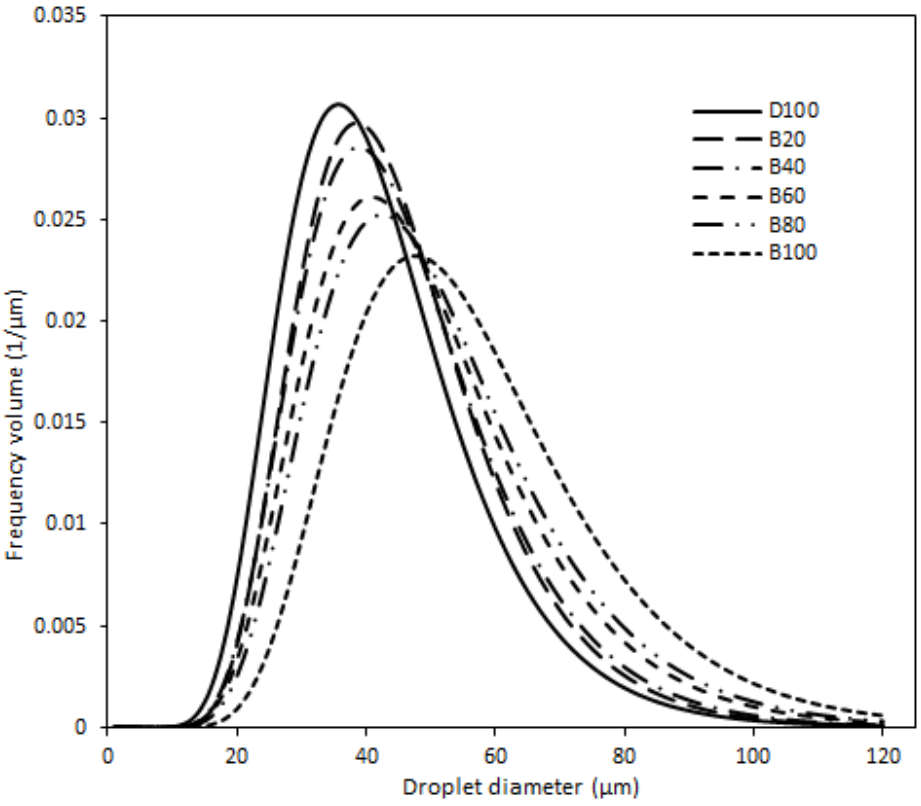

Figure 4- 10: Frequency volume distribution, using pressure-micro whirl atomizer

4.5 Summary

An improved mechanical method has been developed and validated for measuring spray droplets size. The drop coalesce was studied and described by the aperture time as used to control the amount of drops on glass slide and its location during the injection from the nozzle exit. In this way, the effect of overlap drops on $D_{0.9}$ becomes more pronounced when comparison have been done along the downstream position while $D_{0.1}$ is nearly constant. Also critical roundness defined in case of eliminating furthermore overlapped droplets on glass slide. The correlation for the shape correction factor developed which is applicable for wide range of fuel properties. To reduce the evaporation effect on initial drops diameters calculation have been done for all individual drops and the initial drops diameter estimated. The results from diesel, biodiesel and their blends show that the method can be successfully applicable to various fuels.

CHAPTER 5: SPRAY CHARACTERISTICS OF BIO-OIL AND BIOSLURRY BY IMPACT AND TWIN-FLUID ATOMIZERS†

5.1 Introduction

Substantial research efforts are being made to advance the technologies for the production, storage, transportation and utilization of liquid biofuels.[94, 95] In particular, bio-oil and bioslurry (mixture of fine biochar particles with bio-oil) derived from biomass fast pyrolysis are potentially attractive alternatives and becoming an increasingly important for future energy security and sustainable development.[5, 14, 19-21]It is well known that the size of droplets after spray is an important factor in stationary applications (combustion or gasification) of bio-oil and bio-oil/biochar slurry fuels.[22, 23, 111] Fundamentally determined by the atomization characteristics of these fuels, the spray process involves complex fluid dynamics and transport phenomena,[24] which have critical impacts to the exchanges of mass, momentum, and energy between different phases.

As bio-oil and bioslurry fuels have the tendency of plugging during atomization.[112] Two types of atomizers may be used. One type is impact atomizer that has no whirl vanes or internal partsand is commercially available. This type of atomizer was used because of its applicable for fuels with potential plugging issue and a working system where no gas injection is allowed by the nozzle. The other is the twin-fluid atomizer, which was used in previous studies.[23, 42, 47, 111] The twin-fluid atomizer allows the user to control the flow rate for ensuring proper spray distribution regardless of flow rate. The low flow rate and proper atomization of gas atomizing system make the twin-fluid atomizer suitable for laboratory reactors. When air cannot be used for a working system, an inert gas (e.g. N_2 or Ar) can be used under controlled pressure and flow conditions.

As discussed in section 2.2.1.2 of Chapter 2, the most widely used of mean diameter in mass transfer calculation is the Sauter Mean Diameter, which many correlations

have been obtained for different type of atomizers, relating to the fuel properties, geometric parameters, and the atomizer operating conditions.[25] Such correlations, mostly, have not been tested against the bio-oil and bioslurry fuels that are now of growing interest to the researchers.

While the use of impact atomizer and twin-flow atomizer was reported previously for various liquid fuels, there has been no systematic study on the spray characteristics of bioslurry fuels. Nor has been there developed empirical correlations for modeling thermochemical processing of bioslurry fuels. The main objectives of this study are to investigate the spray characteristics of bio-oil and bioslurry using both impact and twin-fluid atomizers and then to develop correlations of atomization for modeling applications.

5.2 Droplet measurement technique

For measuring droplet size distribution of bio-oils and bioslurry, using the modified mechanical method developed in Chapter 4, it was found the optimal distances from the atomizer exit (see Section 4.2.1) to the glass slide are 130-150 mm and 70-90 mm for the impact and twin-fluid atomizers respectively. Furthermore, in this technique estimating shape correction factor from fuel physical properties is important to find out real diameter of drops before strike to solid surface. In this way the contact angle of bio-oil A with viscosity of 15.22E-2 Pa.s and bio-oil B with viscosity of 7.53E-2Pa.s were measured; 25.11° and 25.07° at pressure and temperature close to ambient. In addition, the average contact angle of bio-slurries A and B were measured 25.17° and 25.33° respectively.

5.3 Spray of bio-oil using impact atomiser

In many calculations of mass transfer and flow processes it is convenient to work only with mean or average diameters instead of the complete drop size distribution. Mugele and Evans[32] suggested a list of mean diameters with their application. The most widely used is the Sauter Mean Diameter (SMD or D32), which is proportional to the ratio of the total liquid volume to the total droplet surface area in a spray.[24] This definition of mean drop size has special significance for heat and mass transfer applications, such as spray drying and the combustion of liquid fuel sprays.[25]

Figures 5-1 to 5-7 shows the measurement results of SMDs for bio-oil A and B, injected by impact atomizers at various operating conditions. In these figures the effects of variables: (1) bio-oil flow rate and injection pressure. (2) The size of atomizer as indicated by flow number. (3) Liquid properties such as viscosity on SMD were reported. Figure 5-1indicates the SMD of bio-oil A at different liquid flow rate with other relative importance of nozzle flow number, and liquid differential pressure. In this figure, for a given pressure, an increase in the liquid flow rate (via increases in nozzle orifice diameter) leads to an increase in SMD, due to the increase in diameter of bio-oil jet as it leaves the orifice and impacts the needle shape (obstructed in the orifice outlet of impact atomizer) with lower efficiency. The relative velocity between bio-oil and surrounding gas plays an essential role due to turbulence properties of liquid stream in case of disintegration into waves, ligaments, and drops.[94] The liquid stream with higher relative velocity impacts the needle shape with higher kinetic energy, and therefore, achieves smaller droplet size distribution. Figure 5-1also shows a lower injection pressure led to the change in SMD having a higher sensitivity to bio-oil flow rate. Therefore, the injection pressure of 2.17 MPa has the highest change of SMD around 32.9% when the flow rate increase from 0.003 to 0.006 kg/s, while the 4.96 MPa injection pressures has the lowest change of SMD around 16.3%. It is clear that, a minimum injection pressure is required to achieve effective spray due to the essential disturbance required for jet instability and disintegration.

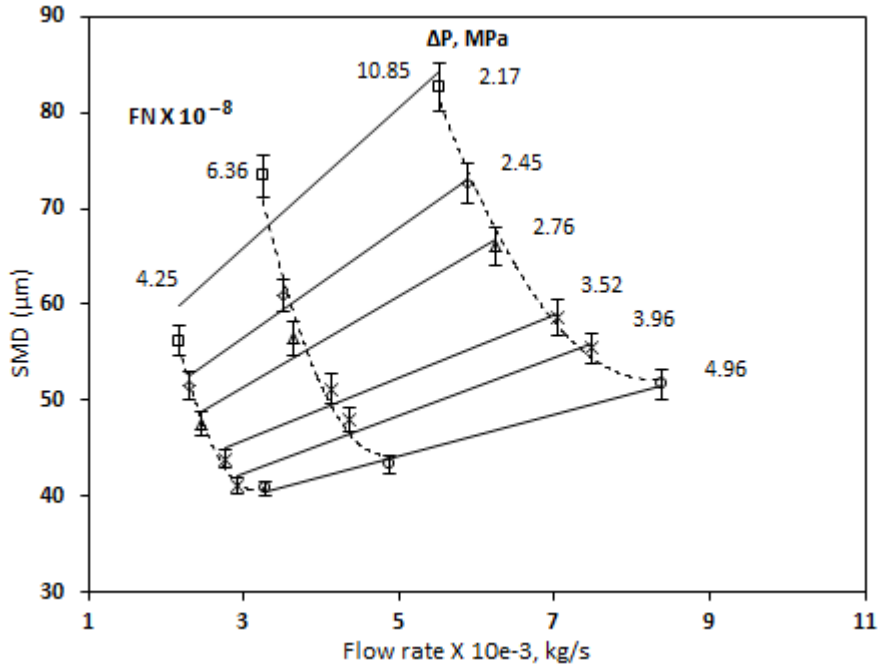

Figure 5- 1: SMD of bio-oil A at different liquid flow rate, nozzle flow number, and liquid pressure differential

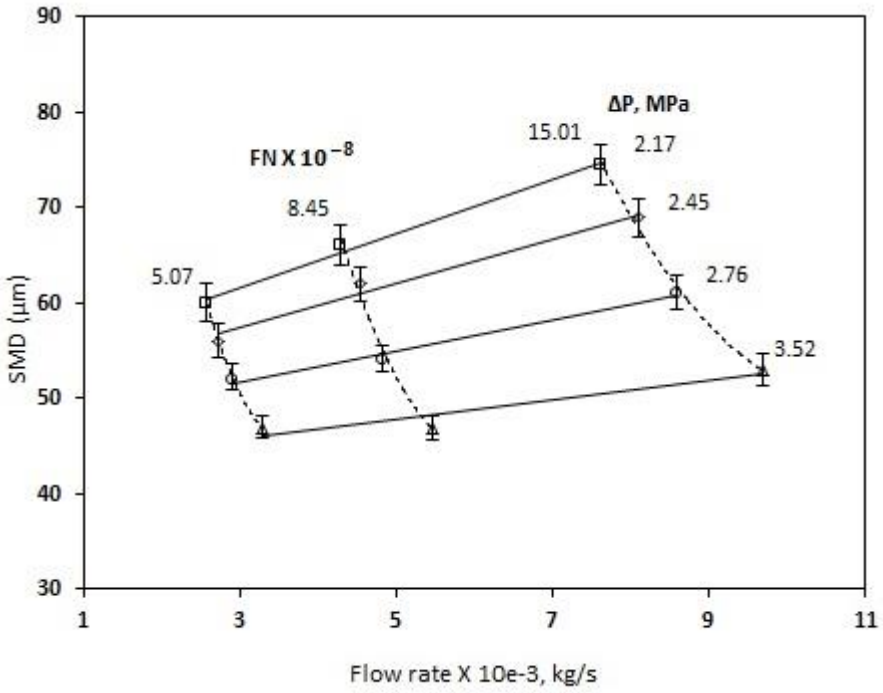

Figure 5- 2: SMD of bio-oil B at different liquid flow rate, nozzle flow number, and liquid pressure differential

A similar trend has been observed for bio-oil B as illustrated in Figure 5-2. However, at same pressure (e.g. 2.17 MPa); the effect of liquid flow rate on SMD is less sensitive due to change in properties of bio-oil. It is also noted that the maximum injection pressure for bio-oil B was reduced to 3.52 MPa while it was 4.96 MPa for bio-oil A (see figure 5-1).

Figures 5-3 and 5-4 further show the SMD of bio-oil A and B at different pressure for given flow numbers respectively. Figure 5-3showsan increase in atomization pressure leads to a reduction in the SMD of bio-oil sprays at a constant flow number. This is reasonable because at a constant flow number, the exit liquid velocity (fluid's kinetics energy) of a jet with higher injection pressure (fluid's potential energy) is higher than that from lower injection pressure. The relative velocity between bio-oil and surrounding gas plays an essential role in atomization due to enhanced turbulence of liquid stream in case of disintegration into waves, ligaments, and drops. A jet with a higher exit liquid velocity has more kinetics energy impacting the needle of atomizer, resulting in better spray performance hence reduced SMD.

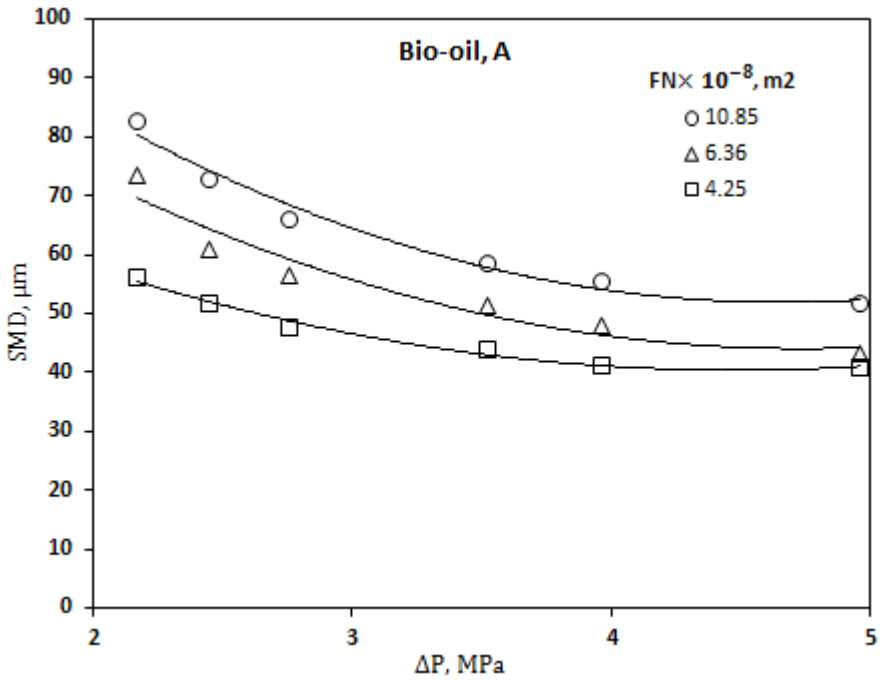

Figure 5- 3: SMD of bio-oil A at different pressure for given flow numbers between 4.25E-8 and 10.85E-8 m^2

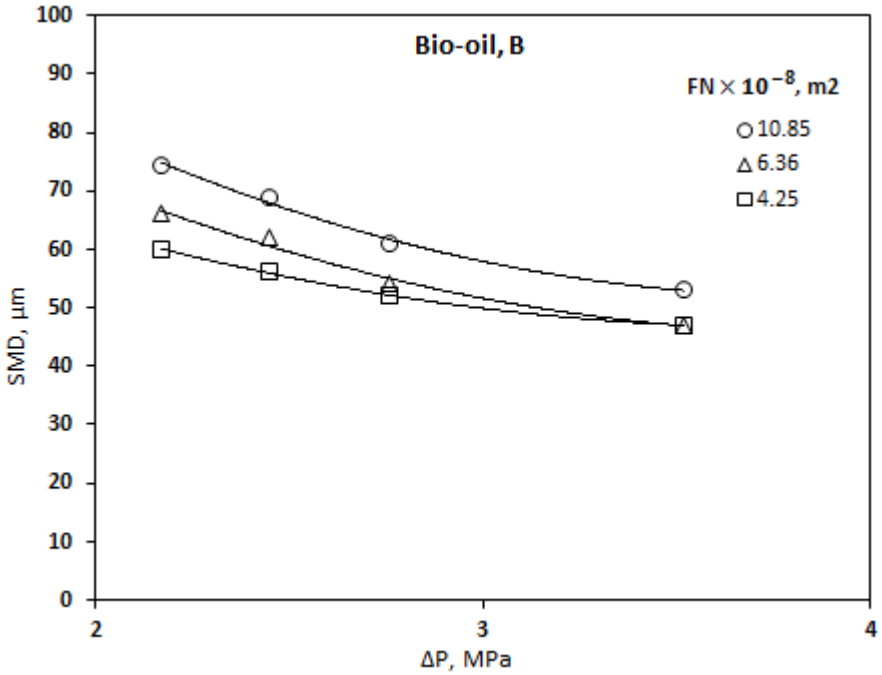

Figure 5- 4: SMD of bio-oil B at different pressure for given flow numbers between 4.25E-8 and 10.85E-8 m^2

Figures 5-5 and 5-6 shows that at a constant atomization pressure, an increase in spray flow number leads to an increase in the spray SMD. This is because for a given nozzle, mass conservation dictates that a reduction in the orifice diameter (corresponding to a reduction in flow number) leads to an increase in the exit velocity hence a decrease in the spray SMD.

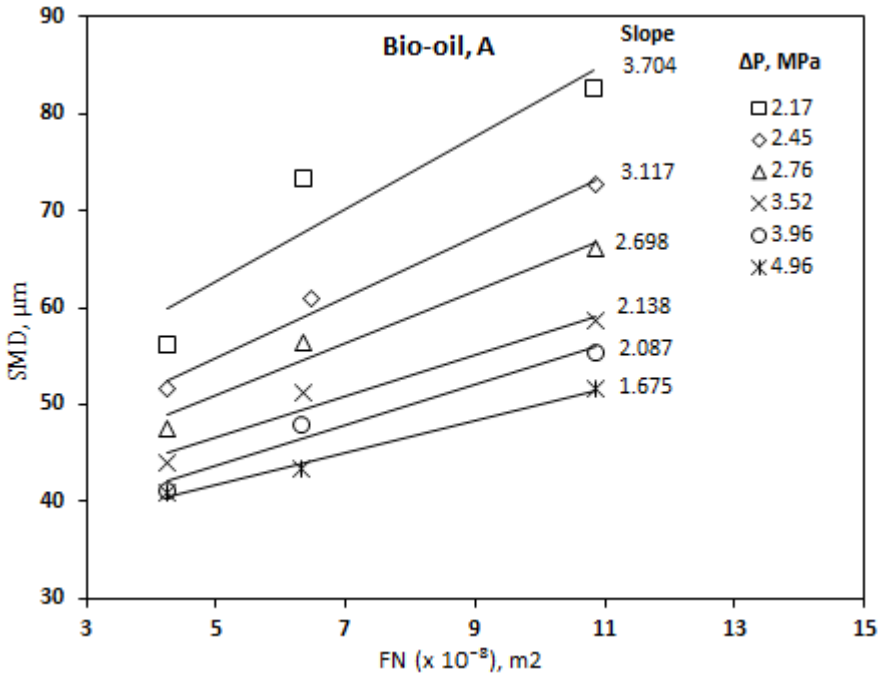

Figure 5- 5: Influence of spray flow number for bio-oil A on SMD for a given pressure between 2.17 and 4.96 MPa

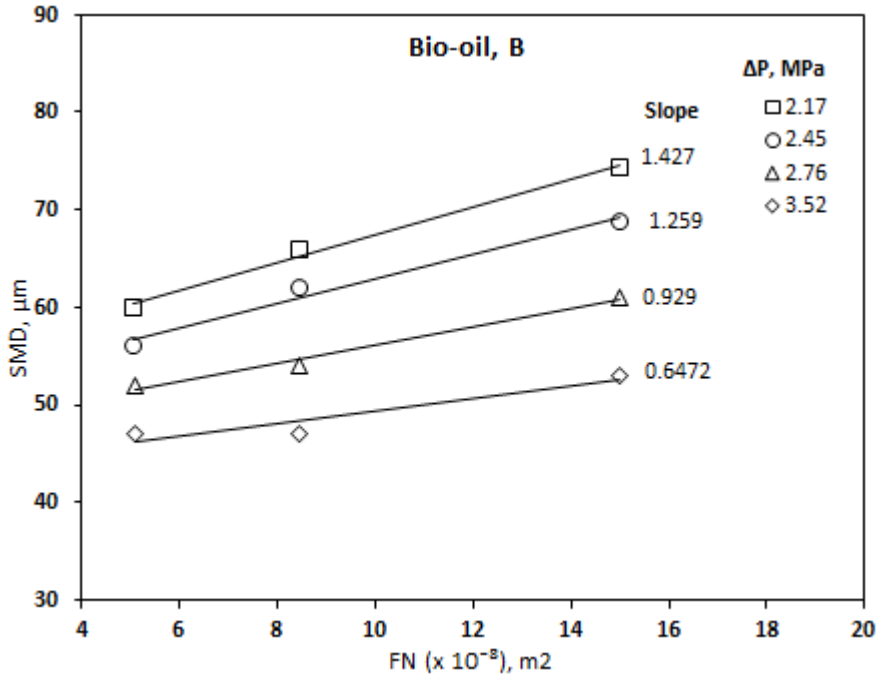

Figure 5- 6: Influence of spray flow number for bio-oil B on SMD for a given pressure between 2.17 and 3.52 MPa

Figure 5-7 illustrates the effect of increasing pressure on SMD for two viscosities of bio-oils. As shown in this figure, the spray SMD of bio-oil A is considerably higher than that of bio-oil B because the viscosity of bio-oil A (~0.1522 pa.s at 21 °C) is much higher than that of bio-oil B (~0.0752 Pa.s at 21 °C). This is expected because the action of liquid with a higher viscosity in atomization would have experienced lower fluctuation in liquid jet (tendency to be damped out) where the high level of turbulence is necessary to achieve enough disturbances during brake up liquid jet into droplets. In other words, more external energy (e.g. more injection pressure) is needed for spray. This is clearly shown by the experimental data, e.g. to achieve the spray SMD of 58.6 μm an injection pressure of 2.8 MPa is required for bio-oil B but 3.5 MPa for bio-oil A.

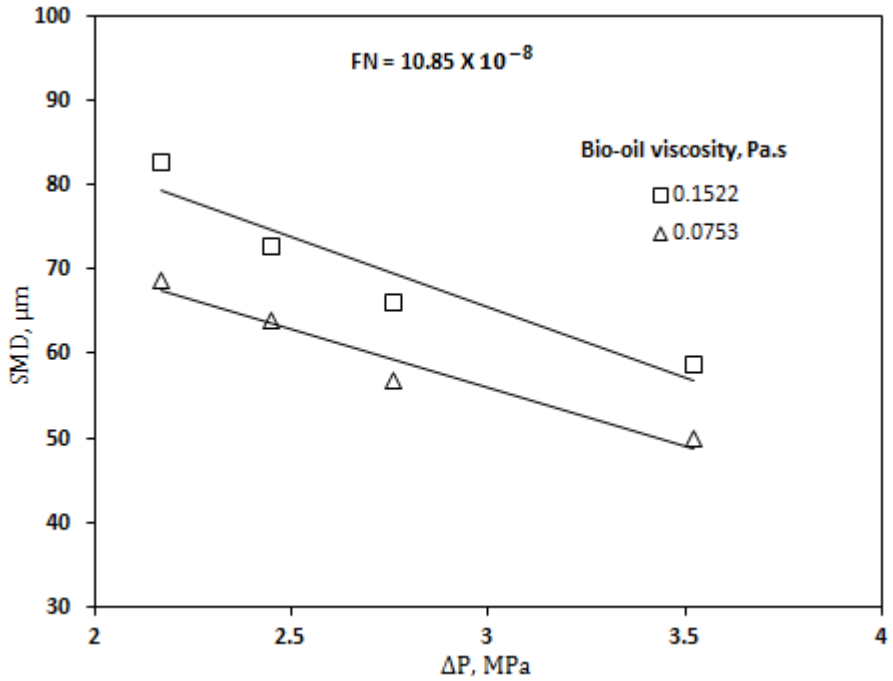

Figure 5- 7: Influence of viscosity on SMD for bio-oil A and B for a given flow number and different nozzle pressure of 7.53E-2 and 15.22E-2 Pa.s

5.4 Spray of bioslurry using impact atomiser

In this study many experimental data were obtained for bioslurry with char loading levels of 5, 10, and 15% (the upper limit of 15% to avoid plugging issue). However,

in order to keep the total length of this paper within reasonable bounds, some typical results illustrated in Figure 5-8. This Figure shows the SMDs for bioslurry A5 at different: (1) Bioslurry flow rate. (2) Injection pressure. (3) Flow number. Figure 5-8a illustrates that an increase in flow rate leads to an increase in the spray SMD at a constant nozzle pressure. It is also clear that the spray SMD strongly depends on the injection pressure of bioslurry but the changes in spray SMD becomes less sensitive to the change in pressure at a lower injection pressure.

Figure 5-8b shows an inverse relationship between SMD and injection pressure. At the constant flow number, the SMD were greatly affected by the increase in injection pressure of bioslurry into lower SMD while it was less for bio-oil (see Figure 5-3). This figure also indicates a higher injection pressure not led to the significant change in SMD at different flow numbers. Therefore, at high injection pressure the reduction in flow number is more effective way to reduce the SMD of bioslurry with Impact atomizer. Figure 5-8c further shows the influence of spray flow number on SMD at constant pressure where, an increase in nozzle flow number leads to an increase in the SMD. Finally, the effect of different char loading level in bio-oil on SMD was considered in following section after developing a correlation for bio-oil and bioslurry due to different rang of experiments.

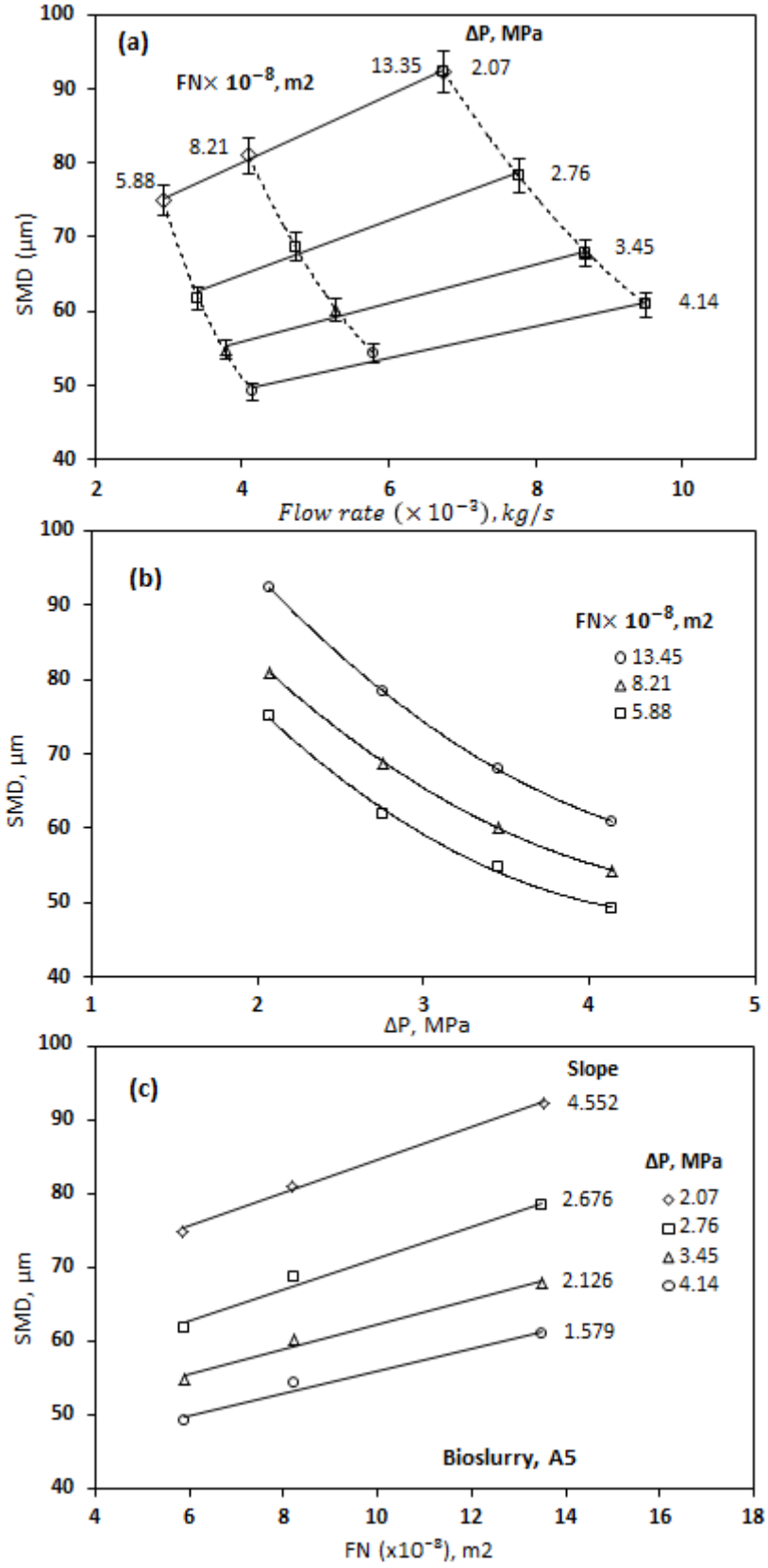

Figure 5- 8: SMD of:(a) bioslurry A5 at different liquid flow rate, nozzle flow number, and nozzle pressure; (b) bioslurry A5 at different pressure for given flow numbers; and (c) bioslurry A5 at different spray flow number for given pressures.

5.5 Empirical Correlation of SMD for bio-oil and bioslurry spray using impact atomizer

Empirical correlations are important for developing models of bio-oil or bioslurry thermochemical processing such as combustion or gasification. Suggested by Lefebvre,[25] the choice of variables for empirical correlation include liquid properties (such as density, viscosity etc.) and atomization operating conditions. For bioslurry spray, the bio-oils have similar surface tension ($\sigma_A = 37.2$ and $\sigma_B = 36$ mN/m) so that the empirical correlation for the spray SMD can be written as $\mathrm{SMD} \propto \mu^a\, \mathrm{FN}^b \Delta \mathrm{P}^c$. The values of the exponents a, b and c can be determined based on the data obtained from experiments where only one of μ, FN and ΔP is varied with the rest two are kept constant. For example, if FN is the variable we have $\mathrm{SMD} \propto \mathrm{FN}^b$ so that the experimental data can be plotted in the form of Ln SMD vs. Ln FN. The average slope of resulting lines gives the value of b. Similar methods can be applied to obtain the values of a and c. Considering the data presented in Figures 4 and 5, the values of a, b and c can be determined as 0.13, 0.26 and -0.58, respectively. Therefore, we have

$$\mathrm{SMD} = \mathrm{A}_0 \times \mu^{0.13} \mathrm{FN}^{0.26} \Delta \mathrm{P}^{-0.58} \tag{5.1}$$

The value of the constant term can then be determined used the experimental data, yielding $\mathrm{A}_0 = 3.175\mathrm{E}7$. The correlation for spray SMD of bio-oils with impact atomizer can be obtained as

$$\mathrm{SMD} = 3.175\mathrm{E}7 \times \mu^{0.13} \mathrm{FN}^{0.26} \Delta \mathrm{P}^{-0.58} \tag{5.2}$$

where $\mathrm{SMD}, \mu, \mathrm{FN}, \text{and } \Delta \mathrm{P}$ denote spray SMD, bio-oil dynamic viscosity, flow number, and injection pressure in $\mu\mathrm{m}, \mathrm{Pa.s}, \mathrm{m}^2$, and Pa respectively. Figure 5-9 shows that the correlation is a good fit with the experimental data in this study.

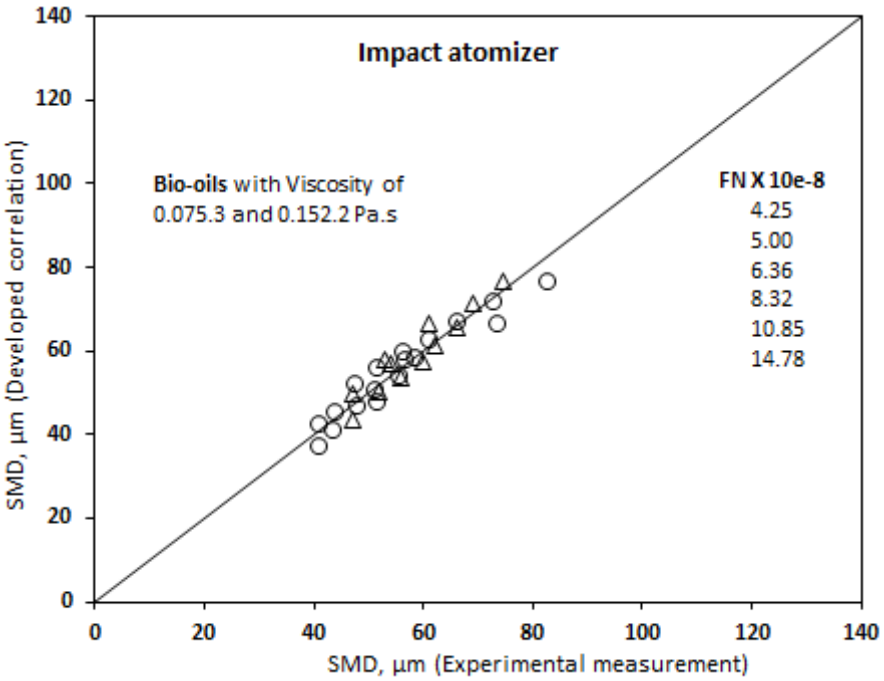

Figure 5- 9: Comparison between experimental data and prediction with Equation 5.3 for bio-oil A and B

In the second part of the empirical analysis, the influence of char in two types of bio-oils on target correlation was investigated. This empirical correlation may be modified for bioslurry atomization, considering the presence of biochar in bioslurry via the introduction of an additional term, in the form of:

$$\mathrm{SMD} = 3.175\mathrm{E}7\mu^{0.13}\mathrm{FN}^{0.26}\Delta\mathrm{P}^{-0.58}\ (\mathrm{Ln}\ (\mathrm{wt}_{\mathrm{char}} + \mathrm{e}))^{\mathrm{d}} \qquad (5.3)$$

where ($\mathrm{wt}_{\mathrm{char}}$) denote the percentage of char in bioslurry and e is an irrational and transcendental constant. Based on the experimental data, it can be derived that $\mathrm{d} = 0.22$. Therefore, a unified SMD correlation can be derived for the spray SMDs (µm) of both bio-oil and bioslurry

$$\mathrm{SMD} = 3.175\mathrm{E}7{\mu_{\mathrm{bio-oil}}}^{0.13}\mathrm{FN}^{0.26}\Delta\mathrm{P}^{-0.58}(\ln(\mathrm{wt}_{\mathrm{char}} + \mathrm{e}))^{0.22} \qquad (5.4)$$

where SMD, µ, FN and ΔP denote Sauter Mean Diameter, bio-oil dynamic viscosity, flow number, and injection pressure in µm, Pa.s, m^2 and Pa, respectively, and $\mathrm{wt}_{\mathrm{char}}$ is the weight percentage of char in bioslurry ($\mathrm{wt}_{\mathrm{char}}$= 0 for bio-oil).

The above equation clearly shows the degree of variables contribution on SMD by four factors: liquid viscosity, flow number, injection pressure, and char percentage in bio-oil. Of these four factors, the most important quantitatively is injection pressure which a small change in injection pressure leads to a large change in SMD. Furthermore, the spray mean diameter (SMD) is directly proportional to the bio-oil viscosity ($\mu_{bio-oil}$), flow number (FN), and the char percentage($\mathrm{wt_{char}}$), and also inversely proportional to the injection pressure with power of 0.579.

As shown in Figure 5-10, the unified correlation can predict the spray SMD reasonably well for both bio-oil and bioslurry. It is noted that an increase in the char percentage in bioslurry leads to an increase in the errors between the prediction and the experimental data. Nevertheless, the correlation is applicable for bioslurry spray with up to15 wt% char loading.

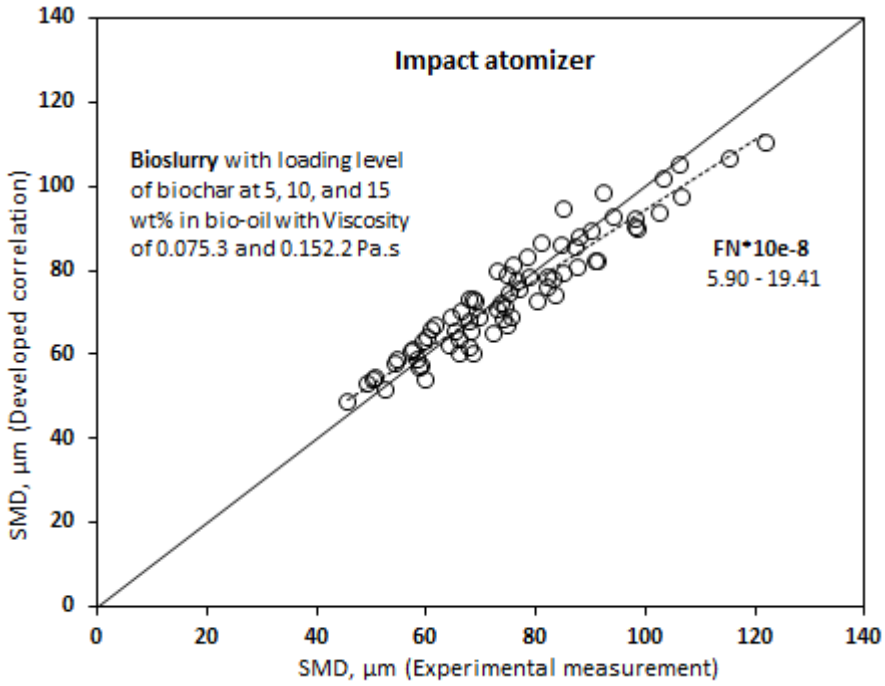

Figure 5- 10: Comparison between experimental data and prediction with Equation 5.4 for bioslurry A5, A10, A15, B5, B10, and B15at different operating conditions by Impact atomizer.

Figure 5-11 further compare the spray SMDs of the bioslurry fuels (A and B) at various char loading levels of 0, 5, 10, and 15 wt% when the impact atomizer was operated at a constant injection pressure.

The results clearly show that an increase in char loading increases the spray SMD significantly. This is largely due to the non-Newtonian and viscoelasticity behaviour of bioslurry with pseudo-plastic characteristics which exhibit a high apparent viscosity at a high shear rate.[113] The restoring force associated with elastic behaviour of bioslurry results in the increase in atomization energy.

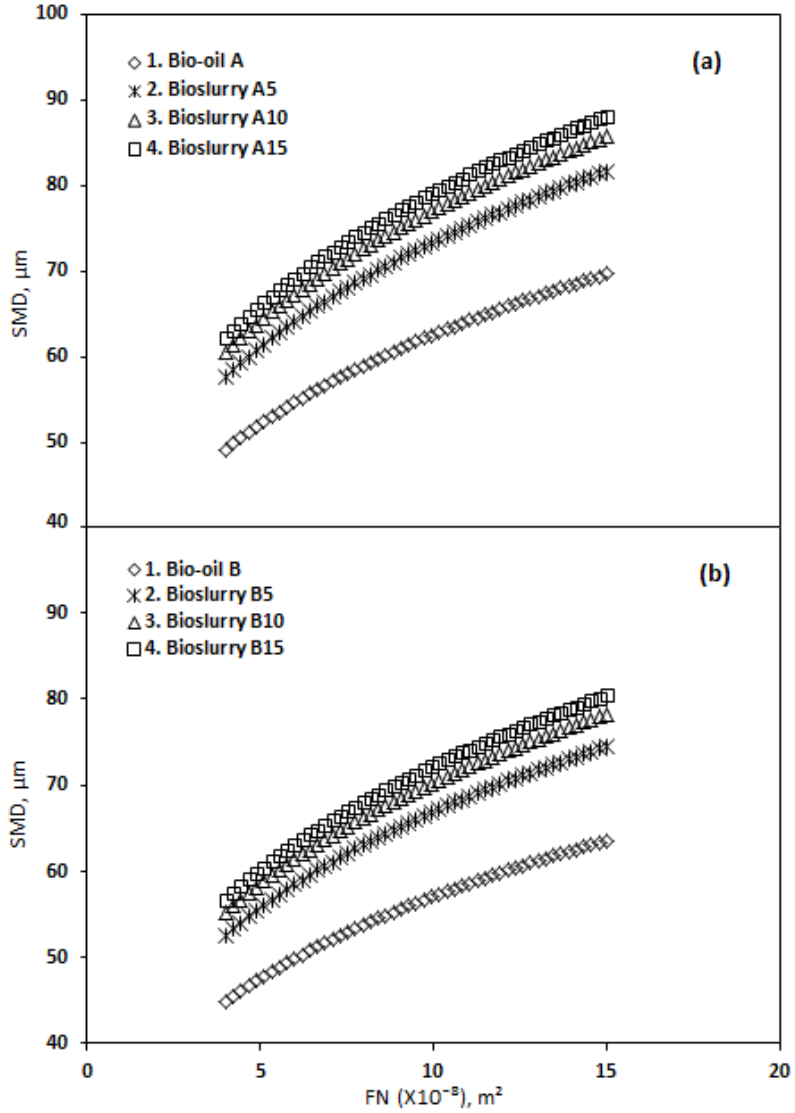

Figure 5- 11: Influence of char loading on SMD (predicted by Equation 5.4) for : (a) Bio-oil and bioslurry A; and (b) Bio-oil and bioslurry B with different loading level of biochar at 5, 10, and 15 wt% by Impact atomizers at different flow number while injection pressure keep constant at 3 MPa.

5.6 Spray of bio-oil and bioslurry using twin-fluid atomizer

Experimental studies are conducted in sprays produced by twin-fluid atomizer where a gas-assisted atomizing system for injection of bio-oil and bioslurry, employed at different operating conditions. This section provides some typical results for the SMDs of bio-oil and bioslurry (char loading levels of 5, 10, 15, and 20%) with other relative importance of bio-oil viscosity, gas to liquid mass ratio (GLR), and char loading levels of bioslurry as illustrated in Figures 5-12 and 5-13.

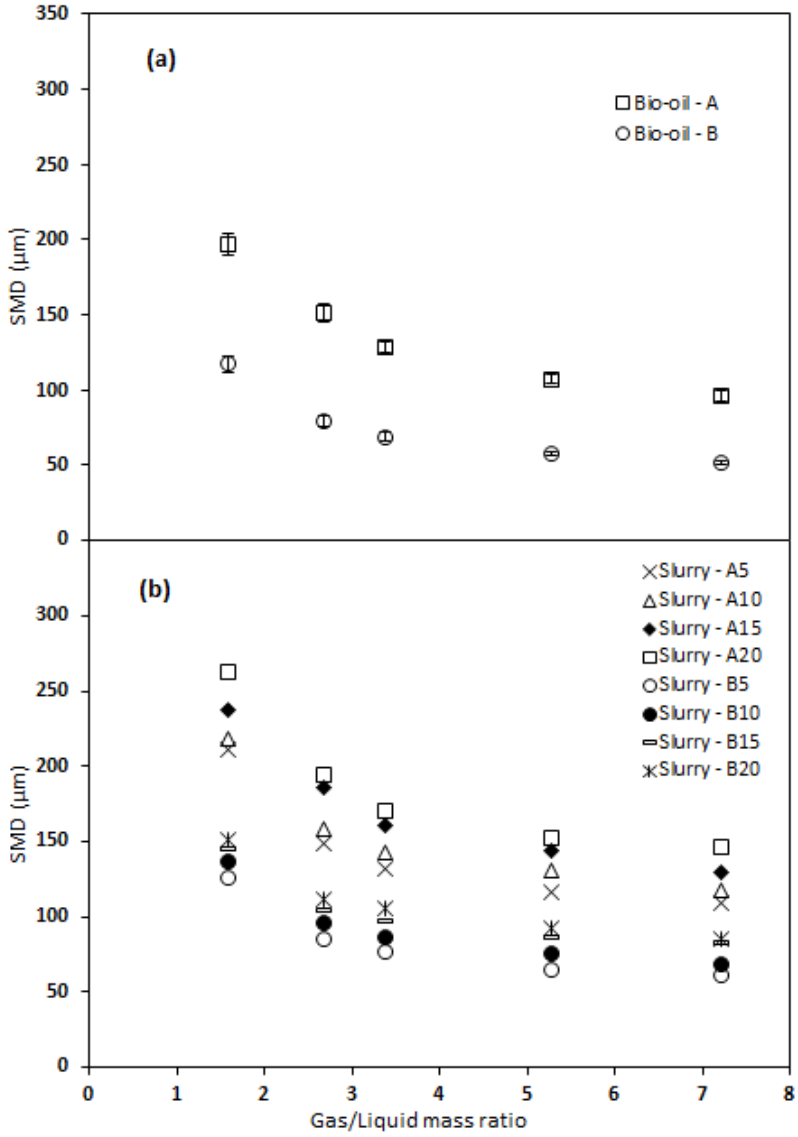

Figure 5- 12: Influence of Gas/Liquid mass ratio on SMD for: (a) bio-oil A and B; and (b) bioslurry (with different loading level of biochar at 5, 10, 15, and 20 wt% into bio-oils A and B) in Twin-fluid Atomizer.

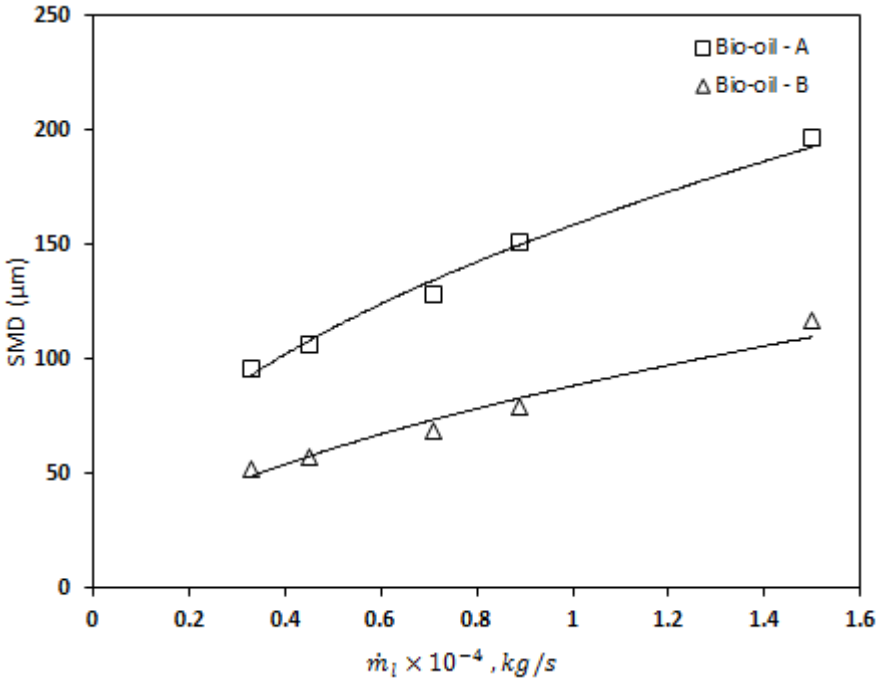

Figure 5- 13: Influence of Liquid mass flow rate on SMD for bio-oil A and B, using Twin-fluid Atomizer.

As shown in Figure 5-12a, at a given gas flow rate, a reduction in the bio-oil flow rate leads to an increases in GLR hence a reduction in the SMD for both bio-oils (A and B). This is because at a constant gas flow rate (constant velocity); a reduction in the liquid flow rate reduces the liquid velocity. This in turn increases the relative difference in velocity between gas and liquid stream which augments the atomization process more effectively.

Figure 5-12b presents the dependence of the spray SMD on gas/liquid mass ratio for bioslurry at different biochar loading levels (A5 to A20 and B5 to B20).At a given GLR, an increase in the char loading level leads to an increase in SMD, due to the change in rheology properties of bioslurry (a higher shear rate resulting in an increase in apparent viscosity[113]). For example, at a GLR of 5.3, increasing the char loading level of bioslurry (prepared from bio-oil A) from 5 to 10, 15 then 20% leads to the spray SMD of bioslurry increasing from 7.7 to 18.1, 25.4 and then 29.7 µm,

respectively. A similar trend is observed for bioslurry samples prepared from bio-oil B as presented in Figure 5-12b.

As shown in Figure 5-13, similarly, the differences in the spray SMD from the two bio-oils using twin-fluid atomizer is mainly due to the difference in bio-oil viscosity. For bio-oil of a lower viscosity, the change in the spray SMD is less sensitive to bio-oil flow rate. For example, the spray SMD increases from 51.87 to 96.24μm (an increase of ~85%) at a liquid flow rate of 0.33×10^{-4} kg/s but it increases from 117.39 to 196.81 μm (an increase of ~68%) at a liquid flow rate of 1.5×10^{-4} kg/s.

5.7 Empirical Correlation of SMD for bio-oil and bioslurry spray using twin-fluid atomizer

For twin-fluid atomizer, the empirical correlation developed for spray SMD of liquid water by Sakai et al[25] includes only two variables as SMD = 14E-6$d_0^{-0.75}(\dot{m}_L/\dot{m}_A)$. For the spray of bio-oil and bioslurry fuels, key parameters to be considered may include viscosity, gas to liquid mass ratio and biochar loading level may be considered in the empirical correlation of spray SMD, in the general form of

$$\text{SMD} \propto \mu^{\text{f}} \left(\frac{\dot{\text{m}}_{\text{G}}}{\dot{\text{m}}_{\text{L}}}\right)^{\text{g}} (\text{Ln}\ (\text{wt}_{\text{char}} + \text{e}))^{\text{h}} \tag{5.5}$$

Following the same approach discussed in Section 3.2, the values of f, g and h can be estimated, resulting in the following correlation

$$\text{SMD} = 3.526\mu^{0.86} \left(\frac{\dot{\text{m}}_{\text{G}}}{\dot{\text{m}}_{\text{L}}}\right)^{-0.56} (\text{Ln}\ (\text{wt}_{\text{char}} + \text{e}))^{0.20} \tag{5.6}$$

where SMD, μ, $\text{wt}_{\text{char}}, \dot{m}_G, and\ \dot{m}_L$ denote spray SMD, bio-oil dynamic viscosity, char loading level, liquid and gas mass flow rate in μm, $Pa.s, \%, m^2, and\ kg/s$ respectively.

The above equation shows, the spray SMD for twin-fluid atomizer is directly proportional to the bio-oil viscosity and char loading with power of 0.86 and 0.20, while it is inversely proportional to the gas to liquid mass ratio with power of 0.56.As shown in Figure 5-14, the predictions of the empirical correlation are in a good fit with the experimental data.

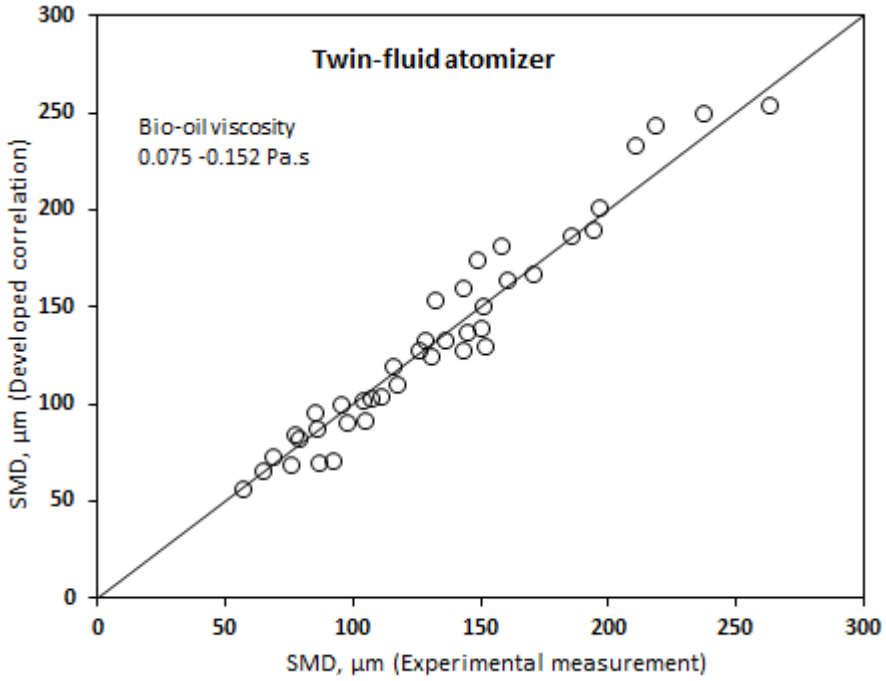

Figure 5- 14: Comparison between experimental data and prediction with Equation 5.6 for two types of bio-oil and bioslurry with loading level between 5 and 20 wt% at different operating conditions by Twin-fluid Atomizer.

5.8 Comparison between twin fluid atomizer and impact atomizer

The approach to the identification and analysis of above discussion in terms of comparison between twin fluid atomizer and impact atomizer are drawn as follows:

- Twin fluid atomizer requires the supply of a source of atomization gas and such supply of high pressure gas can be often costly and also in some applications may not be attractive.

- With the assistance of atomization gas for liquid disintegration, twin-fluid atomizer can be operated at a much lower liquid flow rate and inject pressure than impact atomizer. This makes twin-fluid atomizer be particularly suitable for small-scale applications in laboratory-scale reactors while impact atomizer is more favoured for some large-scale practical applications.

- Impact atomizer is also more suitable for atomizing liquid fuels of high viscosity. This can be clearly seen in the respective empirical correlations, in which the dependence of spray SMD on viscosity is proportional to the power of 0.13 for impact atomizer but 0.86 for twin-fluid atomizer.

- For the atomization of bioslurry fuels, both impact and twin-fluid atomizers exhibit similar dependence of spray SMD on ln $(wt_{char} + e)$ to the power of ~0.20, suggesting that the spray performance of both atomizers have similar sensitivities to biochar loading level.

5.9 Summary

This study reported the experimental data on spray SMD for bio-oil and bioslurry using impact and twin-fluid atomizers. the Sauter Mean Diameter (SMD) of bio-oil and bioslurry increases with increasing flow number at a constant pressure but decreases significantly with increasing pressure at a constant flow number.To evaluate the degree of variables on SMD, a correlation was developed which influenced by change of liquid viscosity, flow number, differential pressure and char concentration in bioslurry with its application for both bio-oil and bioslurry up to 15% char. For twin-fluid atomizer (N_2 as the atomization gas), the spray SMD is mainly influenced by liquid viscosity, Gas/Liquid ratio (GLR) and the biochar loading level. Twin-fluid atomizer has been shown to be more efficient in terms of using low liquid flow rate to conduct laboratory experiments.For both atomizers, biochar loading level is a key parameter influencing bioslurry atomization characteristics. An increasing biochar leading level leads to a drastic increase in the spray SMD.Finally, the twin-fluid atomizer compared in terms of benchmarking against impact atomizer for its performance, application and the influence of different variables on SMD.

CHAPTER 6: MODELLING OF BIO-OIL STEAM GASIFICATION IN A FLUIDIZED BED REACTOR†

6.1 Introduction

Bio-oil is produced from biomass fast pyrolysis and considered as a potential fuel addressing challenges (e.g. low energy density) associated with direct biomass utilisation.[5, 14, 19-21] Bio-oil may be feasible in stationary applications such as gasification for syngas production.[17, 22, 23, 114] Previous studies were carried out on experimental investigations and thermodynamic equilibrium modelling on bio-oil steam gasification.[35, 65, 66] For those models, the predictions were for bio-oil conversion under thermodynamic equilibrium conditions hence may not agree well with the experimental results.[37, 40, 42, 67, 77, 78] A non- equilibrium model which considers more general concepts such as hydrodynamics, heat and mass transfer rate, chemical kinetics, residence time and also particle size distribution might play a major role in transport rate phenomena during bio-oil conversion into product gas.

In Chapter 5 the spray-atomization behaviour was investigated through spray parameters such as the Sauter mean diameter and droplets size distribution data. These measuring were obtained from bio-oil and bioslurry atomization by pressure swirl and twin-fluid atomizers. Also, the spray were produced by twin-fluid atomizer, considered to be exactly, what Sakaguchi[35] used to spray bio-oil and bioslurry. The results of bio-oil droplets measurement by twin-fluid atomizer were used to generate the Rosin-Rammler distribution function for different injection conditions (see Section 6.2.1).

Therefore, in Chapter 6 the cumulative frequency of mass distribution curve with the Rosin-Rammler format has been generated to present mathematical function forms for injection fuels in a fluidized bed reactor. It is the objective of Chapter 6 to develop a bio-oil gasification model based on computational fluid dynamics (CFD), considering atomization, hydrodynamics, heat and mass transfer and chemical

kinetics in a fluidised-bed reactor. A series of simulations were carried out to evaluate the effect of key parameters on bio-oil gasification.

6.2 Methodology

Bio-oil gasification in a fluidised bed includes three phases of solid, liquid and gas and involves injecting bio-oil in the gas-solid fluidized bed. The CFD code was developed based on Eulerian-Eulerian multiphase flow approach which is of relatively low computational cost and suitable for fluidized-bed reactor.[92, 93] The continuity and momentum equations apply for both phases with the equation of particles granular temperature. The Syamlal–O'Brien drag model was employed for predicting the hydrodynamic behaviour of gas-solid fluidized bed reactor.[70] The droplet flow field was examined by Eulerian-Lagrangian approach in which the fluids phase (the gas–solid flow) is treated as continuous and fuel droplets as discrete phase. The discrete phase model (DPM) was used for predicting droplet trajectory, considering interactions with the continuous phase in terms of momentum, heat and mass transfer. The droplet size distribution from atomisation was based on experimental data[115] and presented in terms of the cumulative frequency of mass distribution curve in the Rosin-Rammler format.

As a way of simplifying CFD application in mathematical modelling of bio-oil in a fluidized bed reactor, the following sequence of steps is proposed.

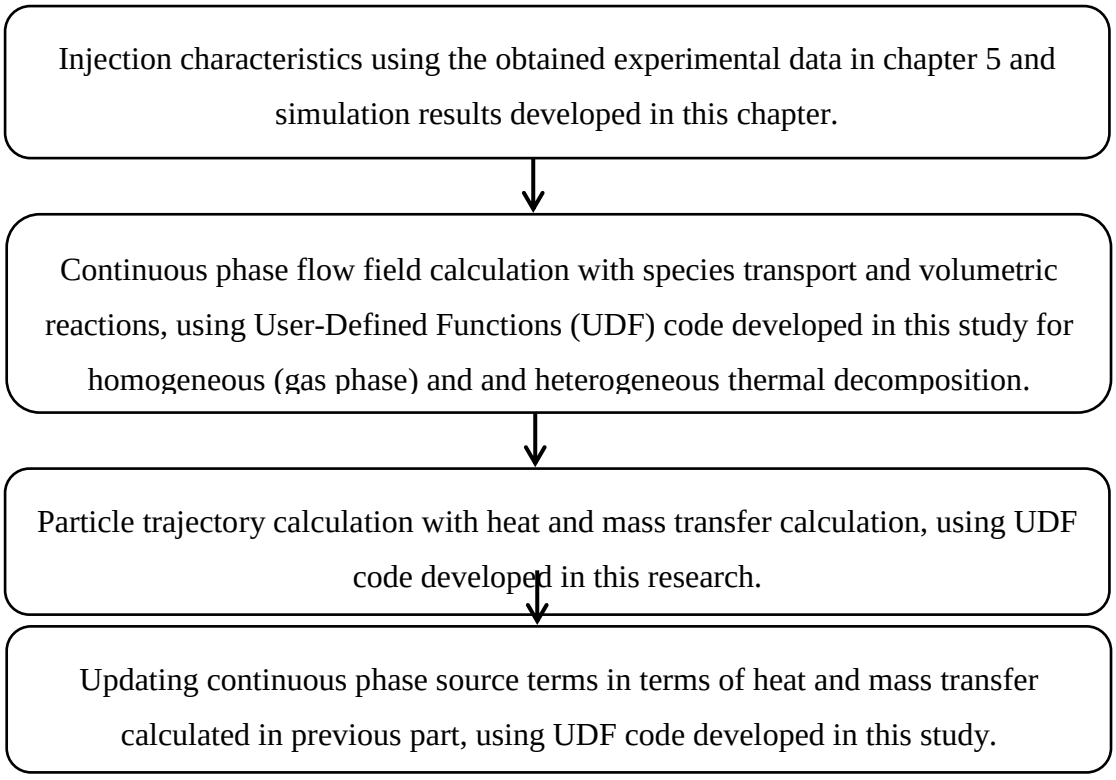

In the first step, the injection characteristics, including droplet size distribution function and particle streams velocity should be specified (see Section 6.2.1).

Once injection steps have been completed, continuous phase flow field calculation can be modelled by Eulerian approach for solid and gas phase in a fluidized bed reactor. In this part, the continuity, volume fraction, momentum and heat transfer equations as well as species transport and volumetric reactions have been considered (see Section 6.2.2).

The third stage is droplets heat and mass transfer calculation base on the droplet mass loss rate during particle trajectory calculation. The standard features of CFD code is not applicable for evaporation and thermal decomposition of bio-oil particles, therefore, the customized UDF code have been written to calculate the heat and mass transfer.

At the end the heat and mass transfer calculated in previous part will be utilized as a source term in conservation equations of continuous phase by using a UDF code developed in this study.

6.2.1 Injection characteristics

6.2.1.1 Droplet size distribution function

For a typical spray, droplets with a wide range of sizes are generated via atomisation. The droplet size distributions of fast pyrolysis bio-oil via atomisation of twin-fluid atomizer can be determined via a procedure developed previous chapter. The Rosin-Rammler distribution function is a cumulative frequency distribution to determine mathematical function for droplet size in sprays. Therefore, in this work the cumulative frequency of mass distribution curve with the Rosin-Rammler format were employed to present the drop size distribution in terms of the two parameters $\overline{D}_d$ and n which provide representative diameter (e.g. mean diameter) and a measure of the spread of drop sizes respectively.

$$\mathrm{Q} = \exp - (\mathrm{D_d}/\overline{\mathrm{D}}_\mathrm{d})^{\mathrm{n}} \tag{6.1}$$

In Equation 6.1, Q is the fraction of the total mass contained in drops of diameter greater thanD_d. Experimental data is needed to determine the size constant $\overline{(\mathrm{D_d})}$ and

the size distribution parameter (n) of Rosin-Rammler equation. The detailed experiments of the bio-oil droplet size distribution were reported in the previous chapter and used in this section to provide the constant parameters of Rosin-Rammler equation in different operating conditions as illustrate in Figure 6-1. This figure presents the experimental results for the cumulative size distribution of spray droplets generated from bio-oil atomisation under three different injection conditions. It can be seen that the experimental data can be well fit with the Rosin-Rammler equation. It is also evident that the Sauter Mean Diameter (SMD) is less than the mean diameter parameter (droplet diameter at $Y_d = 0.368$, Y_d is the mass fraction of droplets with diameter greater than D_p) specified in the Rosin-Rammler distribution function. The spray droplets with the sizes in the form of Rosin-Rammler distribution can then be used for simulation of all droplets generated via bio-oil atomisation.

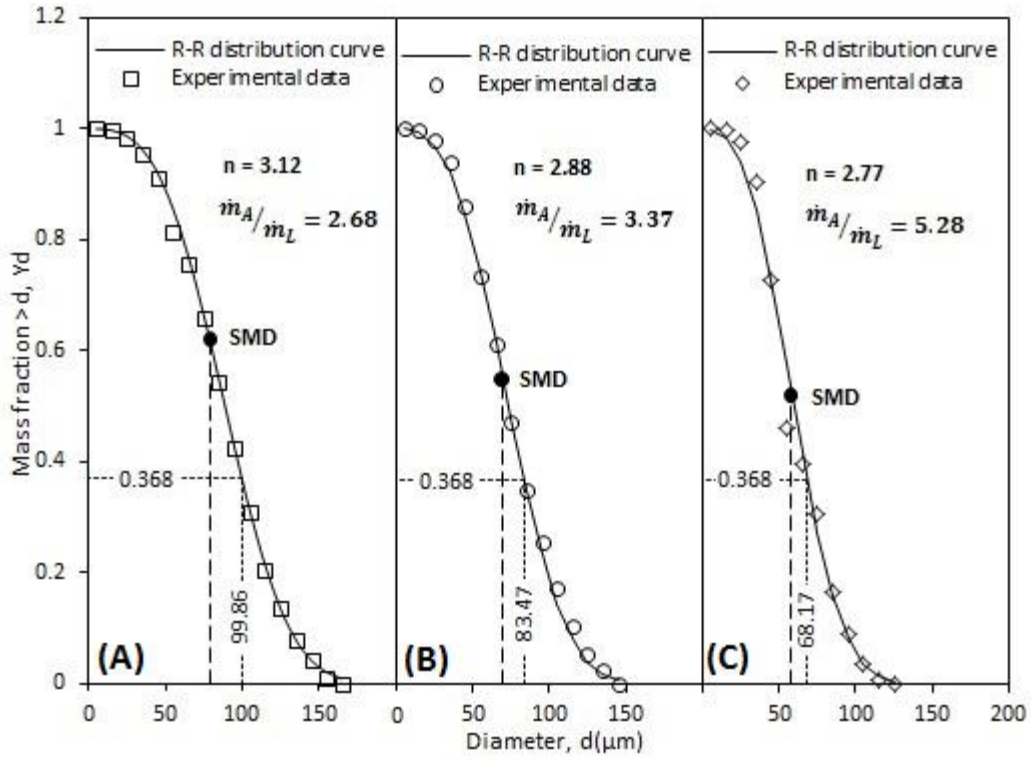

Figure 6 - 1: Comparison between experimental data and fitted curved using Rosin-Rammler equation for the cumulative size distribution of spray droplets generated by the atomisation of bio-oil using twin-fluid atomizer. Three atomisation conditions are considered, including panel (A) n = 3.12 and $\dot{m}_A/\dot{m}_L = 2.68$, panel (B) n = 2.88 and $\dot{m}_A/\dot{m}_L = 3.37$ and panel (C) n = 2.77 and $\dot{m}_A/\dot{m}_L = 5.28$. n and $\dot{m}_A/\dot{m}_L$ indicate the size distribution parameter in the Rosin-Rammler function and atomizer gas to liquid mass ratio respectively.

6.2.1.2 Particle streams velocity with twin-fluid atomizer

The velocity magnitude of the particle streams that will be oriented along the spray cone angle have been estimated by a simulation study of the internal flow field of a twin-fluid atomizer, using three-dimensional computational fluid dynamics (CFD). Details of the average velocities magnitude calculations are described in Appendix A and the result reported in Table 6-1.

Table 6- 1: Velocity magnitude estimated in different position along the spray cone angle at different gas to liquid mass ratio ($\dot{m}_A/\dot{m}_L$)

Continuous phase mass source ($\dot{m}_A$) kg/s	Discrete phase mass source ($\dot{m}_L$) kg/s	$\dot{m}_A/\dot{m}_L$	Average velocity m/s
2.39E-04	8.90E-05	2.68	94.5
2.39E-04	7.10E-05	3.37	85.7
2.39E-04	4.52E-05	5.28	75.4

6.2.2 Conservation equations of flow field (continuous phase)

The continuity, volume fraction and momentum equations for gas and solid phase in fluidized bed reactor are:

$$\frac{\partial}{\partial t}(\alpha_g \rho_g) + \nabla.(\alpha_g \rho_g \nu_g) = S_{mg} \tag{6.2}$$

$$\frac{\partial}{\partial t}(\alpha_s \rho_s) + \nabla.(\alpha_s \rho_s \nu_s) = 0 \tag{6.3}$$

$$\alpha_g + \alpha_s = 1 \tag{6.4}$$

$$\frac{\partial}{\partial t}(\alpha_g \rho_g \nu_g) + \nabla.(\alpha_g \rho_g \nu_g \nu_g) = \alpha_g \nu_g g - \alpha_g \nabla p + \nabla.\bar{\bar{\tau}}_g - K_{sg}(\nu_g - \nu_s) + S_{mg}\nu_d \tag{6.5}$$

$$\frac{\partial}{\partial t}(\alpha_s \rho_s \nu_s) + \nabla.(\alpha_s \rho_s \nu_s \nu_s) = \alpha_s \nu_s g + \nabla.\bar{\bar{\tau}}_s + K_{sg}(\nu_g - \nu_s) \tag{6.6}$$

Whereν and αdenoted the velocity and volume fraction with subscripts g, s and d applied for gas, solid and droplet respectively. Also, $K_{sg}$and$\bar{\bar{\tau}}$ are the interphase momentum exchange coefficient (Ansys Fluent expression for the interphase force) and stress tensor. In addition, S_{mg}in Equation 6.2present the mass transfer rate from bio-oil droplets to gas phase.

The study of Wang et al.[116] shows that the Syamlal–O'Brien drag model predicts solid velocity and volume fraction better than other models. Therefore, the Syamlal–

O'Brien drag model (using the Drag coefficient ($C_{D,s}$) by Dalla Valle[117]) that is based on the relative Reynolds number ($\mathrm{Re_s}$), solid particle diameter ($\mathrm{D_s}$) and terminal velocity ($\mathrm{v_{rs}}$) employed to calculate drag forces and then fluid –solid exchange coefficient as given below:

$$\mathrm{K_{sg}} = \frac{3\alpha_s\alpha_g\rho_g}{4v_{rs}^2 D_s}\mathrm{C_{D,s}}\left(\frac{\mathrm{Re_s}}{\mathrm{v_{rs}}}\right)\left|\mathrm{v_s} - \mathrm{v_g}\right| \tag{6.7}$$

$$\mathrm{v_{rs}} = 0.5\left(\mathrm{A} - 0.06\mathrm{Re_s} + \sqrt{(0.06\mathrm{Re_s})^2 + 0.12\mathrm{Re_s}(2\mathrm{B} - \mathrm{A}) + \mathrm{A}^2}\right) \tag{6.8}$$

$$\mathrm{A} = \alpha_g^{4.14}, \mathrm{B} = \begin{cases} 0.8\alpha_g^{1.28} & \text{if}\alpha_g \le 0.85 \\ \alpha_g^{2.65} & \text{if}\alpha_g > 0.85 \end{cases} \tag{6.9}$$

$$\mathrm{C_{D,s}} = \left(0.63 + \frac{4.8}{\sqrt{\mathrm{Re_s}/\mathrm{v_{rs}}}}\right)^2 \tag{6.10}$$

In Equation 6.6 the solid stress tensor ($\bar{\bar{\tau}}_s$) can be expressed in terms of shear and bulk viscosity which resulted from momentum exchange due to collision and translation of particles:

$$\bar{\bar{\tau}}_s = \alpha_s\mu_s(\nabla\mathrm{v_s} + \nabla\mathrm{v_s^T}) + \alpha_s\left(\lambda_s - \frac{2}{3}\mu_s\right)\nabla.\mathrm{v_s}\bar{\bar{I}} \tag{6.11}$$

The solids shear viscosity can be expressed in terms of the kinetic and collisional viscosity:

$$\mu_s = \mu_{s,kin} + \mu_{s,col} \tag{6.12}$$

In this study for the kinetic and collisional parts, the following expression models employed as given in Equations 6.13 and 6.14 respectively.

$$\mu_{s,kin} = \frac{\alpha_s d_s \rho_s\sqrt{\Theta_s\pi}}{6(3-e_{ss})}\left[1 + \frac{2}{5}(1+e_{ss})(3e_{ss}-1)\alpha_s g_{0,ss}\right] \tag{6.13}$$

$$\mu_{s,col} = \frac{4}{5}\alpha_s\rho_s d_s g_{0,ss}(1+e_{ss})\left(\frac{\Theta_s}{\pi}\right)^{1/2}\alpha_s \tag{6.14}$$

In above equations e_{ss}, $g_{0,ss}$, and Θ_s are the coefficient of restitution for particle collisions, the radial distribution function, and the granular temperature respectively.

The solids bulk viscosity in Equation 6.11 has the following form of Lun-et-al model.[118]

$$\lambda_s = \frac{4}{3}\alpha_s \rho_s d_s g_{0,ss}(1+e_{ss})\left(\frac{\Theta_s}{\pi}\right)^{1/2} \tag{6.15}$$

The granular temperature in Equations 6.13, 6.14, and 6.15 is turbulent fluctuating energy of the solid particle and has been modelled by kinetic theory of granular flow. The transport equation of granular temperature (Θ_s) is given in form of equation6.16.

$$\frac{3}{2}\left[\frac{\partial}{\partial t}(\rho_s \alpha_s \Theta_s) + \nabla.(\rho_s \alpha_s \nu_s \Theta_s)\right] = \left(-p_s \bar{\bar{I}} + \bar{\bar{\tau}}_s\right): \nabla \nu_s + \nabla.\left(k_{\Theta_s} \nabla \Theta_s\right) - \gamma \Theta_s + \emptyset_s \tag{6.16}$$

Where:

$$p_s = \alpha_s \rho_s \Theta_s + 2\mu_s(1+e_{ss})\alpha_s^2 g_{0,ss}\Theta_s \tag{6.17}$$

Equation 6.17 represents the particle pressure (p_s) due to the particles normal force interactions and can be expressed in terms of kinetic and collisional portion, which describes particle translations and the momentum transfer respectively.

In Equation 6.13 the Radial distribution function ($g_{0,ss}$) is a correction factor used for dense solid granular phase to modify the probability of the collisions between particles.

$$g_{0,ss} = \left[1 - \left(\frac{\alpha_s}{\alpha_{s,max}}\right)^{\frac{1}{3}}\right]^{-1} \tag{6.18}$$

The standard $k-\varepsilon$ model is reasonable accurate, robustness, and economic for a wide range of turbulent flows which widely use in the industrial flow and heat transfer simulations. In particular, for multi-phase flow where particles are dispersed through turbulent flow fluctuations, the modified $k-\varepsilon$ model can be used to predict hydrodynamic turbulent parameters, assuming that the turbulent fluctuations of solid phase be affected only by the gas-phase turbulence. The transport equations for the turbulence kinetic energy (k) and its dissipation rate (ε) are:

$$\frac{\partial}{\partial t}\left(\alpha_g \rho_g k_g\right) + \nabla.\left(\alpha_g \rho_g \nu_g k_g\right) = \nabla.\left(\alpha_g \frac{\mu_{t,g}}{\sigma_k} \nabla k_g\right) + \alpha_g G_{k,g} - \alpha_g \rho_g \varepsilon_g + \alpha_g \rho_g \Pi_{k_g} \quad (6.19)$$

$$\frac{\partial}{\partial t}\left(\alpha_g \rho_g \varepsilon_g\right) + \nabla.\left(\alpha_g \rho_g \nu_g k_g\right) = \nabla.\left(\alpha_g \frac{\mu_{t,g}}{\sigma_\varepsilon} \nabla \varepsilon_g\right) + \alpha_g \frac{\varepsilon_g}{k_g}\left(C_{1\varepsilon} G_{k,g} - C_{2\varepsilon} \rho_\varepsilon \varepsilon_g\right) + \alpha_g \rho_g \Pi_{\epsilon_g} \quad (6.20)$$

In above equations, G_k indicated the production of turbulent kinetic energy. σ_k and σ_ε also are the turbulent Prandtl numbers for (k) and (ε), respectively. In addition, $\Pi_{k_g}$and Π_{ϵ_g} represent the influence of the dispersed phases on the continuous gas phase and $C_{1\varepsilon}$, $C_{2\varepsilon}$ are constants.

The internal energy balance for the Eulerian approach can be written for gas and solid phase:

$$\frac{\partial}{\partial t}\left(\alpha_g \rho_g H_g\right) + \nabla.\left(\alpha_g \rho_g \nu_g H_g\right) = -\nabla. q_g + S_{hg} + Q_{sg} \quad (6.21)$$

$$\frac{\partial}{\partial t}\left(\alpha_s \rho_s H_s\right) + \nabla.\left(\alpha_s \rho_s \nu_s H_s\right) = -\nabla. q_s - Q_{sg} \quad (6.22)$$

The term S_{hg}in Equation 6.21 considers the rate of energy transfer between bio-oil droplet and gas while $Q_{sg} = -Q_{gs}$ is the heat transfer rate between gas and solid phase, related to heat transfer coefficient (correlated to the particle Nusselt number) and temperature difference between gas and solid phases.

$$Q_{sg} = h_{sg}\left(T_s - T_g\right) \quad (6.23)$$

$$h_{sg} = \frac{6 k_g \alpha_s \alpha_g Nu_s}{{D_p}^2} \quad (6.24)$$

In the case of granular flows the Nusselt number is determined by Gunn correlation

$$Nu_s = \left(7 - 10\alpha_g + 5{\alpha_g}^2\right)\left(1 + 0.7{Re_s}^{0.2} Pr^{1/3}\right) + (1.33 - 2.4\alpha_g + 1.2{\alpha_g}^2){Re_s}^{0.7} Pr^{1/3} \quad (6.25)$$

The individual species transport equations need to be considered when there is mass transfer happen between bio-oil droplets and gas phase due to droplet vaporization.

$$\frac{\partial}{\partial t}\left(\rho_g Y_i\right) + \nabla.\left(\rho_g v_g Y_i\right) = -\nabla.J_i + R_i + S_i \tag{6.26}$$

where S_i and J_i are the mass source for the bio-oil species due to droplet thermal decomposition and the diffusion flux of species i (due to concentration and temperature gradient) respectively. In additions, R_i is the net rate of production of species i by chemical reactions.

6.2.3 Trajectory, heat and mass transfer of bio-oil droplets

6.2.3.1 Bio-oil droplet trajectories

Lagrangian discrete phase model was employed for tracking bio-oil droplets, considering interactions between droplets and flow field via interphase exchange of momentum, heat, and mass transfer. In this model, droplet is moved along its trajectory, which is based on integrating the particle equation of motion. Interactions between droplet and flow field are computed due to the interphase exchange of momentum, heat, and mass transfer.

The force balance equates the droplet inertia with the forces acting on the droplet. The applied forces on the droplet are the gravitational and drag force and additional acceleration forces neglected.

$$\frac{du_d}{dt} = F_D(v - v_d) + \frac{g(\rho_d - \rho)}{\rho_d} \tag{6.27}$$

In Equation 6.27, v is the fluid phase velocity and v_d is the droplet velocity, and F_D is the drag force and can be written:

$$F_D = \frac{18\mu}{\rho_d {d_d}^2}\frac{C_{D,d}Re}{24} \tag{6.28}$$

The drag model by Saboni and Alexandrov[119] was employed to predict the drag coefficients (C_D)of dispersed liquid phase in gas phase, as a function of Reynolds number, density ratio, and the viscosity ratio ($\kappa = \mu_d/\mu_c$) between the dispersed phase and the continuous phase.

$$C_{D,d} = \frac{\left[\kappa\left(\frac{24}{Re} + \frac{4}{Re^{1/3}}\right) + \frac{14.9}{Re^{0.78}}\right]Re^2 + 40\frac{3\kappa+2}{Re} + 15\kappa + 10}{(1+\kappa)(5+Re^2)} \tag{6.29}$$

Since this model is not available in Fluent the UDF code to consider above drag coefficient has been written (Appendix A).

6.2.3.2 Droplet heat and mass transfer models

As mentioned in previous section the interactions between droplet and flow field are computed due to the interphase exchange of heat and mass transfer. There are two strategies to develop a model for multi component fuel droplet vaporization. One strategy is based on the continuous thermodynamics model that considers a probability density function for molecular weight distribution of the components in the fuel.[120, 121] This model is preferred for fuel vaporization with large number of components and composition of close molecular structure, such as petroleum fuels. The other model strategy is the vaporization of individual components (discrete component model).[122] This model considers each components vaporization rate, for each individual droplet, and is also preferred for fuels with a small number of components with significant variety of molecular structure such as bio-oil.

- **Droplet mass transfer**

Combined heat and mass transfer occurs when bio-oil droplet evaporate. The major emphasis of this study is describing a method to enhance total mass transfer rates from single droplet. The bio-oil vaporization was modelled with a discrete component approach, with the droplet assumed to be ideal liquid mixture. The pseudo-steady species equation[24] in the gas phase is solved, considering the forced convection between the drop and ambient gas.

$$\dot{m}_{tot} = \frac{\dot{m}_i}{\varepsilon_i} = 2\pi R\rho Sh_{i,o} D_{i,g} \ln(1 + B_{M,i}) \tag{6.30}$$

where $\dot{m}_{tot}$ and $\dot{m}_i$ are total evaporation rate and evaporation rate of component i respectively, $Sh_{i,0}$ is Sherwood number, ε_i is the fraction of vaporization rate for component i with $\varepsilon_i = \dot{m}_i/\dot{m}_{tot}\ and \sum \varepsilon_i = 1$, $D_{i,g}$ is the binary diffusivity between fuel component i and ambient gas, and $B_{M,i}$is Spalding mass transfer number. The correlations for the above definitions are given by:

$$Sh_{i,o} = 2 + 0.6Re^{1/2}{Sc_i}^{1/3} \tag{6.31}$$

$$B_{M,i} = \frac{y_{i,s} - y_{i,\infty}}{\varepsilon_i - y_{i,s}} \tag{6.32}$$

$$Sc_i = {}^{v}/_{D_{i,g}} \tag{6.33}$$

$$\varepsilon_i = \frac{\dot{m}_i}{\dot{m}_{tot}} \; and \; \sum \varepsilon_i = 1 \tag{6.34}$$

In above equations $y_{i,s}$ and $y_{i,\infty}$ are mass fraction of species i at droplet surface and free stream. In addition, v, Re and Sc are kinematic viscosity, dimensionless groups known as Reynolds number, and Schmidt number.

Considering the phase equilibrium at interface, the mole fraction of the components of vapor phase at the interface can be estimated by the Raoult's law.[123]

$$Y_{i,s} = X_{i,s} \frac{P_{v,i}(T_s)}{P_{amb}} \tag{6.35}$$

For a liquid droplet with two components i and j, its diffusivity is related to Spalding mass transfer number via Eq (6.36).

$$D_{i,g} \ln\left(1 + B_{M,i}\right) = D_{j,g} \ln(1 + B_{M,j}) \tag{6.36}$$

If identical components are assumed, the above equation reduces to:

$$\frac{y_{i,s} - y_{i,\infty}}{\varepsilon_i - y_{i,s}} = \frac{y_{j,s} - y_{j,\infty}}{\varepsilon_j - y_{j,s}} \tag{6.37}$$

The vapour pressure is estimated using Eq (6.38).[123]

$$\ln\left(P_{vpr}\right) = f^{(0)}(T_r) + \omega f^{(1)}(T_r) \tag{6.38}$$

where $f^{(0)}$ and $f^{(1)}$ are correlations with following form as:

$$f^{(0)} = 5.92714 - \frac{6.09648}{T_r} - 1.28862 \ln(T_r) + 0.16934 T_r^6 \tag{6.39}$$

$$f^{(1)} = 15.2518 - \frac{15.6875}{T_r} - 13.472 \ln(T_r) + 0.43577 T_r^6 \tag{6.40}$$

In above equation ω is the acentric factor which originally proposed by Pitzer, et al.[124] as:

$$\omega = -\log_{10}\left[\lim_{T/T_c=0.7}(P_{vp}/P_c)\right] - 1.0 \tag{6.41}$$

The multicomponent diffusion flux was simplified to binary diffusion flux and the binary diffusion coefficient is determined based on special atomic diffusion volumes.[125]

$$D_{ij} = \frac{10^{-3}T^{1.75}[(M_i+M_j)/M_iM_j]^{1/2}}{P[(\sum v)_i^{1/3}+(\sum v)_j^{1/3}]^2} \tag{6.42}$$

where T is in Kelvin, P is in atmosphere, and D_{ij} is the diffusion coefficient measured in cm^2/s. M_i and M_j are the molecular weight of components i and j, respectively. $\sum v$ is diffusion volume for molecules of components i and j which can be calculated from atomic diffusion volumes.[125]

The latent heat (enthalpy) of vaporization is estimated, using an equation that represents the temperature dependency of two points.[125]

$$\Delta H_{v,i} = \Delta H_{vb,i}\left(\frac{1-T_{r,i}}{1-T_{br,i}}\right)^{0.38} \tag{6.43}$$

where $\Delta H_{vb,i}$, $T_{r,i}$, and $T_{br,i}$ are the latent heat at the normal boiling point,[125] the reduced temperature of component i at actual temperature and boiling point, respectively. Also, The latent heat at the normal boiling point is estimated by the equation proposed by Riedel from Perry's chemical engineers handbook[125] which includes the critical pressure of component i ($P_{c,i}$) in atm.

$$\Delta H_{vb,i} = 1.093RT_{c.i}T_{br,i}\frac{\ln(P_{c,i})-1.013}{0.930-T_{br,i}} \tag{6.44}$$

The overall latent heat of vaporizing fuel can be calculated from following equation:

$$\Delta H_v = \sum_{i=1}^{n} \varepsilon_i \Delta H_{v,i} \tag{6.45}$$

- **Droplet heat transfer**

The droplet temperature should be updated for droplet mass transfer calculation according to the heat balance at the drop surface. Whereas in forced convection between drop and ambient gas the energy balance is:

$$\mathrm{hA_d}\left(T_\mathrm{g} - T_s\right) + \frac{dm_d}{dt}\Delta H_v = m_d C_{pd}\frac{dT_d}{dt} \quad (6.46)$$

where subscripts d, g, and s denote droplet, gas phase, and droplet surface respectively.

The convective heat transfer coefficient (h) of vaporizing and non-vaporizing drop[24] was estimated by:

$$Nu = Nu_0 \frac{\ln(1+B_T)}{B_T} = Nu_0 \frac{z}{e^z - 1} \quad (6.47)$$

where $z = \dot{m}_{tot} C_{pv}/4\pi k_g R$ and Nu_0 is the Nusselt number at non vaporizing condition and calculated by:

$$Nu_0 = 2 + 0.6Re^{1/2}Pr^{1/3} \quad (6.48)$$

The Spalding heat transfer number can be calculated as:[126]

$$B_T = (1 + B_M)^{\varphi} \quad (6.49)$$

$$\varphi = \left(\frac{C_{pv}}{C_{pg}}\right)\frac{1}{Le} \quad (6.50)$$

In the above equations Le is Lewis number ($Le = k_g/\left(C_{pg}\rho_{total}\right)$

6.2.3.3 Reaction scheme

During steam gasification of bio-oil, the following reaction scheme (R1–R13) is considered for modelling of bi-oil gasification:

$$\mathrm{Bio-oil} \rightarrow \mathrm{C_xH_yO_z} + \text{ gas } (\mathrm{H_2}, \mathrm{CO}, \mathrm{CH_4}, \mathrm{C_2^+} \ldots) + \mathrm{C_s} \quad (R1)$$

$$\mathrm{C_xH_yO_z} + (\mathrm{x-z})\mathrm{H_2O} \rightarrow \mathrm{xCO} + (\mathrm{x + y/2 - z})\,\mathrm{H_2}\,(\text{tar steam reforming}) \quad (R2)$$

$$\mathrm{C_s} + \mathrm{CO_2} \rightarrow 2\mathrm{CO} \quad (R3)$$

$$\mathrm{CH_4} + \mathrm{CO_2} \leftrightarrow 2\mathrm{CO} + 2\mathrm{H_2} \quad (R4)$$

$$\mathrm{C_s} + \mathrm{H_2O} \rightarrow \mathrm{H_2} + \mathrm{CO} \quad (R5)$$

$$\mathrm{CO} + \mathrm{H_2O} \leftrightarrow \mathrm{CO_2} + \mathrm{H_2} \quad (R6)$$

$$CH_4 + H_2O \leftrightarrow CO + 3H_2 \quad \text{(R7)}$$

Reaction R1 is bio-oil thermal decomposition. An empirical formula CH_mO_n is considered for bio-oil, with m and n equal to 2.03 and 0.88, respectively.[17] The activation energy, pre-exponential factor and reaction order for R1 are taken as $45.2\ \text{kJ/mol}$ and $459.4\ s^{-1}$, and 3.8 respectively. [127] The yield and properties of tar product in R1 is based on experimental data [128], which is dependent on reactor temperature. The tar product further reacts with steam for reforming reaction (Reaction R2), considering activation energy and pre-exponential equal of $350\ \text{kJ mol}^{-1}$ and 1.7E14 $m^{0.3}mole^{-0.1}s^{-1}$, respectively.[129]

For C_2^+ that is produced via R1, ethane is selected to represent C_2^+ in order to simplify the modelling. Steam reforming of ethane is modelled via a series of reactions (R8 to R13) outlined previously [130-133] with kinetics being reported elsewhere.[134]

$$C_2H_6 + 2H_2O \leftrightarrow 2CO + 5H_2 \quad \text{(R8)}$$

$$C_2H_6 \leftrightarrow C_2H_4 + H_2 \quad \text{(R9)}$$

$$C_2H_6 + C_2H_4 \rightarrow C_3H_6 + CH_4 \quad \text{(R10)}$$

$$C_3H_6 \leftrightarrow C_2H_2 + CH_4 \quad \text{(R11)}$$

$$C_2H_4 + C_2H_2 \rightarrow C_4H_6 \quad \text{(R12)}$$

$$2C_2H_6 \rightarrow C_3H_8 + CH_4 \quad \text{(R13)}$$

The Boudouard reaction rate (R3) can be considered by following equation (p_{CO_2} is partial pressure MPa). [135, 136]

$$r_{R3} = 2.071 \times 10^4 \exp(-26459.9/T)\,.\,{p_{CO_2}}^{0.733} \quad (\text{kmol/m}^3\text{.s}) \quad (6.51)$$

The CO_2 reforming of CH_4 (R4) are considered with the activation energy and pre-exponential factor $217.9\ \text{kJ/mol}$ and $14639\ s^{-1}$ respectively.[137] The production of char (C_s) in R1 is temperature dependent [42]. Steam reforming of C_s (R5) is modelled based on the n-th order kinetic model, with the activation energy, pre-exponential factor and reaction order being $235\ \text{kJ mol}^{-1}$, $6.5\text{E}05\ s^{-1}\text{Pa}^{-0.41}$, and 0.41,

respectively.[35] Water-gas shift reaction (R6) and steam reforming of methane (R7) are considered, with the following rate equations, respectively.[138]

$$r_{R6} = 2.78 \times 10^3 \exp(-1515.43/T)\left(C_{co}C_{H_2O} - \frac{C_{CO_2}C_{H_2}}{0.0265}\right) \quad (kmol/m^3.s) \quad (6.52)$$

$$r_{R7} = 3.015 \times 10^6 \exp(-15096.6/T)\left(C_{CH_4}C_{H_2O}\right) \quad (kmol/m^3.s) \quad (6.53)$$

6.3 Numerical method

6.3.1 Computational domain

Figure 6-2 presents the computational domain that is generated by ANSYS Design Modeler, taken into consideration of an optimised set of parameters (e.g. mesh type, mesh size, time step size and maximum iteration per time step etc). with details, summarized as follows.

- Hexahedral meshes were chosen for simulation because such meshes led to considerably less residual tolerances than tetrahedral meshes (by one order of magnitude) and in many cases tetrahedral meshes resulted in divergence problems.

- During the hexahedral mesh was reordered to obtain bandwidth reduction equal to 1.0.

- The time step sensitivity study have been performed by increasing the time step to find out the maximum value where further increase in time step will result in divergence issue or lower level of accuracy; this was achieved by examining and comparing the residuals (dropping at least three orders of magnitude). The result was reported in Table 6-2 by monitoring the convergence criteria at different time step from 1e-03 to 1e-06. The result shows the maximum time step strongly related to the quality of mesh, determined by aspect ratio and plays a significant role in the accuracy and stability.

- Table 6-2 also shows the five first cases for which the average aspect ratio more than 2 and the time step less than 1.0e-4, resulted in significant increases in computer resources. For example, increasing the average aspect

ratio from 2.3403 to 2.7004 reduce the maximum time step around 10 times (from 1.0e-05 to 1.0e-06) and then increase the resources approximately 7 times. Therefore, five out of nine reported cases in Table 6-2 have higher relative average aspect ratio (depending on the total number of cells) which reduced the time steps about 5-100 times and increased the computational cost. Therefore, the case number 1- 5 with average aspect ratio more than 2 were eliminated in this stage

- The residual values with maximum iteration per time step equal to 5, 10, 25, 50, and 100 were monitored in terms of converging to a reasonable value at each time step. Therefore, the maximum 25 iterations/time step was chosen because the residuals won't be improved significantly by increasing the iteration more than 25 while less than 25 reduce the accuracy. In addition, by increasing the maximum time step from 25 to 50 the CPU time will increase two times approximately.

- The initial mesh size, considering the convergence criteria and time step as explained above, was in hexahedral finite cells/elements with a total number of 142800. The mesh independence study was conducted by increasing the mesh resolution to finer cells as summarised in Table 6-2 (cases number 6 to 9). In this table the maximum percentage change of outlet gas mole fraction based on initial mesh size was reported for different mesh resolution. As summarized in this table, by increasing the mesh resolution to finer cells (for example, from142800 to162567 cells) the solution result differs by less than 1%; which confirms the mesh with total number of 142800 cells is adequate to capture mass and heat transfer during droplets trajectory calculation. Therefore, the unstructured mesh with total number of 142800 hexahedral cells and average aspect ratio of 1.9920 was concluded in terms of assessing grid independence.

Table 6- 2: Statistics of mesh generated by ANSYS DesignModeler software

Case number	Number of nodes	Number of elements	Min Aspect ratio	Max Aspect ratio	Average Aspect ratio	Min time step	Total number of time step required	Running time (One node and 24 cpu), hr	Result
1	50085	46766	1.1675	6.4338	2.0643	2.0e-05	210000	1079 [a]	High running time
2	72027	67950	1.1361	5.0837	2.1040	2.0e-05	210000	1449 [a]	High running time
3	75020	70686	1.1512	5.6336	2.0095	2.0e-05	210000	1520 [a]	High running time
4	110040	104876	1.1388	9.9475	2.3403	1.0e-05	420000	3515 [a]	High running time
5	115276	110400	1.1492	7.2722	2.7004	1e-06	4200000	25591 [a]	High running time
6	149946	142800	1.0909	8.3977	1.9920	1.0e-04	42000	315	The accepted mesh for simulation
7	171136	162567	1.0715	2.9844	1.6525	1.0e-04	42000	326	The outlet, H_2 mole fraction was changed about 1.2%by increasing from 142800 to 162567
8	243784	233168	1.0781	4.3267	1.7236	1.0e-04	42000	429	The outlet, H_2 mole fraction was changed about 0.06%by increasing from 162567 to 233168

"a" Predicted by running a sample of 1000 time steps

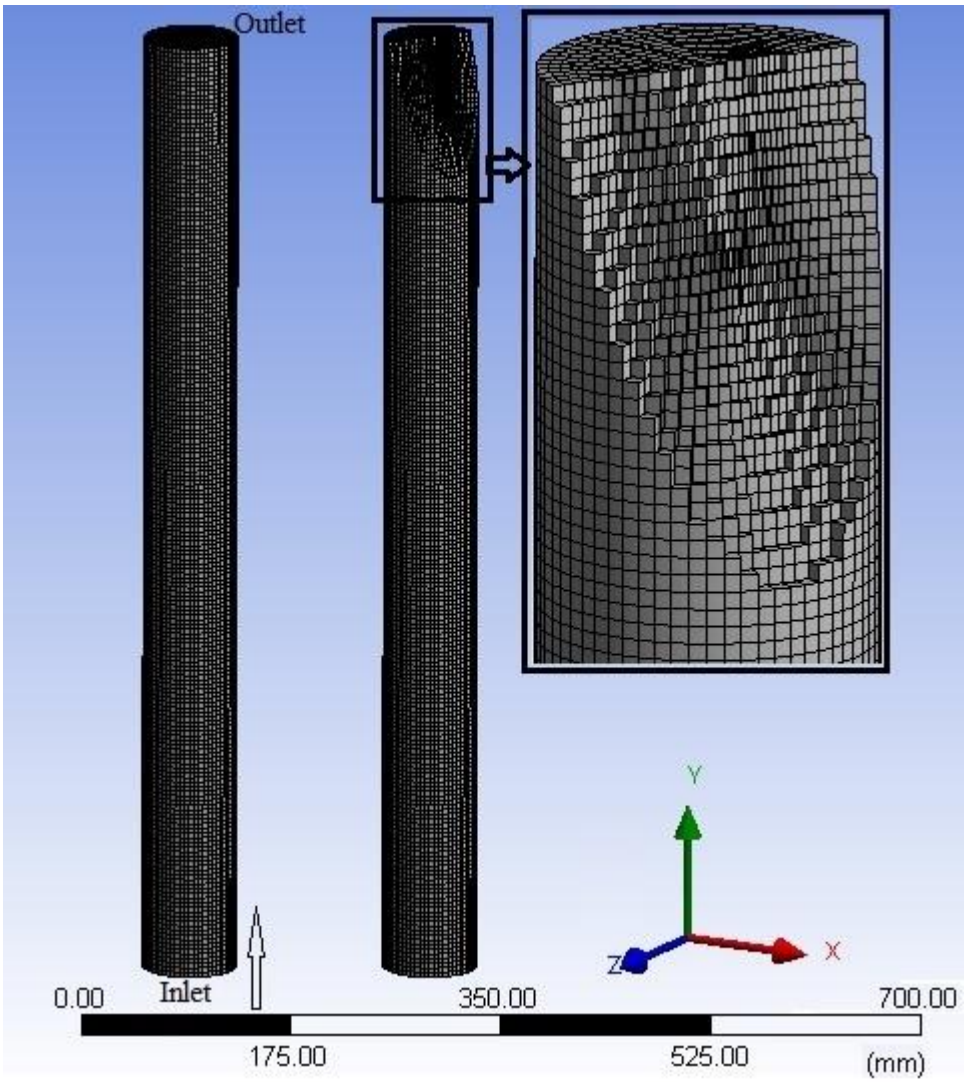

Figure 6 - 2: Computational mesh with the y-direction of the fluid flow

6.3.2 Set up the solver and numerical schemes

A three-dimensional pressure-based solver was used for transient calculations of the continuous phase via first and the second order upwind discretisation schemes where gradients and derivatives are evaluated through the Green-Gauss node-based algorithm. The control volume method was used to convert the governing equations to algebraic equations on a discretised grid system. The Phase Coupled Semi Implicit Method for Pressure Linked Equations (PC-SIMPLE) algorithm, which was developed for multiphase flow to relate the velocity and pressure corrections [139], was employed to recast the continuity equation in terms of a pressure correction calculation. For bio-oil droplets after atomization, the simulation used the Discrete Phase Model (DPM) with droplets tracking and its interactions in continuous phase.

Customized codes (User-Defined Function) were developed to model heat transfer, mass transfer and chemical reactions. To reach a stable converged solution, the continuous phase (gas–solid flow) was solved first. After the basic flow pattern was established, the bio-oil atomization was added to the simulation with a constant time step of 0.1 millisecond and 25 maximum iterations per time step. Considering the need of a large CPU time, an appropriate parallel processing system was performed by employing Epic and Magnus super computers.[140]

6.4 Evaporation of single bio-oil droplet

6.4.1 Bio-oil composition and its model vaporization

Bio-oil is a complex mixture of various type of oxygen-containing organic compounds such as organic acids, aldehydes, alcohols, furans, ketones, esters, dehydrated carbohydrates, and phenols.[141] Simplified methods were previously reported to use different classes or families to represent the major chemical compositions of bio-oil.[56] For modelling multicomponent vaporization, two strategies may be taken. One approach is based on individual components vaporisation (discrete component model [142]) which is more suitable for fuel such as bio-oil that has a small number of major components with a significant variety of molecular structure and weights.[122] The other approach is the use of continuous thermodynamics model [121] that considers a probability density function for molecular weight distribution of fuel components. Such a model is preferred for fuel with a large number of components and close molecular structure, such as petroleum fuels [143]. In this study, the bio-oil vaporization was modelled with a discrete component approach, considering the top ten major components (with the properties[122] listed in Table 6.3) which represent the bio-oil compositions. Evaporation of bio-oil single particle is modelled in a fluidised-bed reactor at 1063 K.

Table 6- 3: Ten major bio-oil components and its properties prediction[122]

Components	Formula	Mass fraction *(%)*	Molecular Weight *(kg/kgmol)*	T_b *(K)*	T_c *(K)*	P_c *(bar)*	Diffusion Volume[125]	Acentric factor $(T/T_c = 0.7)$
Water	H_2O	21.10	18.02	373	647	221	13.1	0.30872
Hydroxyacetaldehyde	$C_2H_4O_2$	21.77	60.05	404	582	64.6	53.26	0.41139
Acetic acid	$C_2H_4O_2$	9.48	60.05	391	588	57.3	53.26	0.2624
Hydroxypropanone	$C_3H_6O_2$	15.06	74.08	418	595	54.8	73.78	0.37772
Levoglucosan	$C_6H_{10}O_5$	17.27	162.14	578	733	57.0	149.05	0.53312
Propionic acid	$C_3H_6O_2$	1.25	74.08	414	609	49.8	73.78	0.23144
(5H)-furan-2-one	$C_4H_4O_2$	2.37	84.07	476	741	56.8	85.06	0.15593
Isoeugenil	$C_{10}H_{12}O_2$	10.79	164.21	540	753	32.8	198.94	0.19621
Phenol	C_6H_6O	0.37	94.11	460	702	61.4	115.37	0.23805
Syringol	$C_8H_{10}O_3$	0.54	154.16	534	767	40.5	168.63	0.20861

6.4.2 Bio-oil vaporization

Figure 6-3 shows the evaporation of a droplet with 100 μm initial diameter when injected into the fluidized bed reactor at 1063 K and 1 atm. As expected, the light components such as acetic acid evaporate rapidly as droplet temperature increases and the evaporation of heavy components (e.g. syringol) takes place mainly at elevated temperatures. The total evaporation time for a droplet with 100 μmdiameter is around 0.045 sec but it only takes ~0.012 s for the droplet depleting to its 50% initial mass as a result of rapid evaporation of light components at early stages. There is also a delay in the evaporation of moisture in the droplet. This can be attributed to the presence of water vapour initially set as the steam-carbon molar ratios within the reactor. The vapour pressure of water at the droplet interface is initially not significant to overcome the partial pressure of water vapour in the reactor.

Figure 6-4 presents the depletion of droplets as a function of time since the droplets are injected into the reactor, for droplets of various diameters. As expected, a larger droplet has longer residence time in the reactor. For example, the lifetime of an

evaporating droplet with an initial size of 500 µm is around 1 sec while it is 0.001 sec for a 10 µm droplet. The prediction of vaporisation time for a100 µm stagnant bio-oil droplet at 1063 K is ~0.12 s, which is in very close agreement with the data (~0.115 s) reported elsewhere[122]. It is further noteworthy in Figure 6-5 that the depletion in bio-oil droplet size as a function of evaporation time cannot be described by the D^2-law (i.e. $D^2 = {D_0}^2 - \lambda t$ that is described elsewhere and generally valid for liquid of simple composition[34]), mostly like due to the continuous changes in the compositions of bio-oil during evaporation.

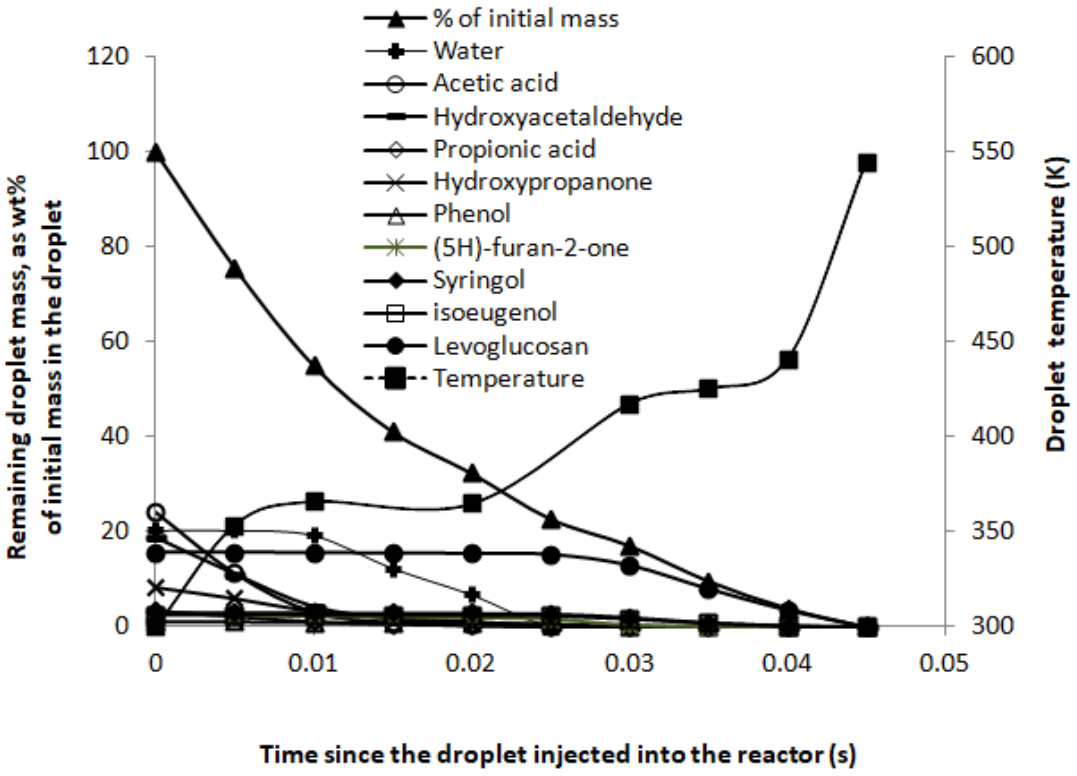

Figure 6 - 3: Changes in droplet mass and temperature as a bio-oil droplet (initial droplet size: 100 µm; initial droplet temperature: 300K) being injected into the fluidised bed that is operated at $T = 1063\ K$, with only evaporation being considered.

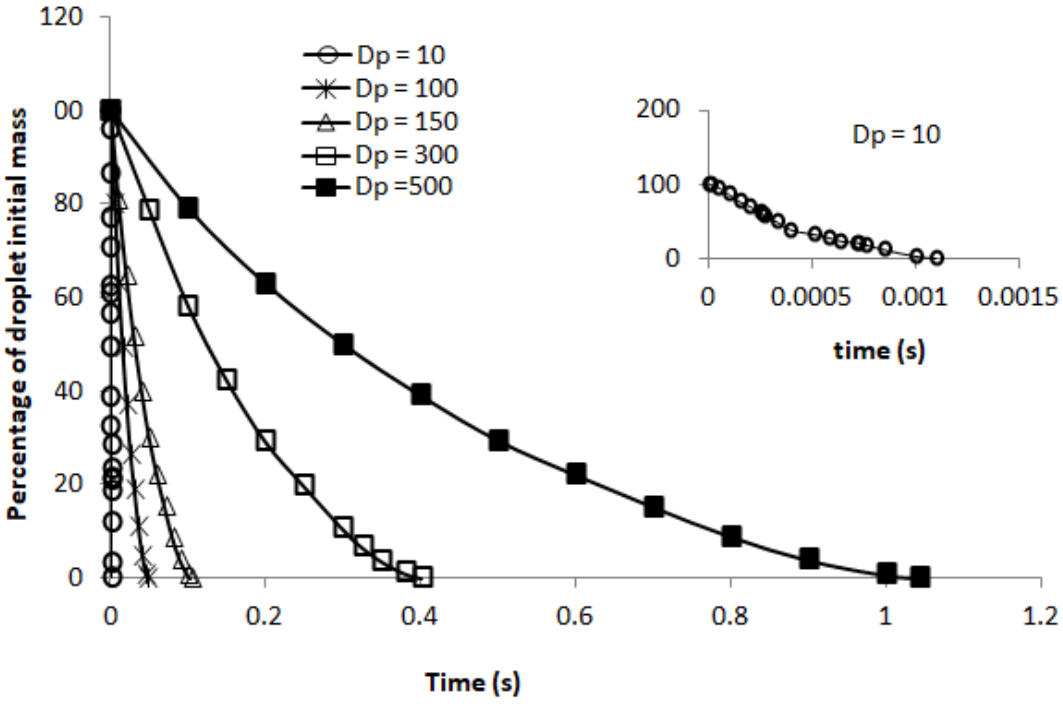

Figure 6 - 4: Simulation results for effect of droplet diameter on the residence time at: T = 1063.15 K.

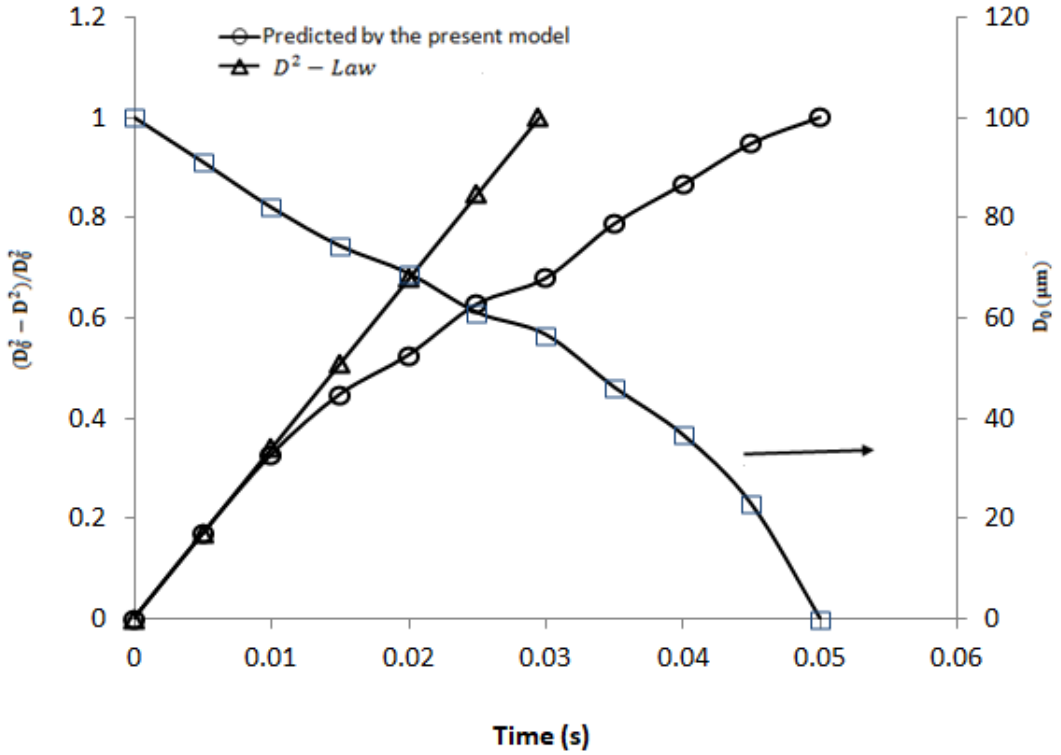

Figure 6 - 5: Comparison between the model prediction and classical $d^2 - law$ (black line) for $100\mu m$ bio-oil droplet ($D_0 = 100\mu m$)vaporisation with initial temperature of 300 K in the fluidized bed reactor at temperature of 1063 K.

6.5 Bio-oil spray droplets in a fluidized-bed reactor

As bio-oil is atomised, droplets of different sizes are sprayed into the reactor. Simulations were then carried out to investigate the penetration of spray droplets into the reactor as a function of droplet size at 1063 K. Considerations are taken for bio-oil injected into the reactor at two locations, bottom injection or side injection, which represent the conditions where the atomizer setup is placed at either the bottom or the side of the reactor, respectively.

Figures 6-6 to 6-8 show the effect of droplets diameter and injection location on droplet distribution, bio-oil vapor, and syngas (H_2+CO) concentration profile inside the reactor during bio-oil vaporisation and gasification. Figure 6-6 indicates that the evaporation of bio-oil droplets with the size of 100 μm(i.e. SMD = 100 μm) in the spray under the injection conditions. It can be seen that the droplets fully evaporate at short penetrations (0.19 and 0.08 m for bottom and side injections, respectively) from

the reactor inlet due to high vaporization rates under the operating conditions. The results also show that side injection results in less droplets penetration than bottom injection. The vaporization and gasification were considered for 0.3 second without aborting trajectory calculations for droplets that no longer exist (fully evaporated), to clarify the lifetime of evaporating droplets.

Figure 6-7 further presents the droplet penetrations into the reactor for bio-oil droplets with the SMDs of 200 and 500 μm, respectively under bottom injection conditions. It can be seen that the spray penetration into the reactor increases substantially with increasing droplet size. Bio-oil droplets with a size of 200 μmcontinue to move upward during evaporation and fully evaporate after exceeding 50% of reactor length. However, the evaporation of bio-oil droplets with a size of 500 μm is incomplete in the reactor, escaping from the reactor outlet with the evaporation of only10% of its initial mass.

A typical spray includes a wide range of drop sizes with different residence time and penetration. The spray droplets with the sizes in the form of Rosin-Rammler distribution can then be used for simulation of all droplets generated via bio-oil atomisation. As shown in Figure 6-8, bio-oil spray (generated under the conditions of panel B in Figure 6-1) reaches full evaporation of all droplets at a short penetration for side injection into the reactor (0.114 m) because the vaporization rate is high and the droplets are small (with maximal droplet sizes of 160 μm). The results clearly demonstrate that efficient atomization of bio-oil is of critical importance to generate spray of small sizes for effective droplet vaporisation.

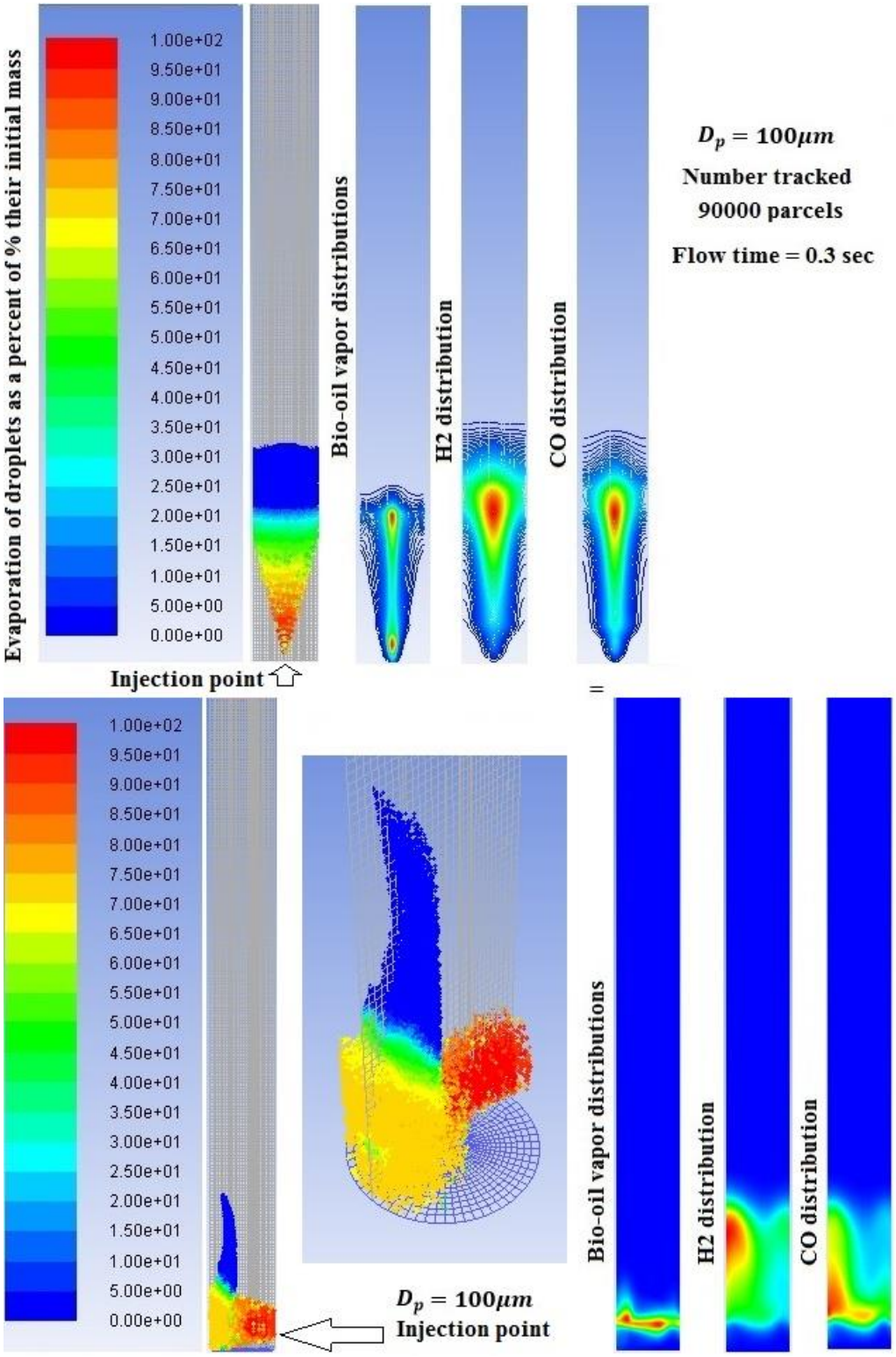

Figure 6 - 6: Effect of injection location on droplets penetration and product gas distribution inside the reactor. The blue colour represents 0% of the initial mass of droplet during trajectory calculations without aborting fully evaporated droplets from calculation and the grey colour is the inside the reactor with 0% of droplets.

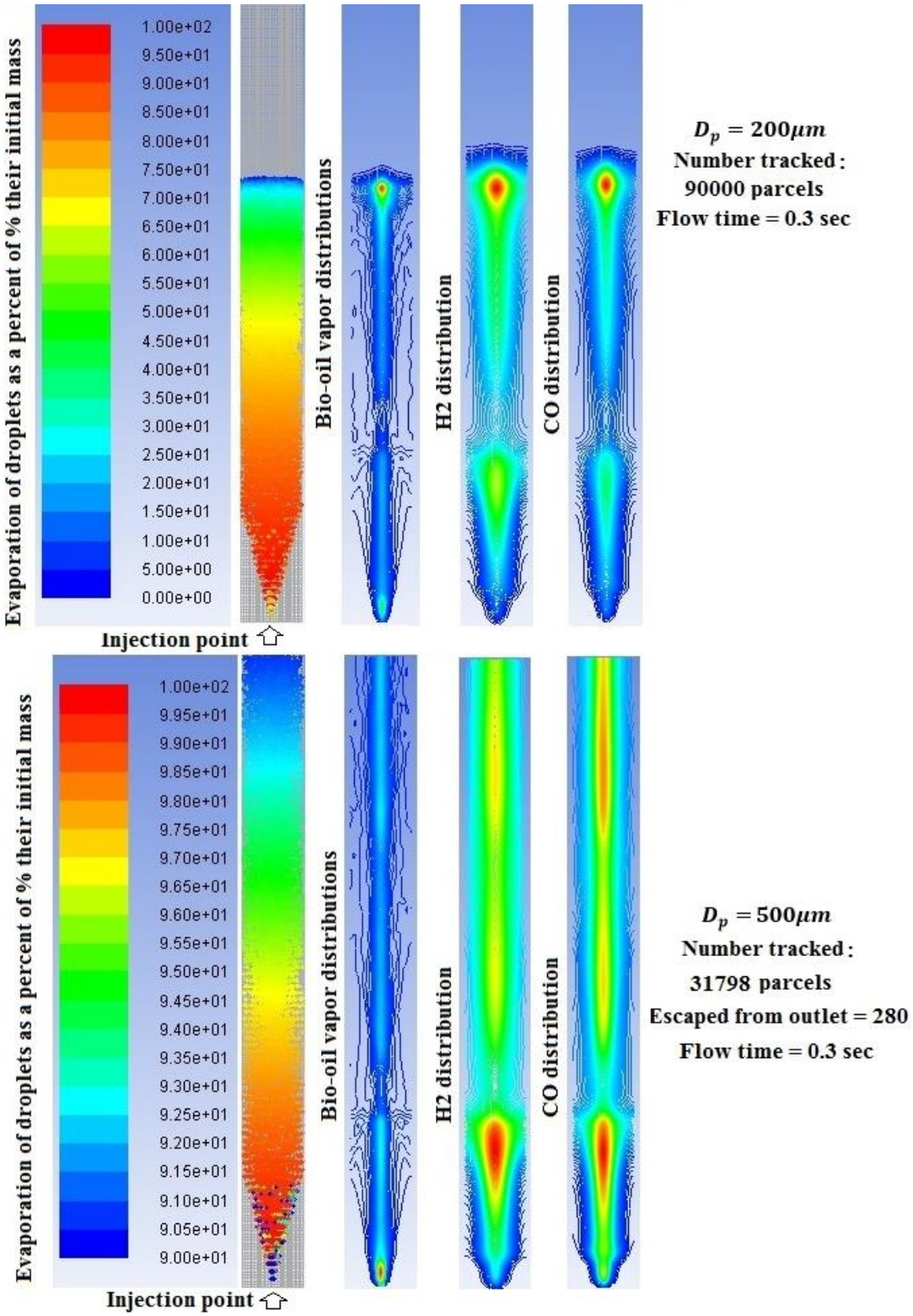

Figure 6 - 7: Effect of initial droplet diameter on droplets penetration and product gas distribution inside the reactor. The blue colour represents 0% of the initial mass of droplet during trajectory calculations without aborting fully evaporated droplets from calculation and the grey colour is the inside the reactor with 0% of droplets.

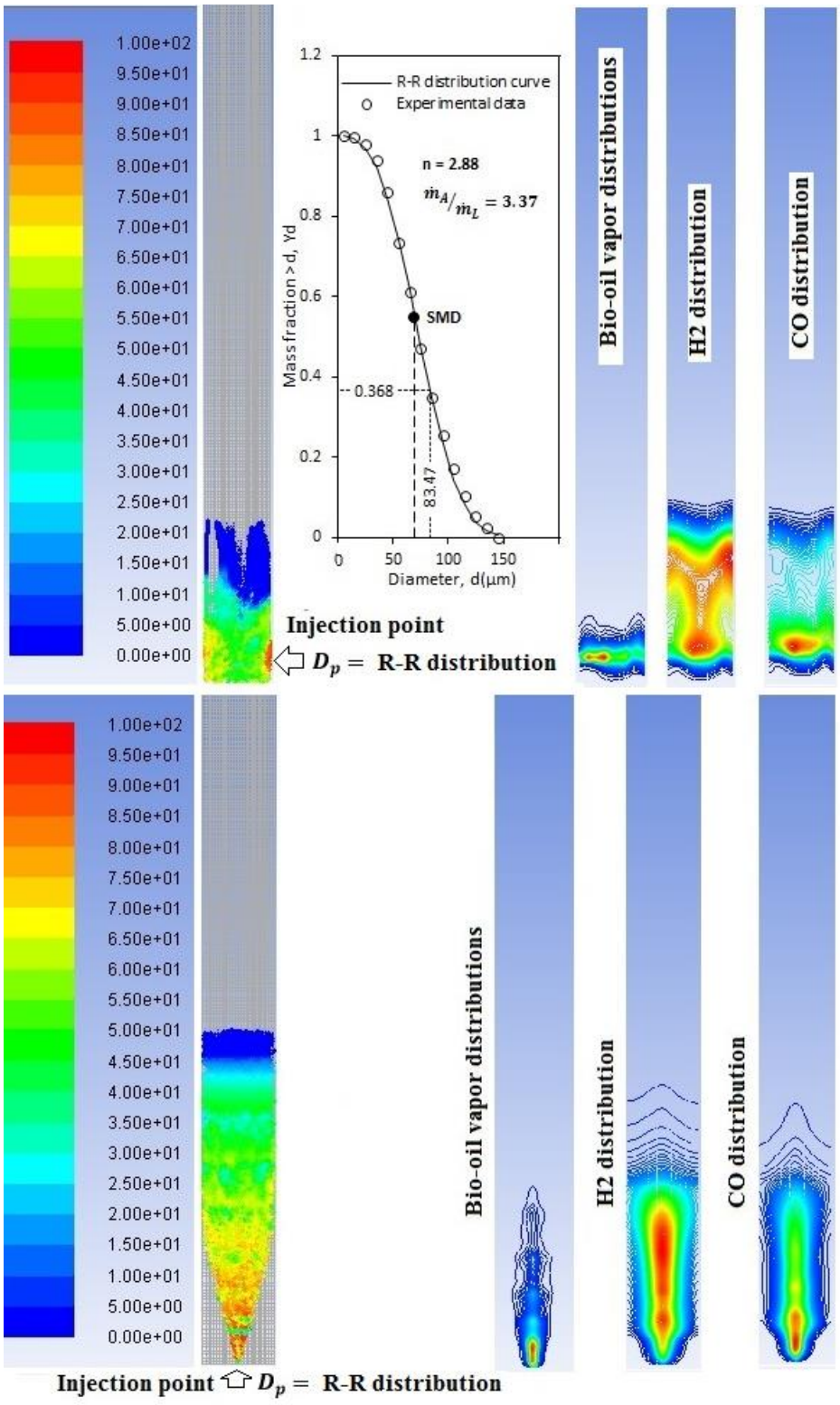

Figure 6 - 8: Spray penetration into the reactor, taking into account all droplets in the spray according to the Rosin-Rammler distribution under either bottom injection or side injection. The atomisation conditions are given in each panel (n = 3.12 and $\dot{m}_A/\dot{m}_L = 2.68$). n and $\dot{m}_A/\dot{m}_L$ indicate the size distribution parameter in the Rosin-Rammler function and atomizer gas to liquid mass ratio respectively.

6.6 Bio-oil gasification in fluidised-bed gasifier

For the simulation of bio-oil gasification, this study considers the geometry (height of 800 mm and inner diameter of 78 mm) of a fluidised-bed reactor in a previous study[35] that considered various experimental parameters (see Table 6-4). Three different side injections were defined by fitting the experimental data to the Rosin-Rammler equation with maximum droplet diameter around $150\ \mu m$ as shown in Figure 6-1.

6.6.1 Model validation: Comparison between model prediction and experimental data

Validation of current model have been done by comparison of simulation results and experimental data over a wide range of operating conditions reported by Sakaguchi[35] and summarised in Table 6-4. In this table the operation conditions of bio-oil steam gasification in fluidized bed reactor are classified by temperature, steam-to-carbon ratios (H_2O /C), and methane-equivalent gas hourly space velocity (G_{C1}HSV), and injection characteristics. In addition, the simulated cases are denoted by gasifier temperature such as1020_B.

Figure 6-9 shows the experimental data and model predictions on the syngas products at the reactor exit at 1063 K (see case 1063_B in Table 6-4). In this figure, the molar percentage was reported on both wet-basis (including N_2) and dry-basis. However, more efficient comparison has been done on dry-basis because of the large variations of gas compositions on wet-basis. Therefore, to provide more comparison with the available experimental data, several simulation results at different operating conditions (see Table 6-4) were reported in Figure 6-10 on dry basis. In this figure, the molar percentage of the outlet gas mixture was reported, using the surface integrals by selecting area-weighted average of species in Fluent.

- Panels A to C compare the syngas gas compositions at various temperatures (corresponding to the operating conditions in Table 6-4). The results clearly show that the simulation results and the experimental data are broadly in good agreements.

- Panel D compares the H_2/CO ratio of the syngas under various operating conditions. It can be seen that the predictions are in good agreements with experimental data and the H_2/CO ratio of the product gas at the reactor exit increases with increasing temperature.

- Figure 6-10E also shows that the predicted cold gas efficiency (CGE) is in good agreement with the CGE calculated based on the experimental data.

- Finally, the model predictions and experimental data on carbon conversion are also very close, as shown in Figure 6-10F.

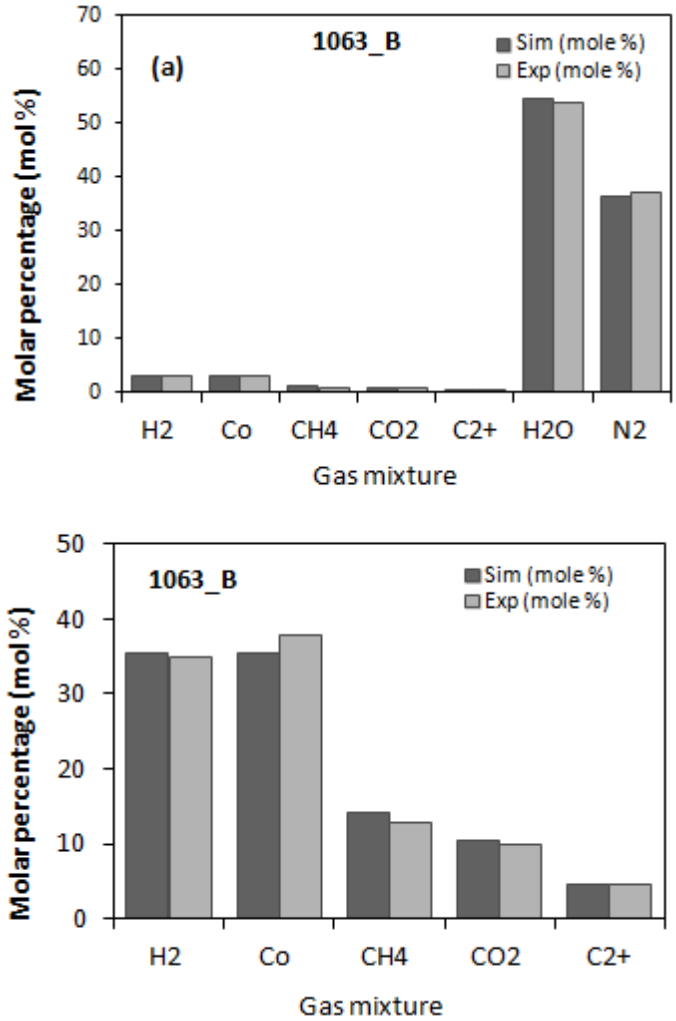

Figure 6 - 9: Simulation result of molar percentage of syngas (H_2+CO), CO_2, C_2^+ and CH_4 with operating conditions: T = 1063.15 K, mole H_2O/mole C = 5.446, GC1HSV = 331.81 m3/m3 (Run name 1063_B in Table 6-4): (a) Dry-basis; (b) Wet-basis

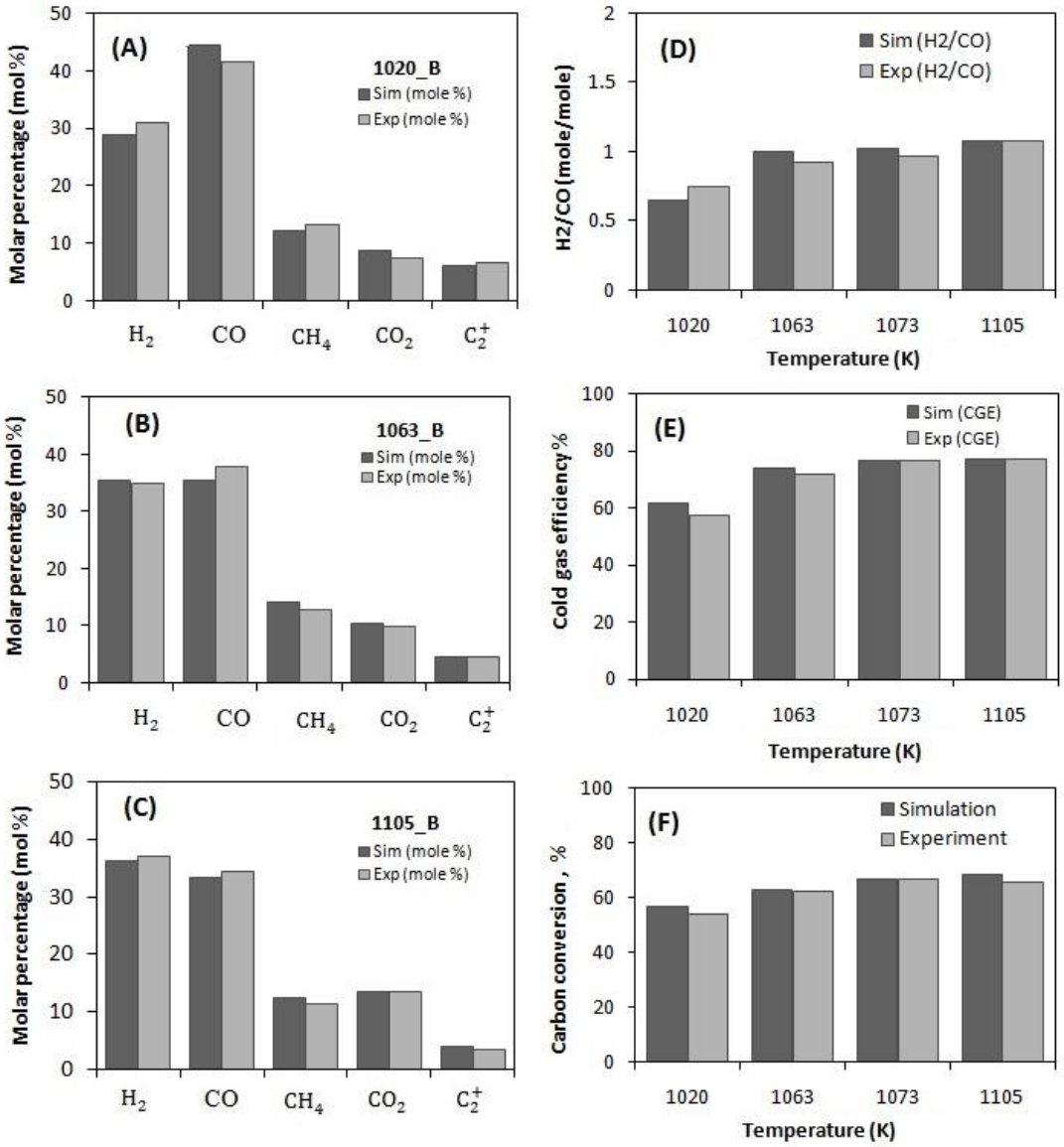

Figure 6 - 10: (A), (B) and (C) Simulation result of molar percentage of syngas (H_2+CO), CO_2, C_2^+ and CH_4 at different operating conditions (Run name 1020_B to 1105_B in Table 6-4) at reactor exit for bio-oil side injection on dry-basis. Comparison of simulation and experimental result at reactor exit at different operation conditions: H_2O/C between 2.7 and 7.5, $G_{C1}HSV$ =215 and 424 h^{-1} and 1020 to 1105 K for temperature differences for (D) the ratio of H_2/CO, (E) Cold gas efficiency and (F) Carbon conversion.

Table 6- 4:Different operating conditions of bio-oil steam gasification in fluidized bed reactor[35]

Run name	Temperature	H_2O /C	$G_{C1}HSV$	Discrete phase flow rate	Injection velocity magnitude[a]	Mass source of steam and nitrogen	Mole fraction of N_2 inlet
	K	*mole/mole*	h^{-1}	*kg/s*	*m/s*	*kg/s*	*mole %*
1020_B	1020.15	5.225	338.53	7.12E-05	85.4	4.63E-04	58.2
1053_B	1053.15	5.402	423.73	8.90E-05	94.5	5.23E-04	64.9
1063_B	1063.15	5.446	331.81	6.97E-05	85.7	4.63E-04	59.4
1073_B	1073.15	5.833	215.23	4.52E-05	75.4	3.95E-04	50.5
1079_B	1079.15	2.675	338.53	7.10E-05	85.7	3.40E-04	40.4
1081_B	1081.15	7.451	343.02	7.20E-05	85.7	5.64E-04	67.7
1105_B	1105.15	5.718	334.05	7.00E-05	85.7	4.73E-04	61.2

"a" Estimated in this study (see Appendix A)

6.6.2 Prediction of the cold gas efficiency (CGE)

Figure 6-11 presents the effect of temperature, hourly space velocity and H_2O /C on CGE. Figure 6-11a shows that the CGE increases with temperature, reaches to the maximum (at 1083K) then levels off with further increasing temperature. As per reactions scheme (R1-R13), R1-R8 are mainly responsible for the generation and consumption of syngas (H_2 +CO) under the operating conditions. The thermal decomposition reaction (R1) is fastest and it proceeds first rapidly to consume the bio-oil and produce gas which consists mostly of H_2 and CO. The contribution of tar steam reforming reaction (R2) to syngas (H_2+CO) is insignificant because the tar concentration is low (~1.5 wt%) after R1 and also the steam reforming of tar (R2) is a slow reaction at 1020 – 1105K. The Boudouard reaction (R3) also is very slow reaction and with very small concentration of CO_2 atmosphere (around %1) is even much more slow reaction. For the reset of reactions (R5-R8), under the reactions conditions, the relative reaction rates of coke gasification reaction (R3), methane reforming reaction (R7) and C_2^+ (represented by C_2H_6) steam reforming reactions (R8) over water gas shift reaction (R6) are 1.5E-10, 3E-3 and 5E-3, respectively. In other words, R6 is much faster than R5, R7 and R8. As a result, an initial increase in reactor temperature increases R1 and the forward water gas shift reaction (R6) resulting in increasing conversion of chemical energy of the bio-oil into the product gas hence increasing cold gas efficiency. However, further increase in temperature leads to the level-off of the CGE because the enhanced reaction R6 to shift towards reactants ($\text{more CO and less } H_2$). Figure 6-11b also shows that the CGE reduces continuously as the gas hourly space velocity increases, mainly due to less production of syngas gas as a result of reduced residence time of feedstock in the reactor. Figure 6-11c shows that the CGE is almost insensitive to H_2O /C ratio. This can be explained by the opposite effect of H_2O / C on CGE via the two significant reactions (R1 and R6). On one hand, increasing H_2O / C ratio decreases the resident time of feedstock in the reactor hence leads to decreased CGE. On the other hand, increasing H_2O /C ratio increases the rate of forward reaction R6 to produce more H_2 hence increase CGE. Figure 6-11c suggests the two opposite effects cancel each other and result in CGE being insensitive to the H_2O / C ratio (in the range of 2.5–8.5).

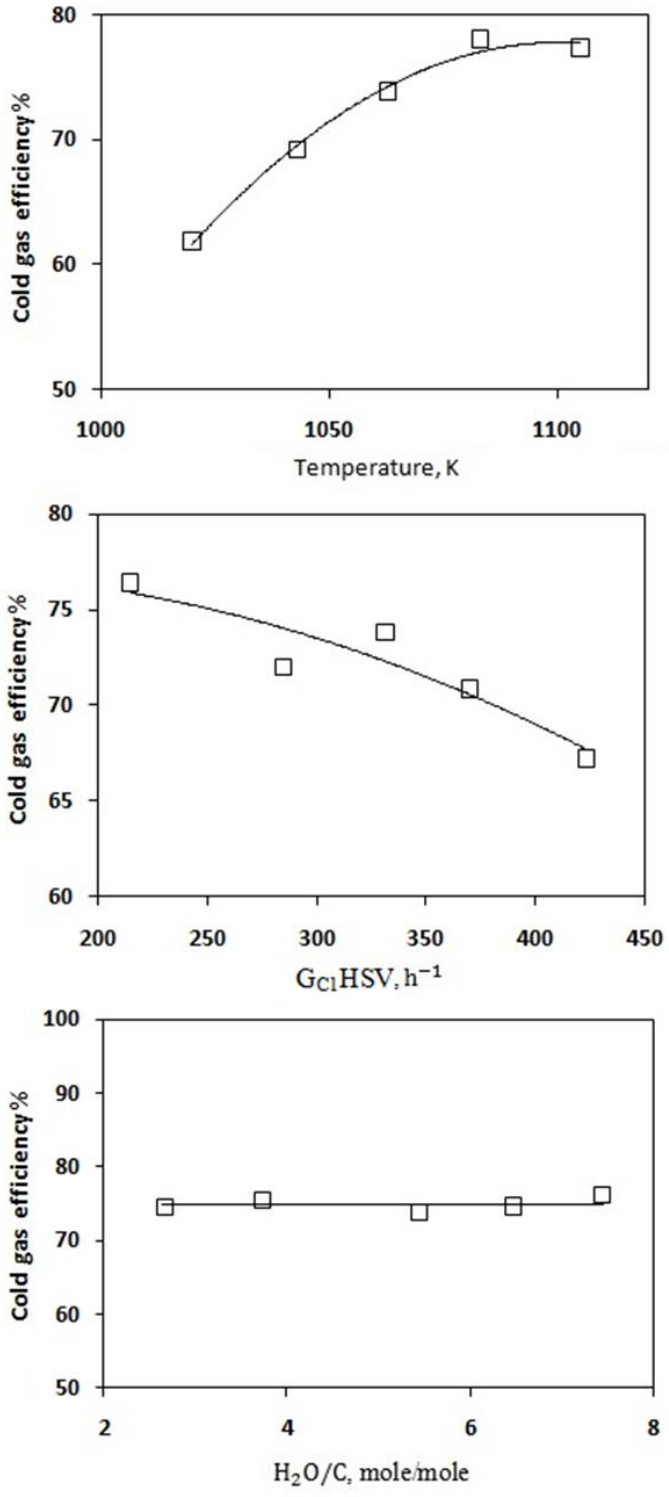

Figure 6 - 11: Model predictions on the effect of operating temperature, $G_{C1}HSV$ and H_2O/C ratio on cold gas efficiency (CGE) during bio-oil steam reforming under side injection conditions.

6.6.3 Prediction of the chemical species distribution

Figures 6-12 to 6-16 illustrates the simulated Z-Y surface plane (X = 0) distribution of the molar concentration of syngas (H_2, CO, CO_2 and CH_4) in the fluidized bed reactor at T = 1063 K, H_2O / C = 5.446, and G_{C1}HSV = 331.81h^{-1}. It can be seen that upon the injection of bio-oil into the gasifier, the concentrations of all gases increase significantly due to the bio-oil thermal decomposition reaction (R1). The production of syngas are in transient state till 4.40 sec after which when the concentrations of each gas product in the syngas reaches steady state and remain almost constant in the gasifier. It is also evident that the molar concentration of CH_4 is mainly non-uniform at the gasifier bottom (i.e. near the range close to the bio-oil injection point) where the bio-oil thermal decomposition reaction mainly takes place.

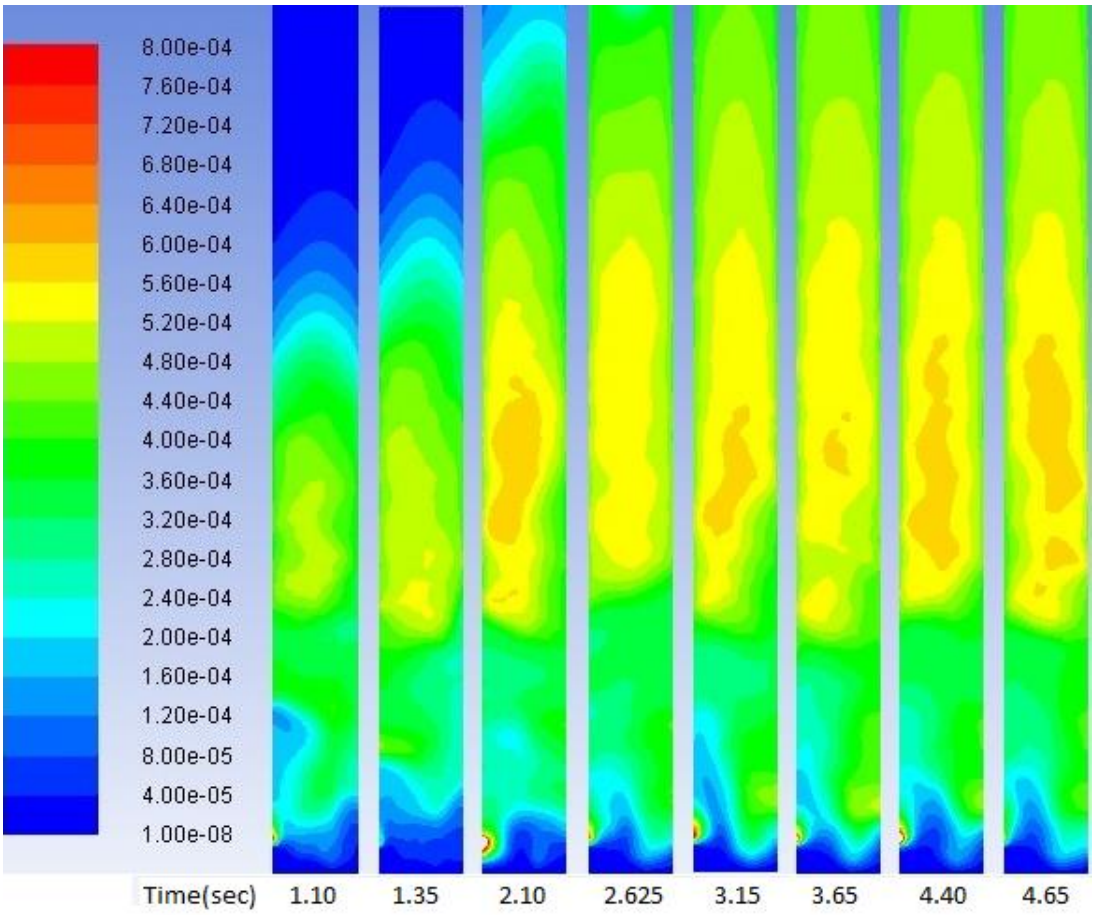

Figure 6 - 12: Simulation results of bio-oil side injection for Z-Y surface plane (X = 0) molar concentration distribution of H_2 with operating conditions: T = 1063 K, mole H_2O/mole C = 5.446, G_{C1}HSV = 331.81 h^{-1} (Run name 1063_B in Table 6-4)

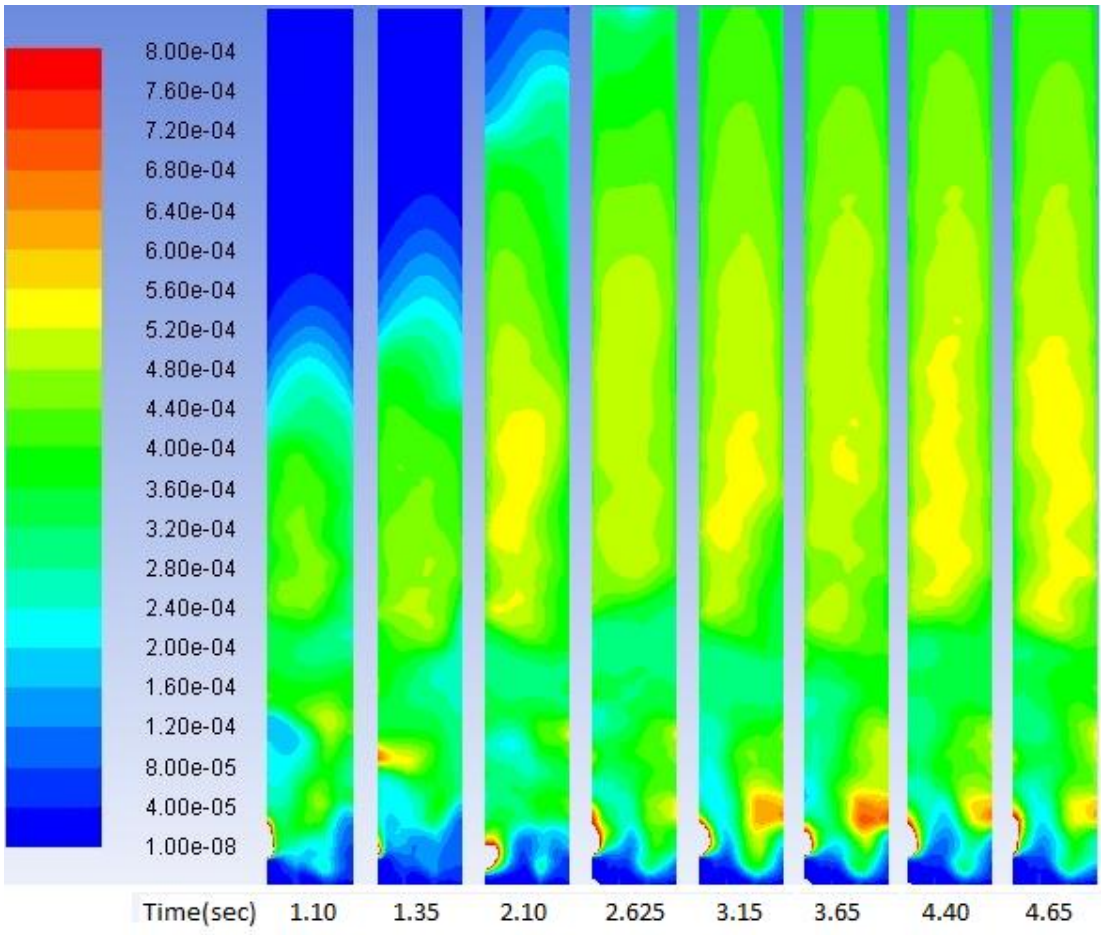

Figure 6 - 13: Simulation results of bio-oil side injection for Z-Y surface plane (X = 0) molar concentration distribution of CO with operating conditions: T = 1063 K, mole H_2O/mole C = 5.446, G_{C1}HSV = 331.81 h^{-1} (Run name 1063_B in Table 6-4)

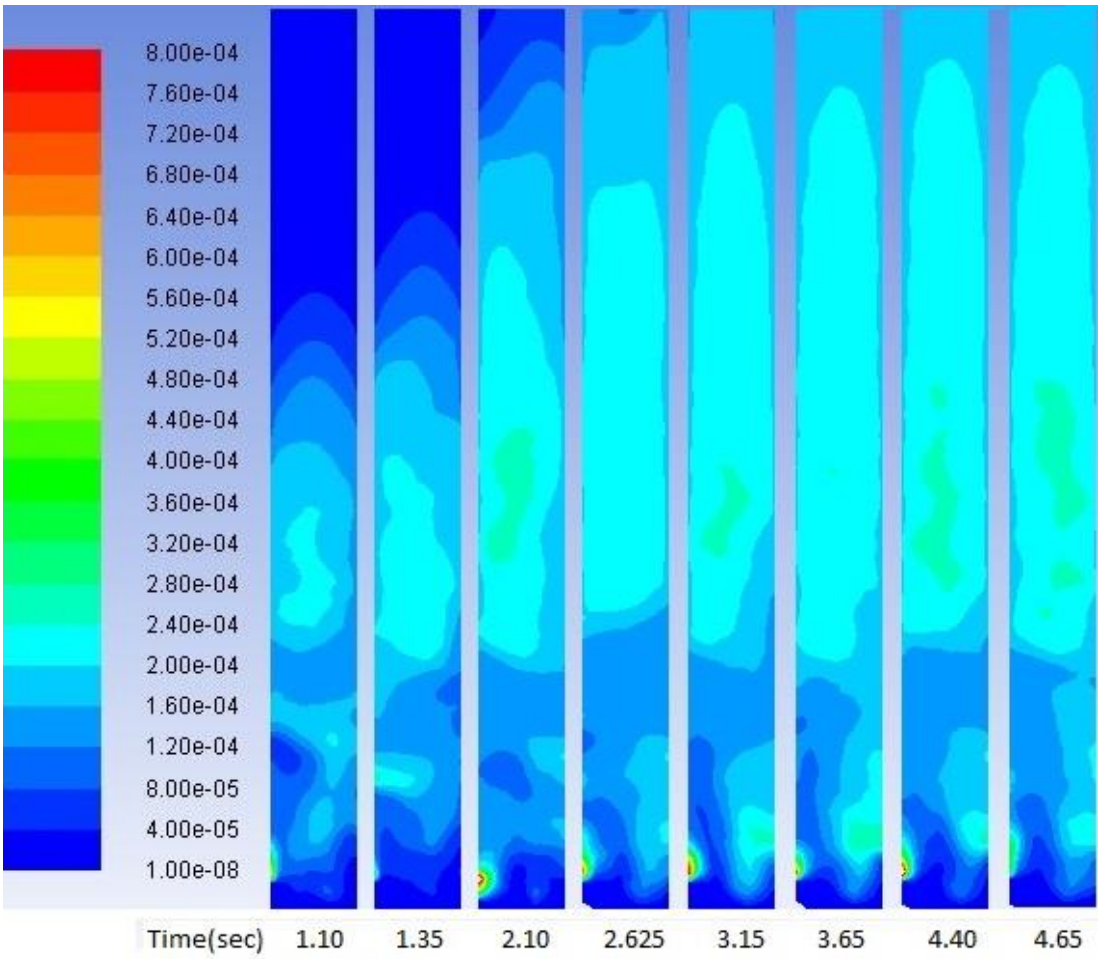

Figure 6 - 14: Simulation results of bio-oil side injection for Z-Y surface plane (X = 0) molar concentration distribution of CH_4 with operating conditions: T = 1063 K, mole H_2O/mole C = 5.446, G_{C1}HSV = 331.81 h^{-1} (Run name 1063_B in Table 6-4)

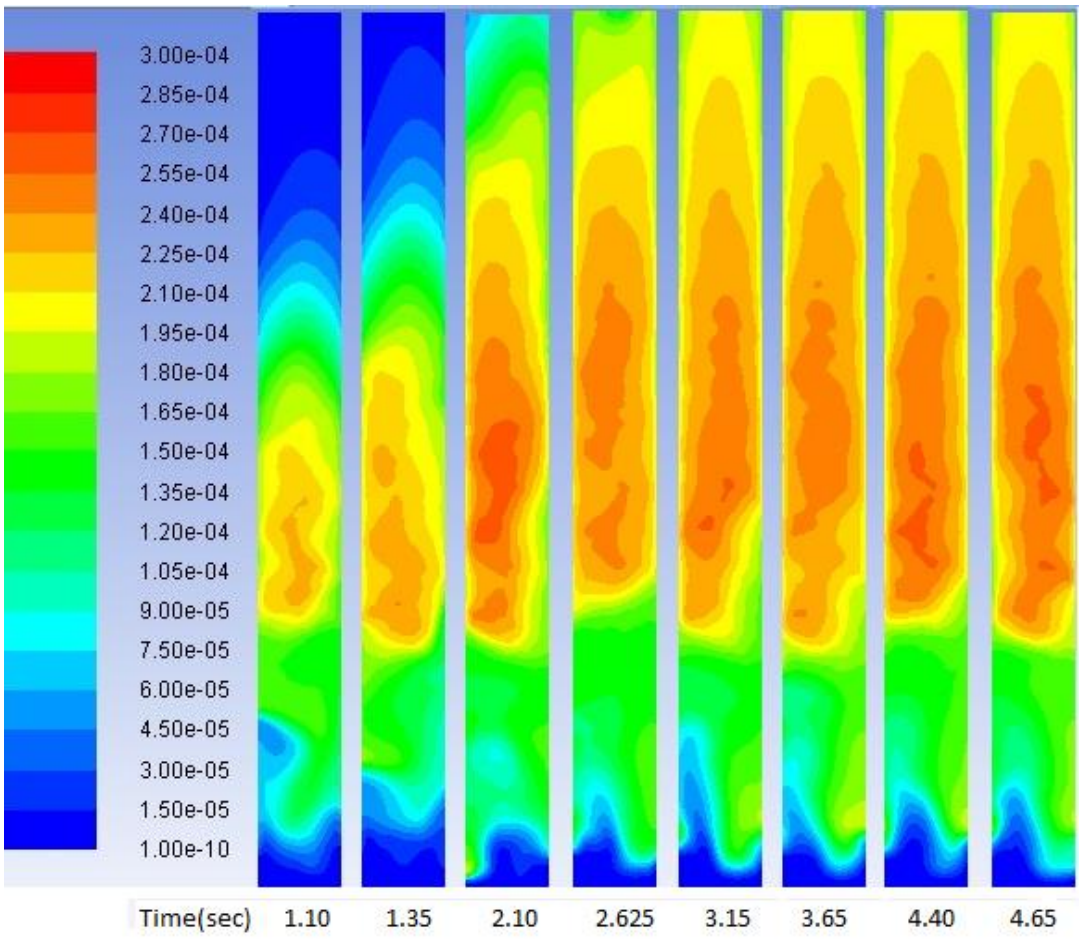

Figure 6 - 15: Simulation results of bio-oil side injection for Z-Y surface plane (X = 0) molar concentration distribution of CO_2 with operating conditions: T = 1063 K, mole H_2O/mole C = 5.446, G_{C1}HSV = 331.81 h^{-1} (Run name 1063_B in Table 6-4)

6.6.4 Effect of temperature, space velocity of feed, and steam to carbon feeding ratio on product gas yields

Figures 6-16 to 6-18 present the sensitivities of carbon (in forms of CO, CO_2, CH_4 and C_2^+) and hydrogen (in forms of H_2, CH_4 and C_2^+) yields against temperatures, space velocity (G_{C1}HSV) and steam to carbon feeding ratio (H_2O/C). Figures 6-16 indicates the carbon and hydrogen yield at various temperatures with constant G_{C1}HSV and H_2O/C of 334.8 and 5.5 respectively. An increase in temperature from 1020 to1063 K leads to an increase in carbon and hydrogen yields around 10.8% and 35%, respectively. This is largely due to the enhanced thermal decomposition of bio-oil (resulting in higher total carbon conversion to gas) and water-gas shift reaction (R6). Further increase in temperature from 1063 to 1105 K leads to limited increase in the yields of carbon and hydrogen by 9.5% and 6.2%, respectively. The yield of

carbon is more sensible than hydrogen yield in the increase because the water gas shift reaction (R6) is sensitive to temperature and has a tendency to shift towards left side as temperature increases. As shown in Figures 6-17, an increase in the G_{C1}HSV from 215.2 to 331.8 h^{-1} at given temperature and H_2O/C ratio (1073 K and 5.6, respectively) results in a reduction in the total conversion by 9.8%. Such reduction is further increased to 16.1% when the G_{C1}HSV increases further from 331.8 to 423.7. This is largely because an increased G_{C1}HSV leads to lower residence time of bio-oil droplets hence reduced conversion in the gasifier. Figures 6-18 further shows that at given temperature and G_{C1}HSV (1073 K and 337.8 h^{-1}, respectively), an increase in H_2O/C ratio from 2.7 to 5.45 results in limited changes in carbon and hydrogen yields. However, as the H_2O/C ratio increases further from 5.45 to 7.45 the carbon yield reduced by 11.2% while the hydrogen yield increases by 9.6%. This can be mainly contributed to the enhanced water-gas shift reaction (R6) for increased hydrogen production.

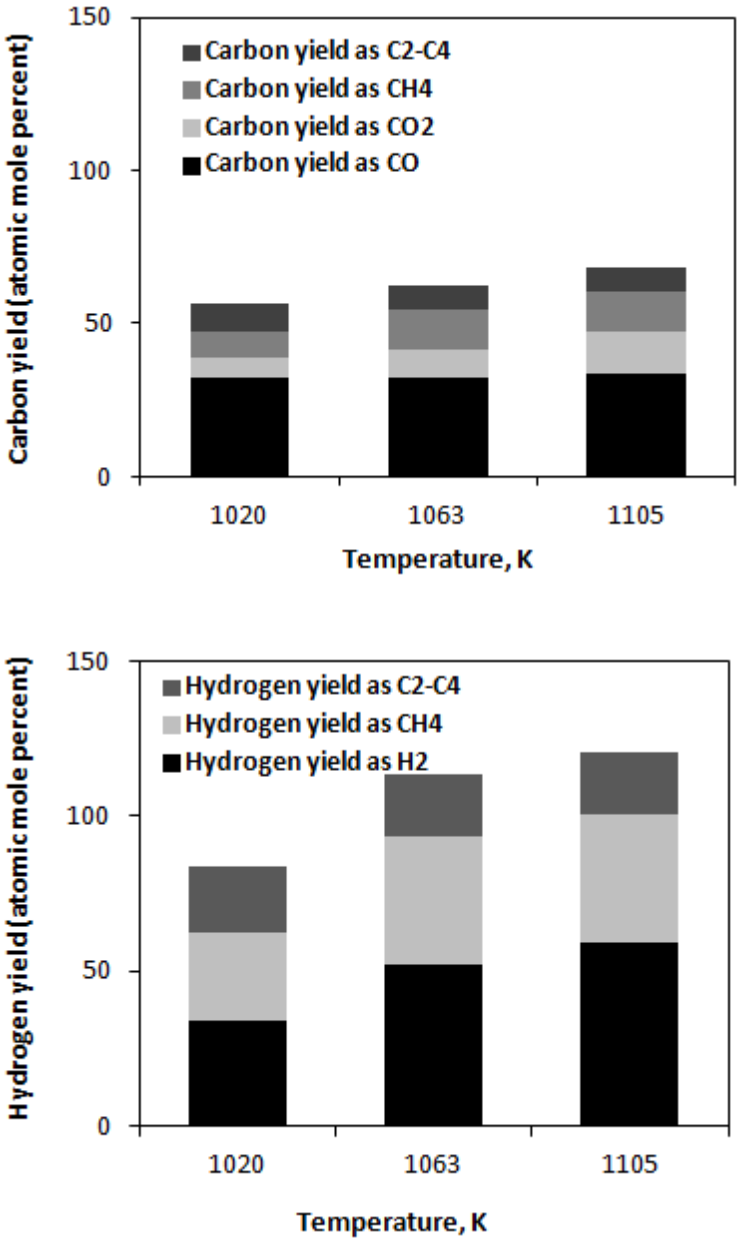

Figure 6 - 16: Simulation results for effect of temperature with $H_2O/C \cong 5.5$ and $G_{C1}HSV \cong 334.8 h^{-1}$ on carbon yield (CO, CO_2, CH_4 and C_2^+) and hydrogen yield (H_2, CH_4 and C_2^+) under dry feedstock basis.

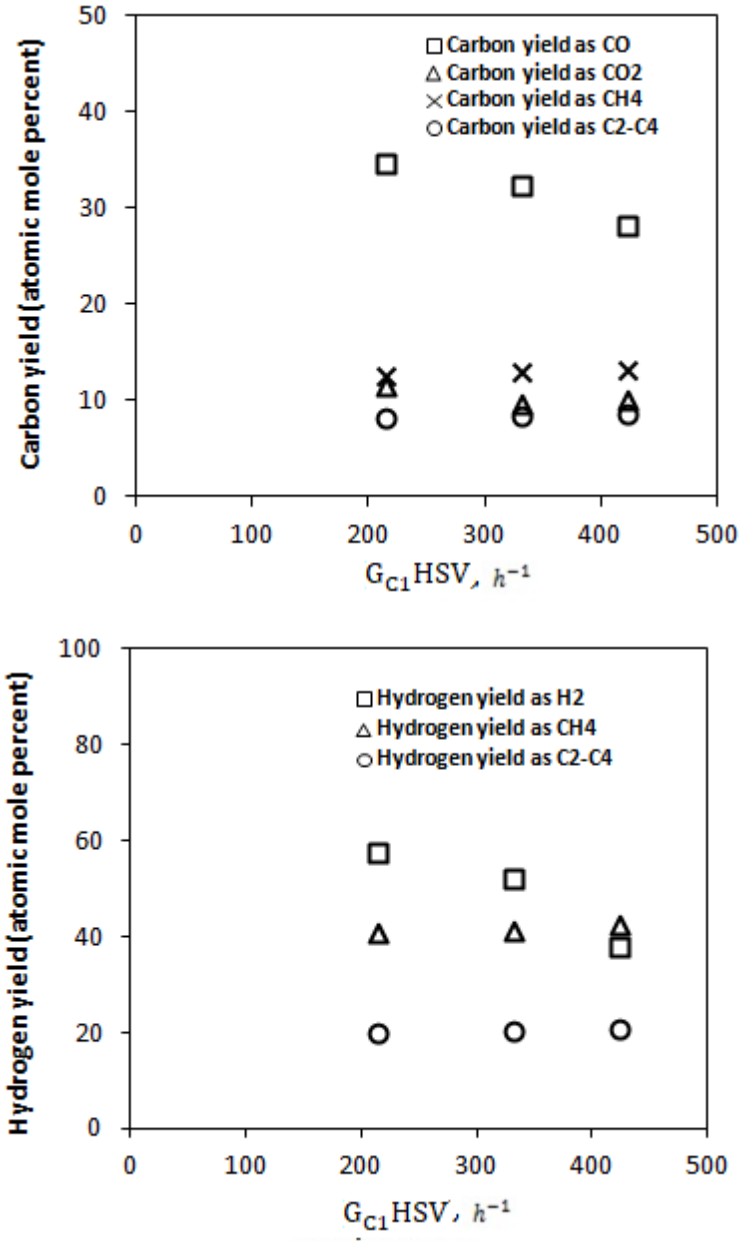

Figure 6 - 17: Simulation results for effect of space velocity of feed ($G_{C1}HSV$) with $H_2O/C \cong 5.6$ and $T \cong 790$ on carbon yield (CO, CO_2, CH_4 and C_2^+) and hydrogen yield (H_2, CH_4 and C_2^+) under dry feedstock basis.

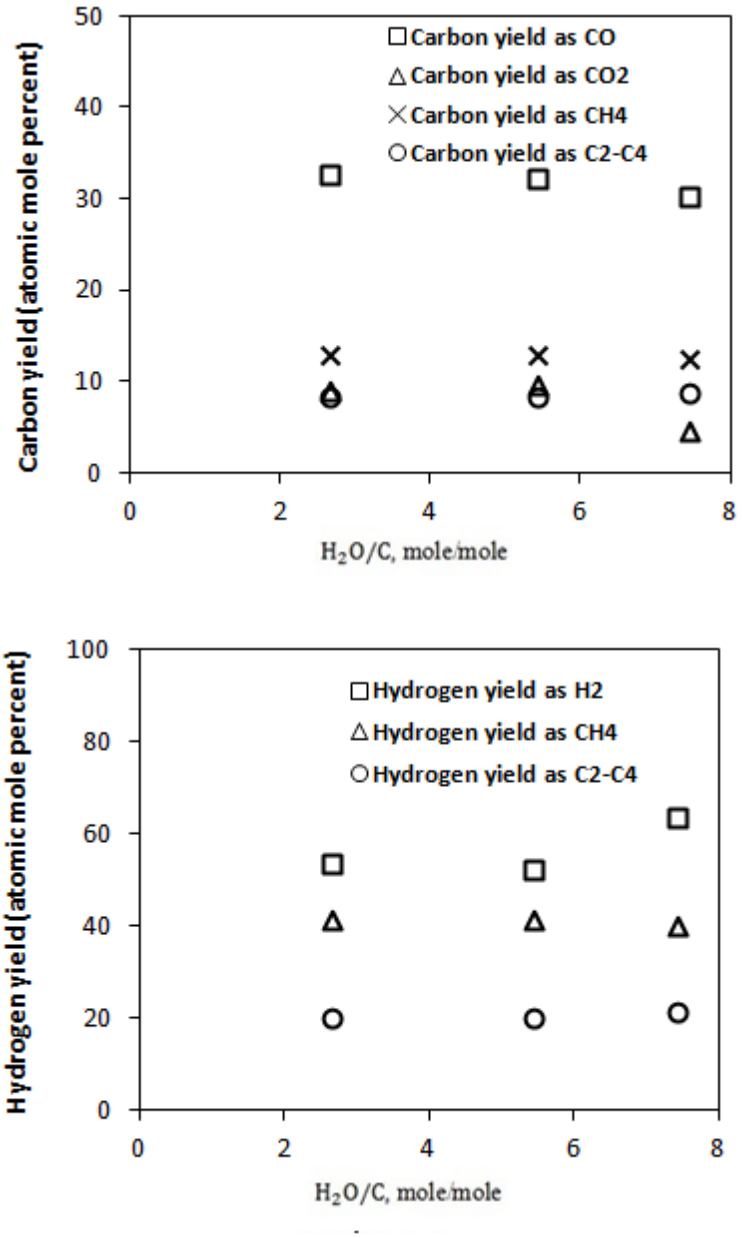

Figure 6 - 18: Simulation results for effect of H_2O /C with $T \cong 1073\ K$ and $G_{C1}HSV \cong 337.8 h^{-1}$ on carbon yield (CO, CO_2, CH_4 and C_2^+) and hydrogen yield (H_2, CH_4 and C_2^+) under dry feedstock basis.

6.7 Summary

A three-dimensional CFD model was developed to simulate bio-oil gasification in a fluidized bed reactor. The model takes into account three-phase hydrodynamics, heat and mass transfer, droplet atomisation, droplet vaporization and thermal decomposition in a gas–solid flow. Several user-defined functions (UDFs) have been developed for the model. The experimental data in Chapter 5 have been incorporated into the model to generate the Rosin-Rammler distribution function for different

injection conditions. The CFD is capable of predicting the synthesis gas product composition at different bed temperatures, steam-carbon molar ratios, methane equivalent gas hourly space velocity ($G_{C1}HSV$) of feed and the sizes of droplets injected into the gasifier. The simulation shows that an increase in gasification temperature leads to an increase in the hydrogen and carbon yields and fuel conversion during bio-oil gasification. This is largely due to enhanced thermal decomposition and water-gas shift reactions. It is also clearly demonstrated that the droplet size has a significant effect on droplet residence time and fuel conversion.

CHAPTER 7: MODELLING OF BIOSLURRY STEAM GASIFICATION IN A FLUIDIZED BED REACTOR

7.1 Introduction

Biosulrry is mixing of bio-oil and biochar,[14-16] produced from distributed pyrolysis located in or near the biomass growth areas. The excellent grindability and desirable particle size of biochar[14] have enabled it to be mixed with bio-oil to produce bioslurry, while the direct use of biomass as a fuel addresses multiple disadvantages such as low energy density, high transportation cost, and poor grindability.[14] As was discussed in Chapter 2 (literature review) a simplified assumption was made, only for the purpose of the maximum feedstock conversion calculation with the equilibrium model. However, as analysed in the previous section, the equilibrium limitation for bio-oil gasification is not likely to occur in a realistic gasifier, and also the bioslurry, prepared from suspending of fine biochar particles into bio-oil at 20 wt%, might operate in the far-from-equilibrium system. A non- equilibrium model which considers transport processes such as the heat and mass transfer of the particles inside the gasifier; where the heterogeneous reaction rates, and hence particle diameters may play a major role during bioslurry conversion into product gas.

In Chapter 6 the three-dimensional CFD model was developed to simulate bio-oil gasification in a fluidized bed reactor (the spray were produced by twin-fluid atomizer, considered to be exactly, what Sakaguchi [35] used to spray bio-oil and bioslurry). The model takes into account three-phase hydrodynamics, heat and mass transfer, droplet atomisation, droplet vaporization and thermal decomposition in a gas–solid flow. The synthesis gas product composition at different bed temperatures, steam-carbon molar ratios, methane equivalent gas hourly space velocity ($G_{C1}HSV$) of feed was predicted.

Therefore, the objective of Chapter 7 is to propose a flow simulation for bioslurry injected into a reactor by the twin-flow atomizer and calculate flow characteristics such as the outlet gaseous concentration by the ANSYS-Fluent software, in regard to the forth research objective outlined in Chapter 2. Furthermore, the impact of alkali and alkaline earth metallic (AAEM) species on the reaction rate of biochar

gasification is considered because it might play a significant role on gasification result in terms of validation with experimental data. Finally, a series of simulations are necessary to investigate the contributions of different variables on total feedstock conversion and product gas composition.

7.2 Methodology

The bioslurry gasification model is based on the previous model simulation for bio-oil as discussed in Chapter 6. During the complementation of this model for bio-slurry application, the main assumption was made. The mathematical model simulation of bioslurry gasification in a fluidized bed reactor includes two parts: the bio-oil and biochar injection at the same time in order to represent bioslurry injection. This assumption is reasonable due to higher vaporization rate of bio-oil against the steam reforming of char. The first part includes the bio-oil model vaporization and gasification which was presented and validated in Chapter 6 and the second part is biochar trajectory calculation with heat and mass transfer and its interaction with continues phase. The principle of bio-char particles trajectory calculation is the same as bio-oil droplets and it is applicable for any type of particle, including solid particles such as biochar. However, the UDF code for trajectory calculation with heat and mass transfer (steam reforming of char), and the code for updating the source terms of continues phase are different.

7.2.1 Bioslurry injection in fluidized bed reactor

As discussed in section 6.2.1.1, the mathematical function for droplet size in spray was presented by the Rosin-Rammler distribution function (see Equation 6.1) for bio-oil injected by the twin-fluid atomizer. The same calculation was done for bioslurry and the result for the Rosin-Rammler parameters indicated in Figure 7-1. This figure shows the particles size distribution data for bioslurry with gas to liquid mass ratio ($\dot{m}_G/\dot{m}_L$) equal to 4.15. The Rosin-Rammler parameters, including droplet mean diameter (when Q≈0.368) and spread parameter were obtained at $\overline{D}_d = 130.27\ \mu m$ and $n = 2.76$ respectively. These parameters were used to set up bioslurry injection in Fluent Discrete Phase Model (DPM).

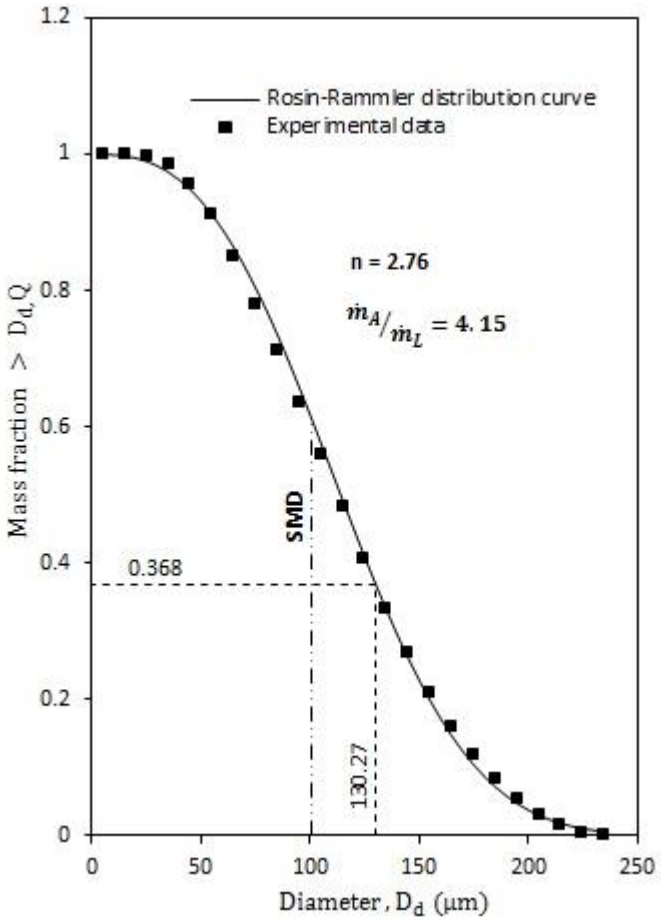

Figure 7- 1: Comparison between experimental data and fitted curved using Rosin-Rammler equation for the cumulative size distribution of spray droplets generated by the atomisation of bioslurry using twin-fluid atomizer with n =2.76 and $\dot{m}_A/\dot{m}_L = 4.15$, indicate the size distribution parameter in the Rosin-Rammler function and atomizer gas to liquid mass ratio respectively.

7.2.2 Conservation equations of flow field (continuous phase) and bioslurry trajectory calculation

The continuity, volume fraction and momentum equations for gas and solid phase in fluidized bed reactor are based on the previous model simulation for bio-oil as discussed in Chapter 6 equations 6.2 to equations 6.26.

Lagrangian discrete phase model was employed for tracking bioslurry droplets, considering interactions between droplets and flow field via interphase exchange of momentum, heat, and mass transfer. In this model, droplet is moved along its trajectory, which is based on integrating the particle equation of motion. Interactions

between droplet and flow field are computed due to the interphase exchange of momentum, heat, and mass transfer. The details were discussed in Chapter 6.

7.2.3 Reaction scheme

In this study, a simplified model is defined for the gasification of bioslurry in the fluidized bed reactor. It is assumed that the char steam reforming takes place at the same time as the onset of bio-oil vaporization. This simplifying assumption appears reasonable because the rate of bio-oil vaporization is too fast as discussed in chapter 6.

During steam gasification of bioslurry, the following reaction scheme (R1–R15) is considered for modelling of bio-oil gasification:

$$\text{Bio} - \text{oil} \rightarrow \mathrm{C_xH_yO_z} + \text{ gas } (\mathrm{H_2}, \mathrm{CO}, \mathrm{CH_4}, \mathrm{C_2^+} \ldots) + \mathrm{C_s} \quad \text{(R1)}$$

$$\mathrm{C_xH_yO_z} + (\mathrm{x} - \mathrm{z})\mathrm{H_2O} \rightarrow \mathrm{xCO} + (\mathrm{x} + \mathrm{y}/2 - \mathrm{z})\,\mathrm{H_2} (\text{tar steam reforming}) \quad \text{(R2)}$$

$$\mathrm{C_s} + \mathrm{CO_2} \rightarrow 2\mathrm{CO} \quad \text{(R3)}$$

$$\mathrm{CH_4} + \mathrm{CO_2} \leftrightarrow 2\mathrm{CO} + 2\mathrm{H_2} \quad \text{(R4)}$$

$$\mathrm{C_s} + \mathrm{H_2O} \rightarrow \mathrm{H_2} + \mathrm{CO} \quad \text{(R5)}$$

$$\mathrm{CO} + \mathrm{H_2O} \leftrightarrow \mathrm{CO_2} + \mathrm{H_2} \quad \text{(R6)}$$

$$\mathrm{CH_4} + \mathrm{H_2O} \leftrightarrow \mathrm{CO} + 3\mathrm{H_2} \quad \text{(R7)}$$

Reaction R1 is bio-oil thermal decomposition. An empirical formula $\mathrm{CH_mO_n}$ is considered for bio-oil, with m and n equal to 2.03 and 0.88, respectively.[17] The activation energy, pre-exponential factor and reaction order for R1 are taken as $45.2\ \mathrm{kJ/mol}$ and $459.4\ \mathrm{s^{-1}}$, and 3.8 respectively. [127] The yield and properties of tar product in R1 is based on experimental data,[128] which is dependent on reactor temperature. The tar product further reacts with steam for reforming reaction (Reaction R2), considering activation energy and pre-exponential (for temperature range of 700-1400℃) equal of $350\ \mathrm{kJ\ mol^{-1}}$ and 1.7E14 $m^{0.3}mole^{-0.1}s^{-1}$, respectively. [129].

For C_2^+ that is produced via R1, ethane is selected to represent C_2^+ in order to simplify the modelling. Steam reforming of ethane is modelled via a series of reactions (R8 to R13) outlined previously [130-133] with kinetics being reported elsewhere. [134]

$$C_2H_6 + 2H_2O \leftrightarrow 2CO + 5H_2 \quad \text{(R8)}$$

$$C_2H_6 \leftrightarrow C_2H_4 + H_2 \quad \text{(R9)}$$

$$C_2H_6 + C_2H_4 \rightarrow C_3H_6 + CH_4 \quad \text{(R10)}$$

$$C_3H_6 \leftrightarrow C_2H_2 + CH_4 \quad \text{(R11)}$$

$$C_2H_4 + C_2H_2 \rightarrow C_4H_6 \quad \text{(R12)}$$

$$2C_2H_6 \rightarrow C_3H_8 + CH_4 \quad \text{(R13)}$$

The Boudouard reaction rate (R3) can be considered by equation (6.51).

The CO_2 reforming of CH_4 (R4) is considered with the activation energy and pre-exponential factor $217.9\ \mathrm{kJ/mol}$ and $14639\ \mathrm{s^{-1}}$ respectively. [137] The production of char (C_s) in R1 is temperature dependent [42]. Steam reforming of C_s (R5) is modelled based on the n-th order kinetic model, with the activation energy, pre-exponential factor and reaction order being $235\ \mathrm{kJ\ mol^{-1}}$, $6.5\mathrm{E}05\ \mathrm{s^{-1}Pa^{-0.41}}$, and 0.41, respectively. [35] Water-gas shift reaction (R6) and steam reforming of methane (R7) are considered, with the equations of (6.52) and (6.53) respectively.

The bioslurry gasification model also incorporates another reaction, including char steam reaction as shown by the following equation.

$$\mathrm{Char} + H_2O \rightarrow CO + H_2 \quad \text{(R14)}$$

Reaction R14 is Char steam gasification. The char represents the elemental formula of carbon, considered for simplification. The kinetic parameters of char gasification (R14), reported by M. Sakaguchiet.al.[35] was considered with the *n*-th order kinetic model. In their model the kinetic parameters, including activation energies (E), frequency factors (A), and reaction order (n) determined for the char resulted from bioslurry gasification (called slurry char) and was compared to the original char.

Therefore, the following description refers to kinetic parameter of slurry char, employed in this study.

The overall char reaction rate, considered to be controlled only by steam pressure and temperature between 800 and 1000℃is given by the following n-th order reaction kinetic:

$$r = kP_{H_2O}^{n} \quad (7.1)$$

In above equations r, P_{H_2O}, n, and k are reaction rate (s^{-1}), steam pressure (Pa), reaction order, and rate constant ($s^{-1}Pa^{-n}$) respectively. In addition, the rate constant (k), depends on temperature, (T), frequency factor (k_0), and activation energy (E) with the Arrhenius' equation.

$$k = k_0 \exp(-\frac{E}{RT}) \quad (7.2)$$

The activation energy, and pre-exponential factor, and reaction order were reported [35] in the range of $218E6$ (J/kmol), 2.7E5 ($s^{-1}Pa^{-0.34}$), and 0.34 respectively.

However, the interactions between char and volatiles during gasification can generate abundant radicals occupying the char surface. During pyrolysis and gasification, the volatile–char interactions could cause drastic volatilisation of alkali and alkaline earth metallic (AAEM) species (especially Na) largely due to the (H) radicals from volatiles, [57, 60-62] which might otherwise serve as excellent catalysts for char gasification. Studies conducted by Wu and Li [57-59] shows that the interactions between the volatiles and char particles enhanced the volatilization of AAEM species. Meanwhile, the activity of AAEM species was deeply dependent on the interaction between AAEM species and char structure. This is not necessarily but might be attributed to the effect of AAEM species on char steam reforming reaction.

Steam gasification of char

$$\text{Char} + H_2O \xrightarrow{\text{AAEM species}} CO + H_2 \quad (R15)$$

This catalyst effect of AAEM species on the above reaction was considered by lowering its activation energy to speed up the rate of a chemical reaction in order to predict accurate results for bioslurry steam gasification. For this purpose, multiple

simulations, using different activation energy were run to find out the activation energy, which would result in a valid product gas composition and total bioslurry conversion. Therefore, the activation energy, considering catalyst effect of AAEM species reduces from $218E6$, to $135\mathrm{E}6$ $(\mathrm{J/kmol})$ (around 38% reduction).

7.3 Numerical method

7.3.1 Initial conditions, boundary conditions and numerical scheme

In this chapter, all calculations are performed on the fluidized bed reactor with the same geometry and grid specification, presented in Chapter 3 and 6 (see Sections 3.5.1.1and 6.3.1). At the inlet, the velocity, temperature and species mole fraction for a binary mixture of steam and nitrogen gas are specified. The pressure outlet boundary condition is used at the outlet with temperature, species mole fraction, and back flow quantities (backflow turbulent intensity at 10% and backflow hydraulic diameter at 0.077 m) specifications. As in the case of the convergence minimization problem, the inlet operating conditions is used as a first guess for outlet boundary condition because the details of the flow temperature and species mole fraction at the outlet are not known prior to the solution. In the next step, the stationary wall boundary condition is maintained at inlet temperature and the specified shear at zero is assumed. Finally, the bioslurry inlet is specified in the setup injection of Fluent Discrete Phase Model (DPM).

Initially, the bed material is adapted with the volume fraction of 0.598 and velocity equal to zero. The simulations are implemented in three dimensions with transient calculation and first and second order upwind discretisation schemes (for more detail on numerical scheme see the section 6.3.2 in Chapter 6).

7.4 Evaporation of single bioslurry droplet

The vaporization model is based on the assumption was made to reduce the complementation of this model for bio-slurry application. Due to the higher vaporization rate of bio-oil against the steam reforming of char, the bio-oil vaporization and char steam reforming start at the same time during the injection of bioslurry in the fluidized bed reactor. The bio-oil vaporization model has been discussed in the previous chapter (section 6.4.2) and the results are applicable for

bioslurry vaporization. Biochar trajectory calculation with heat and mass transfer and its interaction with continues phase considered during bio-oil vaporization.

7.5 Bioslurry gasification in fluidised-bed gasifier

For the simulation of bioslurry gasification, this study was carried out to predict the change of product gas yields when all variables are constant except one, in order to determine the contributions of each variable on the result. Table 7-1 shows a wide range of operating conditions, determined for simulation of bioslurry. In this table the operating conditions are presented by temperature, steam-to-carbon ratios (H_2O /C), methane-equivalent gas hourly space velocity ($G_{C1}HSV$), injection characteristics, and gaseous species in the inlet. In addition, depending on the selected variable, the fuel type, and range of variables, the run name is denoted as either "xxxx_B_yyyy" or "xxxx_S_yyyy" where B and S stands for bio-oil and slurry respectively; while xxxx and yyyy represent the selected variable and its range respectively.

Table 7- 1: Different operating conditions of bioslurry steam gasification in fluidized bed reactor

Run name[a]	Temperature	H_2O /C	$G_{C1}HSV$	Discrete phase flow rate	Mass source of steam and nitrogen	Mole fraction of H_2O inlet
	℃	*mole/mole*	h^{-1}	*kg/s*	*kg/s*	*mole %*
T_S_1109	836	5.804	311.63	5.73E-05	4.66E-04	60.4
T_S_1003	730	6.388	311.63	5.73E-05	5.15E-04	60.4
T_S_1058	785	6.071	311.63	5.73E-05	4.89E-04	60.4
CHD_S_10	836	5.804	311.63	5.73E-05	4.66E-04	60.4
CHD_S_25	836	5.804	311.63	5.73E-05	4.66E-04	60.4
CHD_S_45	836	5.804	311.63	5.73E-05	4.66E-04	60.4
SV_S_200	836	5.606	199.53	3.67E-05	3.69E-04	49.4
SV_S_400	836	5.606	401.31	7.38E-05	5.12E-04	66.3
HC_S_7.5	836	7.24	311.63	5.73E-05	5.17E-04	66.6

HC_S_10	836	9.651	311.63	5.73E-05	6.17E-04	72.9

"a" T, CHD, SV, and HC stand for temperature, char particle diameter, G_{C1}HSV and H_2O /C respectively

7.5.1 Model validation: Comparison between model prediction and experimental data

Similar to the bio-oil gasification model (See Chapter 6), validation of bioslurry gasification model has been done by comparison of simulation result and experimental data.[35] Figure 7-2 includes the model prediction of the syngas products at the gasifier exit at 1109 K (run name 1109_S in Table 7-1). In this figure, the molar percentage, using the surface integrals by selecting area-weighted average of species in Fluent was reported on both wet-basis (including $N_2$and H_2O) and dry-basis (excluding $N_2$and H_2O). The results clearly show that the simulation result and the experimental data are in very good agreement because the relative percentage errors for H_2 and CO are -0.2% and 0.8% respectively.

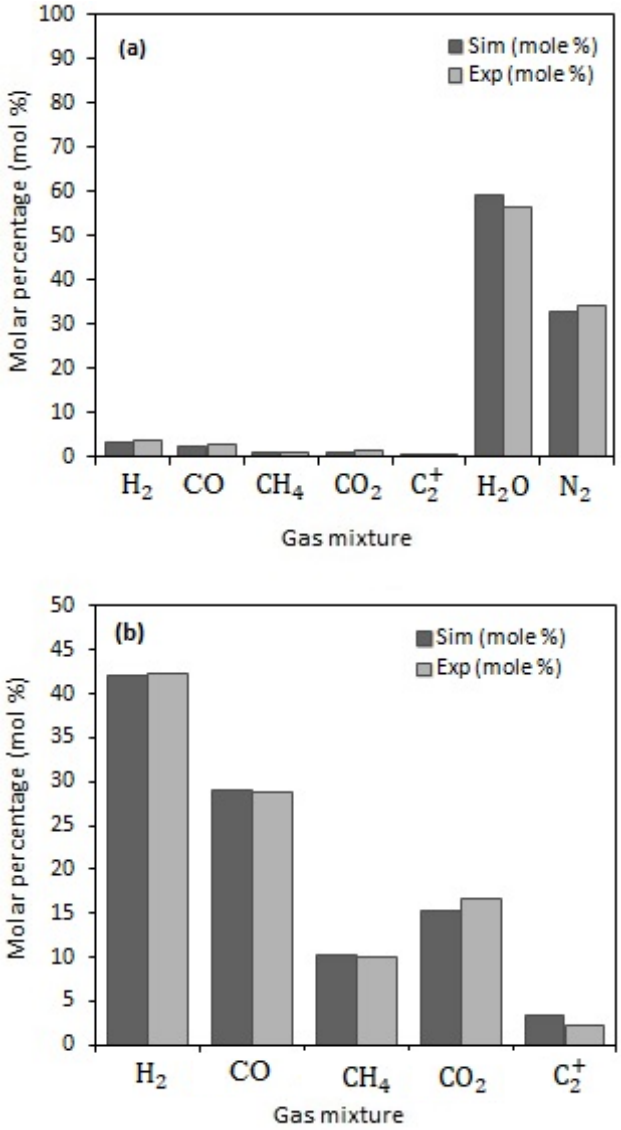

Figure 7- 2: Comparison of simulation and experimental results for molar percentage of syngas (H_2+CO), CO_2, C_2^+ and CH_4 at reactor exit under operating conditions of: T = 1109 K, mole H_2O /mole C = 5.804, G_{C1}HSV = 311.63 h^{-1} (Run name 1109_S in Table 7-1) for bioslurry side injection in a fluidized bed reactor on (a) Wet-basis (b) Dry-basis.

7.5.2 Contribution of bio-oil fraction and biochar fraction to bioslurry conversion

Figures 7-3 shows the simulation result for contribution of biochar in bio-oil (bioslurry with biochar loading levels of 20 wt%) on molar percentage of syngas (H_2+CO), CO_2, C_2^+ and CH_4 at constant temperature of T = 1107 K, H_2O / C = 5.76, and G_{C1}HSV = 322.84 h^{-1}. In this figure, the 20 wt% biochar in bioslurry leads to an increase in H_2 and CO_2 around 16.4% and 11.9% respectively. This is largely due to

the enhanced thermal decomposition of char particles steam gasification reaction (R15) and water-gas shift reaction (R6) which results in higher hydrogen and carbon dioxide gaseous. On the other hand, CO, CH_4, and C_2^+ reduced around 13%, 18.7%, and 20% respectively. This is largely because the char part in bioslurry only generates syngas (H_2+ CO) with reaction R15 (carbon dioxide then reduced by water gas shift reaction) with very lower reaction rate than bio-oil thermal decomposition reaction rate (R1). Figure 7-4 shows the comparison of cold gas efficiency (CGE) for bio-oil and bioslurry at the constant operating condition with $T \cong 1107\,K$, $H_2O/C \cong 5.76$ and $G_{C1}HSV \cong 322.84\,h^{-1}$. In this figure, the cold gas efficiency of bioslurry reduced by increasing 20% char to the bio-oil. The total carbon conversion in bioslurry steam gasification reduced from 65.7% to 49.3% because the char steam gasification reaction rate in bioslurry (R15) is lower than bio-oil thermal decomposition reaction rate (R1).

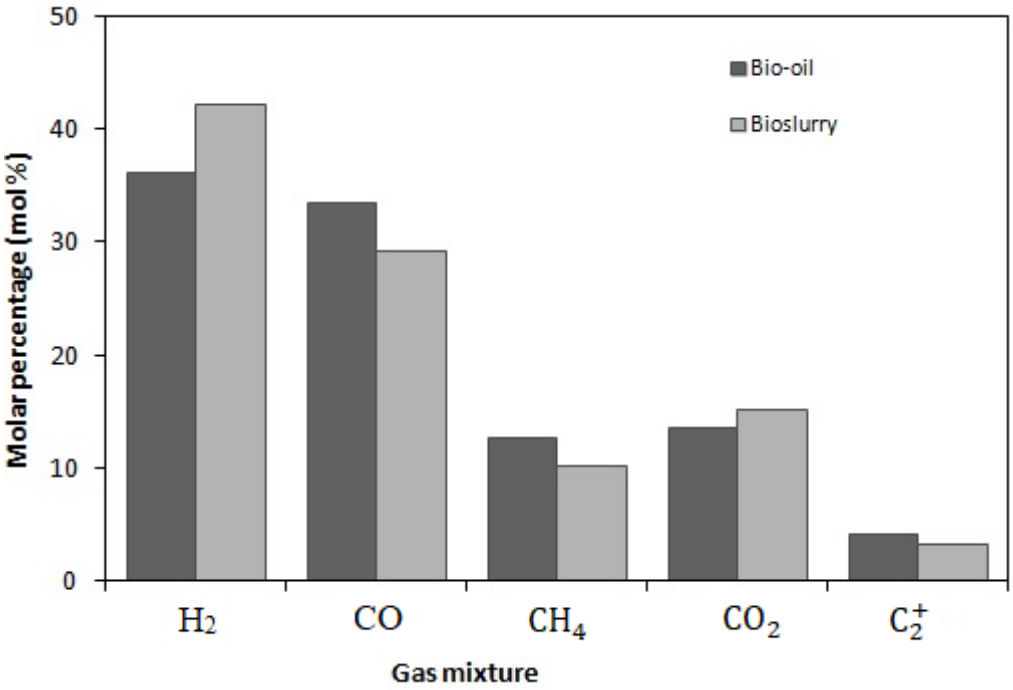

Figure 7- 3: Contribution of biochar in bio-oil (bioslurry) on molar percentage of syngas (H_2+CO), CO_2, C_2^+ and CH_4 at reactor exit under operating conditions of: T = 1107 K, mole H_2O /mole C = 5.76, $G_{C1}HSV$ = 322.84 h^{-1}.

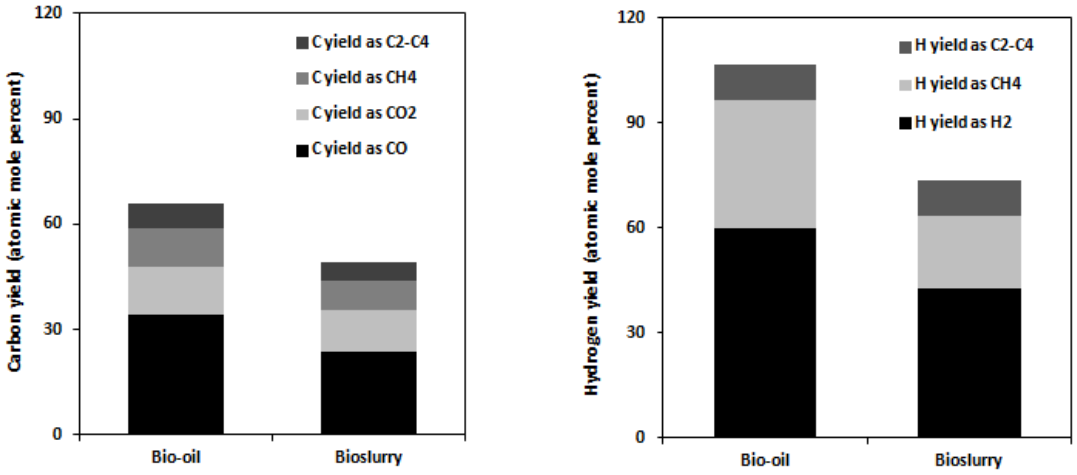

Figure 7- 4: Simulation results of bio-oil and bioslurry steam gasification for contribution of biochar in bioslurry on carbon yield (CO, CO_2, CH_4 and C_2^+) and hydrogen yield (H_2, CH_4 and C_2^+) under dry feedstock basis with $T \cong 1107$ K, $H_2O/C \cong 5.76$ and $G_{C1}HSV \cong 322.84\ h^{-1}$.

7.5.3 Prediction of the cold gas efficiency (CGE)

Figure 7-5 presents the effect of temperature, hourly space velocity and H_2O /C on cold gas efficiency (CGE). Figure 7-5a shows that the CGE increases with temperature. As per reactions scheme (R1-R13) explained in chapter 6, R1and R6 is mainly responsible for the generation and consumption of syngas (H_2+ CO) for bio-oil in bioslurry. The char part in bioslurry also generates syngas (H_2+ CO) with reaction R15. An initial increase in reactor temperature increases R1, R6 and R15, resulting in increasing the cold gas efficiency. However, further increase in temperature leads to the level-off of the CGE because the water gas shift reaction (R6) produces more CO and less H_2 with less CGE. Moreover, Figure 7-6 shows the comparison of cold gas efficiency (CGE) for bio-oil and bioslurry at different operating conditions (temperature, $G_{C1}HSV$ and H_2O/C ratio). In this figure, the cold gas efficiency of bio-oil is more than bioslurry mainly due to less production of syngas gas as a result of very low reaction rate of biochar in bioslurry (R15). This also can be explained by Figure 7-4 where carbon yield (CO, CO_2, CH_4 and C_2^+) and hydrogen yield (H_2, CH_4 and C_2^+) of bioslurry are lower than bio-oil hence leads to decreased CGE of bioslurry. Figure 7-5b also shows that the CGE reduces

continuously as the gas hourly space velocity increases, mainly due to less production of syngas gas as a result of the reduced residence time of feedstock in the reactor. Figure 7-5c shows that the CGE increases as the H_2O/C ratio increases while it was almost insensitive for bio-oil as discussed in Chapter 6 (see section 6.2.2). Increasing H_2O /C ratio decreases the residence time of feedstock in the reactor hence leads to decreased CGE. On the other hand, increasing H_2O /C ratio increases the rate of forward reaction R6 and R15 to produce more H_2 hence increase CGE.

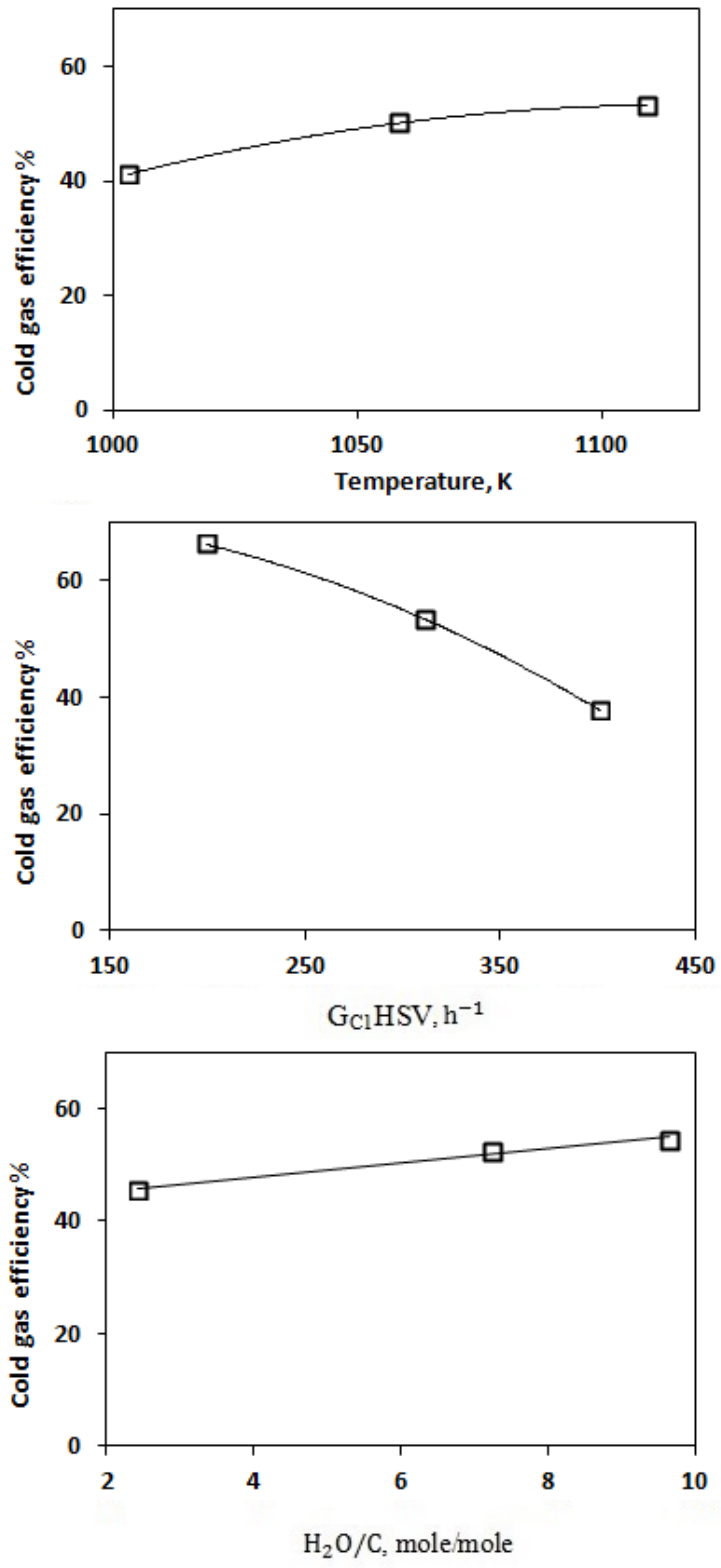

Figure 7- 5: Model predictions on the effect of operating temperature, $G_{C1}HSV$ and H_2O/C ratio on cold gas efficiency (CGE) during bioslurry steam reforming under side injection conditions.

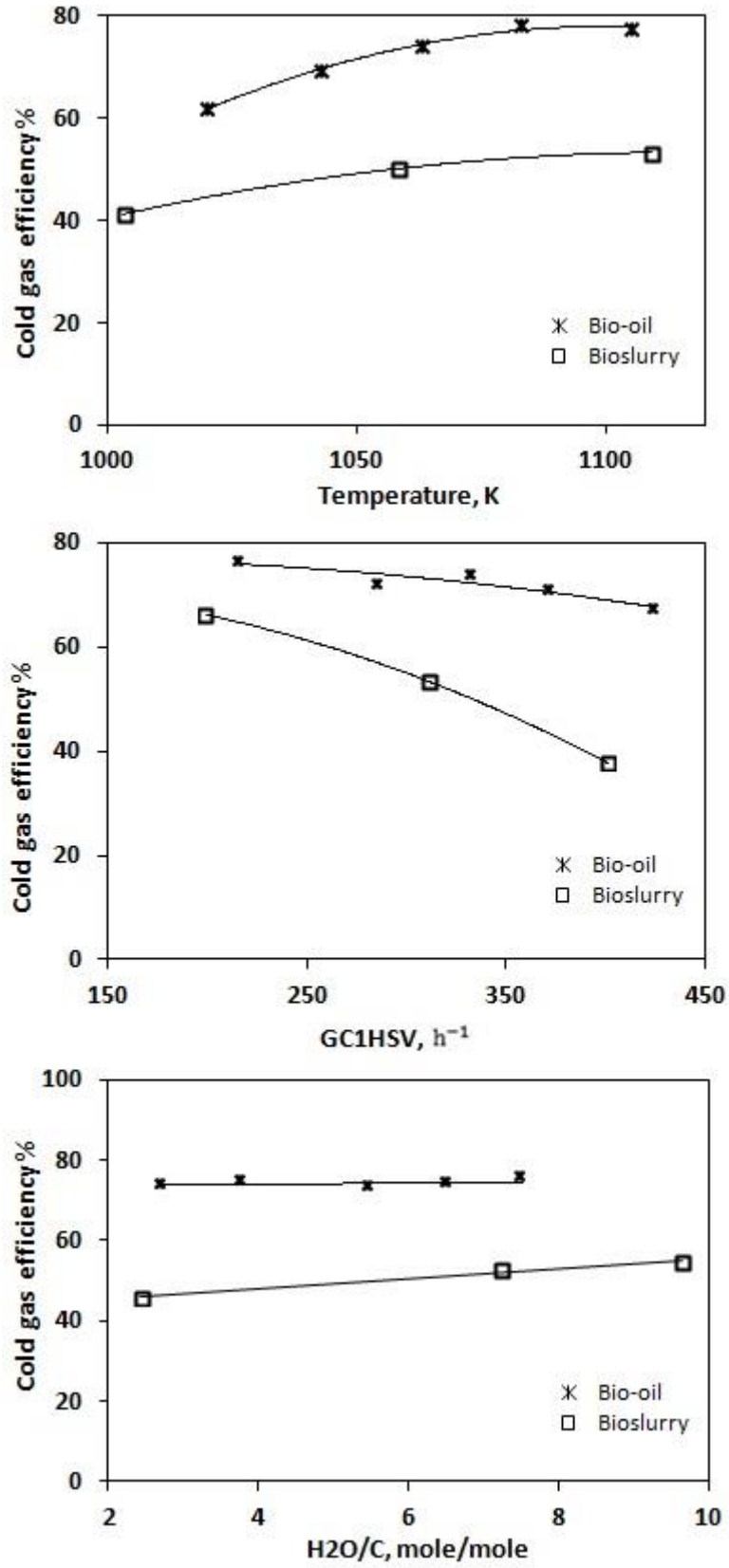

Figure 7- 6: Comparison of cold gas efficiency (CGE) of bio-oil and bioslurry at different operating conditions (temperature, $G_{C1}HSV$ and H_2O/C ratio).

7.5.4 Effect of temperature, space velocity of feed, and steam to carbon feeding ratio on product gas yields

Figures 7-7 to 7-9 present the sensitivities of carbon (in forms of CO, CO_2, CH_4 and C_2^+) and hydrogen (in forms of H_2, CH_4 and C_2^+) yields against temperatures, space velocity (G_{C1}HSV) and steam to carbon feeding ratio (H_2O/C). Figure 7-7 indicates the carbon and hydrogen yields at various temperatures with constant G_{C1}HSV and H_2O/C of 311.6 and 6.1 respectively. An increase in temperature from 1003 to 1058 K, leads to an increase in carbon and hydrogen yields around 11.6% and 25.3% respectively. This is largely due to the enhanced thermal decomposition of bio-oil in bioslurry and char particles steam gasification reaction (resulting in higher total carbon conversion to gas) and water-gas shift reaction (R6). Further increases in temperature up to 1109 K lead to a small increase in the yields of carbon and hydrogen by around 6.9% and 4.3% respectively. As mentioned in chapter 6, the yield of carbon is more sensible than hydrogen yield in the increase because the water gas shift reaction (R6) is sensitive to temperature and has a tendency to shift towards left side as temperature increases. However, bio-oil (see section 6.6.4) is more sensitive than bioslurry to temperature because the char steam gasification reaction rate (R15) is very lower than bio-oil thermal decomposition reaction rate (R1).

Figure 7-8 shows the carbon and hydrogen yields at various G_{C1}HSV with constant temperature and H_2O/C of 1109 K and 5.7 respectively. In this figure, an increase in G_{C1}HSV from 199.5 to 311.6 results in a reduction in the total conversion by 19.4%. Such reduction is further increased to 27.1% when the G_{C1}HSV increases further from 311.6 to 401.3. This is largely because an increased G_{C1}HSV leads to lower residence time of bioslurry droplets hence reduced conversion in the gasifier. The results of bioslurry in this chapter and bio-oil in the previous chapter clearly show the influence of G_{C1}HSV on the total conversion of bioslurry to product gas yield is more sensitive than bio-oil. This is might be related to lowest conversion and also larger droplet diameter of bioslurry which leads to more reduction in product yields.

Figure 7-9 shows the influence of H_2O /C on product gas yields at given temperature and G_{C1}HSV by 1109 K and 311.63h^{-1} respectively. From the figure, it is clear that an increase in H_2O/C ratio from 5.804 to 7.24 results in a reduction of 5.3% in the

carbon yields and an increase of 5.7 in the hydrogen yields. A further increase in the H_2O/C from 7.45 to 9.65 leads to an increase of about 7.2% in total hydrogen yields while the total carbon yields is almost constant. This can be mainly contributed to the enhanced water-gas shift reaction (R6) and char steam gasification (R15) for increased hydrogen production.

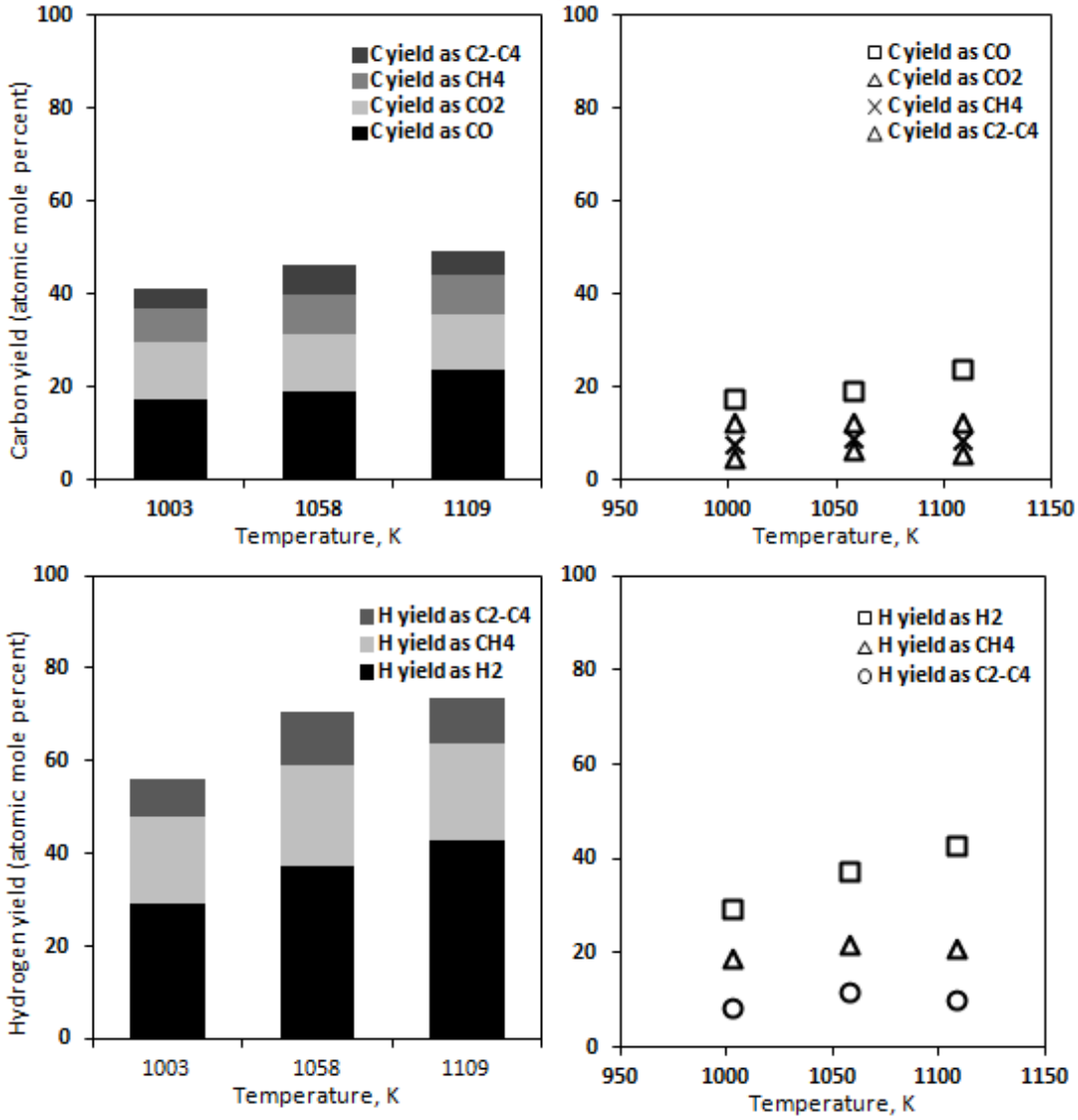

Figure 7- 7: Simulation results of bioslurry steam gasification for effect of temperature on carbon yield (CO, CO_2, CH_4 and C_2^+) and hydrogen yield (H_2, CH_4 and C_2^+) under dry feedstock basis with H_2O /C ≅6.09 and G_{C1}HSV ≅311.63h^{-1}.

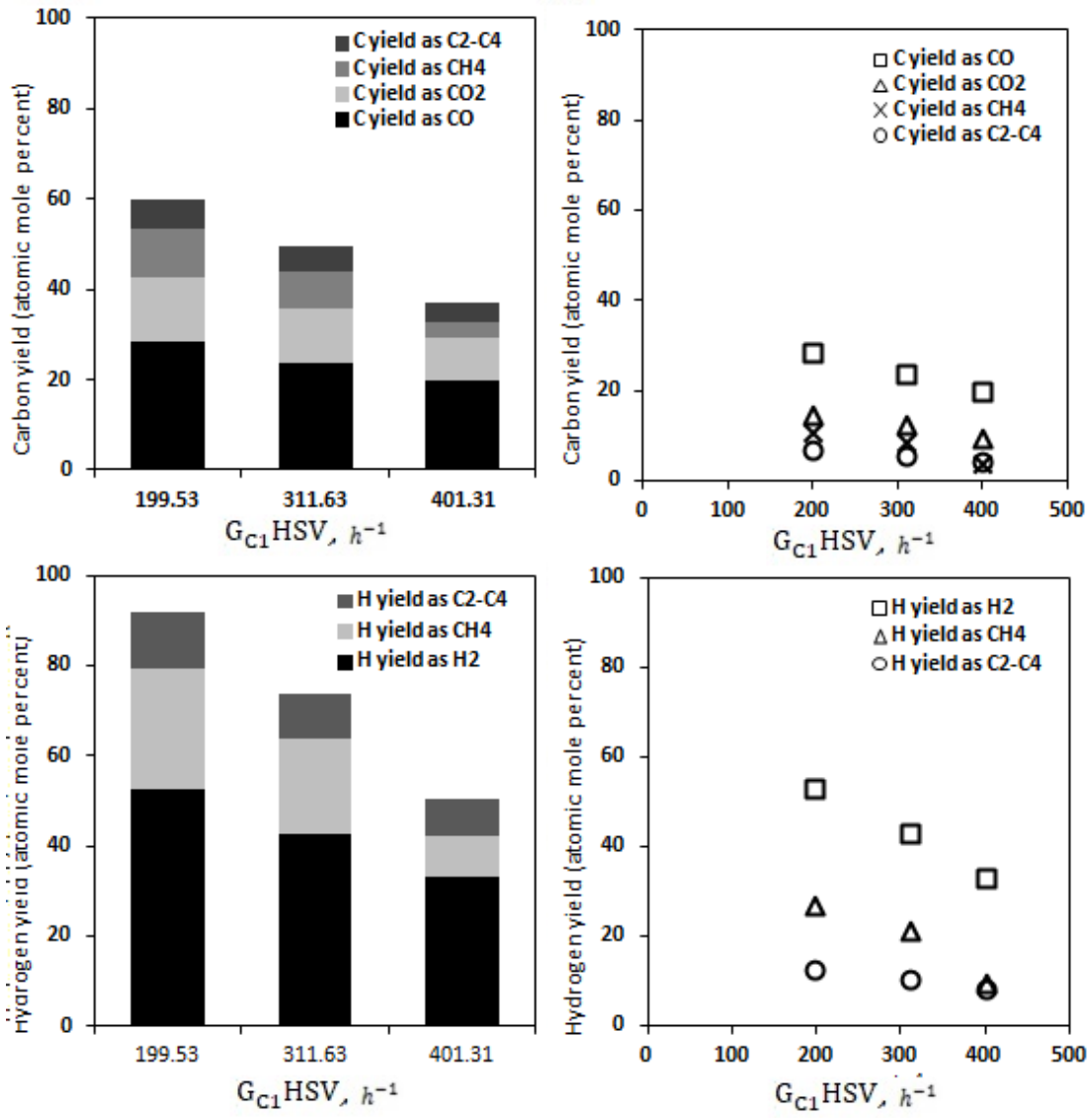

Figure 7- 8: Simulation results of bioslurry steam gasification for effect of $G_{C1}HSV$ on carbon yield (CO, CO_2, CH_4 and C_2^+) and hydrogen yield (H_2, CH_4 and C_2^+) under dry basis with $T \cong 836℃$, and $H_2O/C \cong 5.67$.

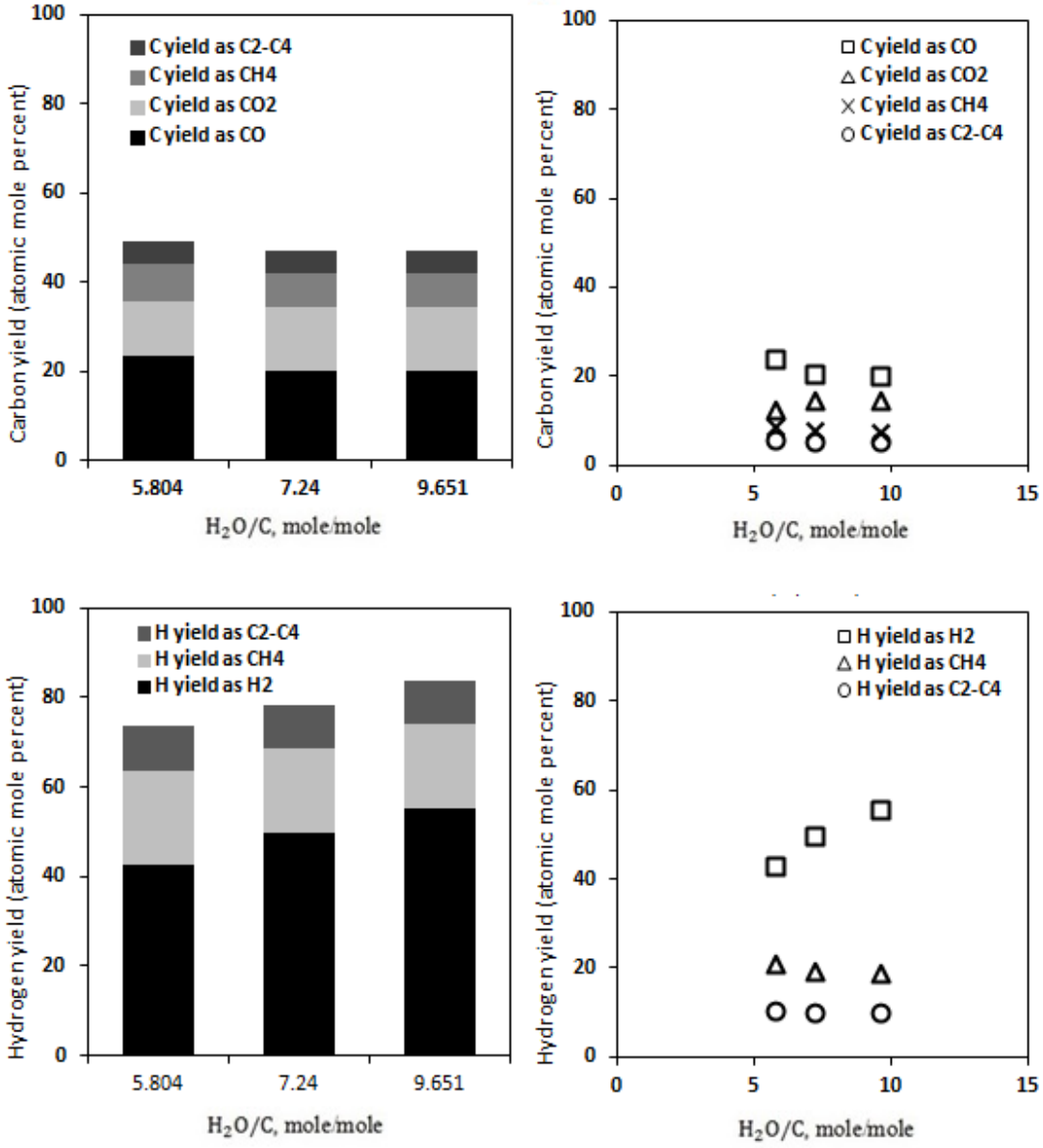

Figure 7- 9: Simulation results of bioslurry steam gasification for effect of H_2O/C on carbon yield (CO, CO_2, CH_4 and C_2^+) and hydrogen yield (H_2, CH_4 and C_2^+) under dry feedstock basis with $T \cong 836℃$ and $GC_1HSV \cong 311.63h^{-1}$.

7.5.5 Effect of char diameter on product gas yields

In chapter 6, it was demonstrated that the droplet size has a significant effect on droplet residence time and fuel conversion. In this chapter then taken to investigate the effects of char particles diameter on product gas yields when other variables are kept constant. The range of char particles diameter is much less than the range for bio-oil droplets (as discussed in Chapter 6 which was between 50 and 500 µm)

because this is a realistic range where fine biochar particles are considered to be suspended into bio-oil droplets. Figure 7-10 presents the carbon and hydrogen yields for char particles with a mean diameter in the range of 10 - 45μm at constant temperature, G_{C1}HSV, H_2O /C at 1109 K, 311.63 $h^{-1}$and 5.804 respectively. It is clear that the total hydrogen and carbon yields remain nearly constant for different char particles between 10 and 45 micron. This is not surprising, given the low impact of char particle diameter (range of 10 - 45 micron) on product gas yields due to the very low reaction rate of char steam reforming (R15). Therefore, the result of this study clearly indicates that the role of char particle diameters in the formation of hydrogen and carbon monoxide from biochar steam gasification is not important and char particle diameters do not control the overall feedstock conversion to product gas yields.

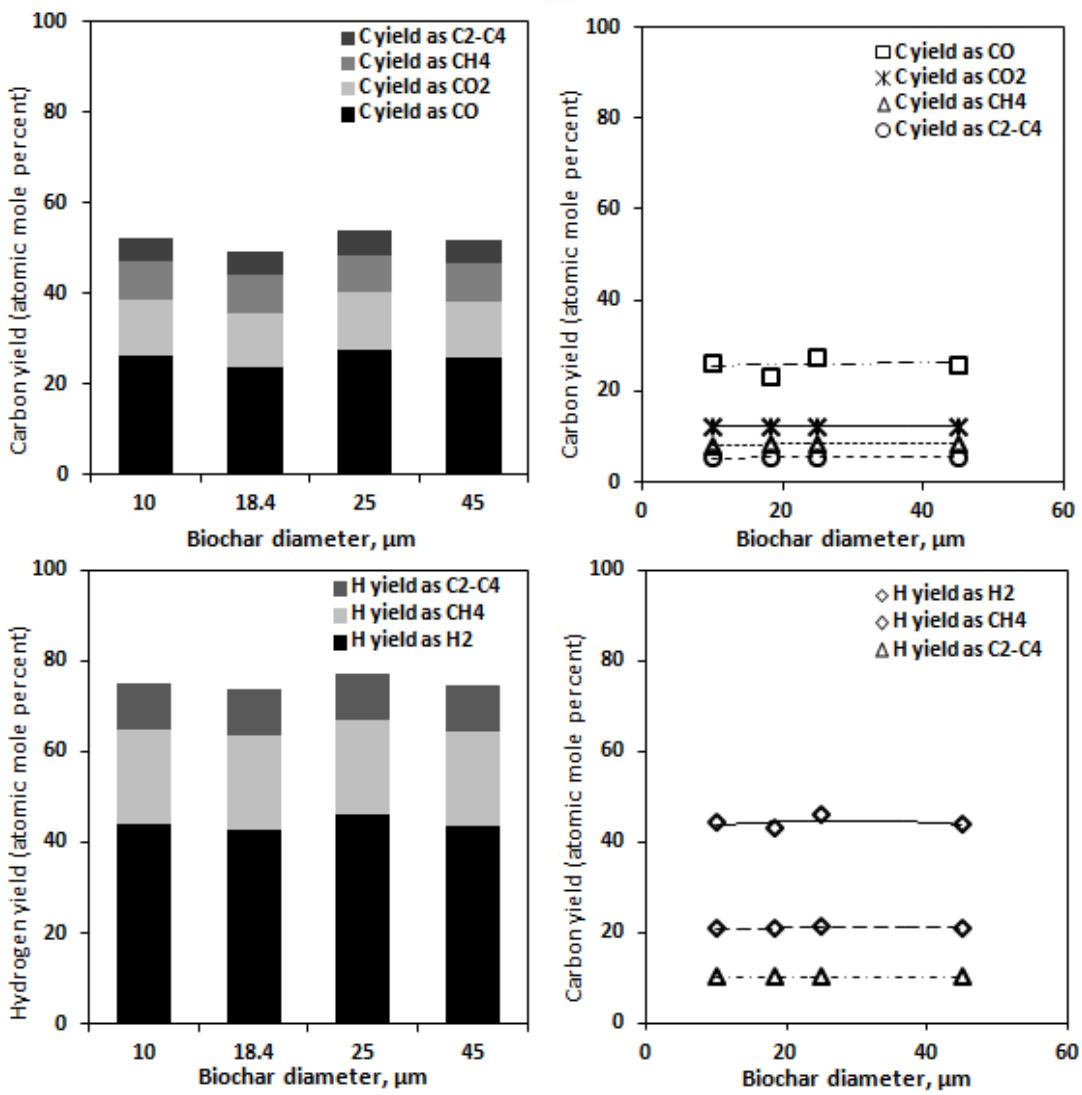

Figure 7- 10: Simulation results of bioslurry steam gasification for effect of biochar diameter on carbon yield (CO, CO_2, CH_4 and C_2^+) and hydrogen yield (H_2, CH_4 and C_2^+) under dry basis with $T \cong 836℃$, $H_2O/C \cong 5.804$ and $GC_1HSV \cong 311.63h^{-1}$.

7.6 Summary

A three-dimensional CFD simulation, using the Euler-Lagrange approach for a fluidized bed reactor with bioslurry (20 wt% biochar) injection into hot bed in the presence of steam and nitrogen gas has been developed to investigate the influence of flow characteristics on bioslurry steam gasification process. The significant roles of alkali and alkaline earth metallic (AAEM) species, in the presence of biochar have been studied by altering the activation energy required for the chemical reaction of biochar gasification, and hence, considering that AAEM speeds up the rate of a chemical reaction by lowering its activation energy to approximately a half. After validation, the sensitivity study of the associated parameters including, temperature, space velocity of feed, steam to carbon feeding ratio, and biochar particles diameter in slurry in case of the quantifications of individual parameters on feedstock conversion have been done. The CFD simulation results indicate that the biochar particles diameter (with mean diameter between 10 and 45μm) had no significant effect on total bioslurry conversion to product gas yield due to very low reaction rate, which controlled the total conversion of feedstock to product gas. However, the gasification temperature and also the H_2O /C lead to an increase in the biochar steam reforming reaction rate, which increases the hydrogen and carbon yields.

CHAPTER 8: CONCLUSION AND FUTURE WORK

8.1 Introduction

Bio-oil and/or bio-char are products from fast pyrolysis of biomass. It is becoming an increasingly important sustainable energy used to address the challenges of energy security, climate change, greenhouse gas emissions and economics of carbon price.[5, 14, 19-21] As compared with biomass, bio-oil and bioslurry (mix fine biochar into bio-oil) have higher energy density, for example, the volumetric energy density of bio-oil is roughly five times higher than biomass.[22] Also bio-oil and bioslurry are easier to be transported, processed, pressurized and stored. Using bio-oil as fuel for boilers, furnaces, diesel engines and gas turbines has been proved feasible, while gasification of bio-oil and bioslurry for synthesis gas which is an important intermediate product for many processes has also attracted considerable attention recently.[17, 18, 22, 23]

Therefore, this chapter summarises the key research outcomes from this PhD study. Firstly, this research has developed a new methodology that minimizes several drawbacks related to mechanical approach for measuring the droplet size of the sprays. Secondly, this research has developed empirical correlations for bio-oil and bioslurry sprays via atomization using several types and sizes of atomizers. Thirdly, a three-dimensional CFD model has been developed for bio-oil gasification in a fluidized bed reactor. The model considers three-phase hydrodynamics, heat and mass transfer, fuel atomization, droplets evaporation and thermal decomposition a gas–solid flow. It predicts fuel conversion and the composition of synsis gas products. Finally, the model is also developed for bioslurry steam gasification in fluidized bed. This chapter also includes a list of some future work recommended in this research area.

8.2 Conclusions

8.2.1 Development and validation of a modified method for droplets size distribution measurement

- An improved mechanical method has been developed for measuring spray droplet size distribution of liquid fuel atomization.

- Minimum distance of captured plate from nozzle was determined for minimising droplets overlapping.

- Critical roundness was determined for eliminating overlapped droplets on glass slide for image analysing. At the threshold of critical roundness0.75, there are less than 5% of the overlapped droplets which were eliminated.

- The method also considers fuel-dependent correction factor for fuel droplets. This allows the application of the method to a wide range of fuels because the ratio of droplet size to impression size is determined by fuel properties.

- Evaporation effect on initial droplets sizes is considered. The result shows evaporation for diesel and biodiesel at low temperatures is low because of low vapour pressure.

With these considerations, the Sauter mean diameters (SMD) were measured for diesel, biodiesel and diesel/biodiesel blends, with average standard deviation of 0.7μm.The comparisons between the experimental measurements and analytical calculations are within the average relative error of 1.2%.

8.2.2 Atomization of bio-oil and bioslurry by impact and twin-fluid atomizer

8.2.2.1 Impact atomizer

- Mean droplet sizes of bio-oil and bioslurry fuels were measured for impact atomizers (of different sizes) at injection pressure of 2.07–4.96 MPa and feeding rate of 108–490 ml/min. Two types of fast pyrolysis bio-oil samples (with different viscosities 0.0753 and 0.1522 Pa.s, respectively) were considered. Bioslurry samples have biochar loading levels of 5, 10, 15 and 20 wt%, respectively.

- At a given pressure, the SMDs of bio-oil and bioslurry increase as the flow numbers increase and the SMD is more sensitive to the reduction of the pressure by increasing the liquid flow rate.

- The SMD can be approximated by an empirical correlation developed for both bio-oil and bioslurry. The mean diameter is proportional to liquid

viscosity by ($SMD \propto \mu_{bio-oil}^{0.131}$), flow number ($SMD \propto FN^{0.26}$), and the level of char loaded ($SMD \propto (\ln(wt_{char} + e))^{0.22}$) while it is diminished by an increase in injection pressure differential ($SMD \propto \Delta P^{-0.58}$).

8.2.2.2 Twin-fluid atomizer

- Droplet size distribution was investigated for bio-oil and bioslurry atomization by a twin-fluid atomizer (N_2 fed in the outer tube) at a flow rate of 2–6 ml/min.

- The SMD of twin-fluid atomizer relates to the gas/liquid ratio and char loading level. An increase in char loading level leads to an increase in the SMD of spray while an increase in GLR results in a reduction in the SMD.

- The SMD can be approximated by an empirical correlation developed for both bio-oil and bioslurry by twin-fluid atomizer. The SMD is proportional to liquid viscosity ($SMD \propto \mu_{bio-oil}^{0.86}$), and the level of char ($SMD \propto (\ln(wt_{char} + e))^{0.20}$) while it is diminished by an increase in Gas/Liquid ratio ($SMD \propto \left(\frac{\dot{m}_G}{\dot{m}_L}\right)^{-0.56}$).

8.2.3 Mathematical modelling of bio-oil steam gasification in a fluidized bed reactor

- A three-dimensional CFD model was developed to simulate bio-oil gasification in a fluidized bed reactor. The model takes into account three-phase hydrodynamics, heat and mass transfer, droplet atomisation, droplet vaporization and thermal decomposition in a gas–solid flow. Several user-defined functions (UDFs) have been developed for the model.

- The experimental data in Chapter 5 have been incorporated into the model to generate the Rosin-Rammler distribution function for different injection conditions.

- The CFD is capable of predicting the synthesis gas product composition at different bed temperatures, steam-carbon molar ratios, methane equivalent

gas hourly space velocity ($G_{C1}HSV$) of feed and the sizes of droplets injected into the gasifier.

- The simulation shows that an increase in gasification temperature leads to an increase in the hydrogen and carbon yields and fuel conversion during bio-oil gasification. This is largely due to enhanced thermal decomposition, water-gas shift reactions.

  It is also clearly demonstrated that the droplet size has a significant effect on droplet residence time and fuel conversion.

8.2.4 Modelling of bioslurry steam gasification in a fluidized bed reactor

- The CFD model was further extended for simulating bioslurry steam gasification in a fluidized bed reactor. Analysis was also carried out for the sensitivities of fuel conversion and synthesis gas compositions to gasification temperature, space velocity of feed, steam to carbon feeding ratio, droplet size and biochar diameter.

- Catalytic effect of alkali and alkaline earth metallic (AAEM) species in biochar was considered as the presence of these catalysts alters the activation energy of biochar gasification reactions.

- The size of biochar in bioslurry has insignificant effect on bioslurry gasification as the biochar size is small (10–45μm).

- The reactor temperature has significant effect on bioslurry gasification to the syngas production and also cold gas efficiency as the thermal decomposition of bio-oil and biochar steam reforming reaction rate increase by temperature rising.

8.3 Recommendations

Based on the conclusions in this study, the following future research suggestions have identified.

1. Empirical correlations on atomisation are needed for more nozzles of different types.

2. Future research is also needed on the kinetics of the bio-oil steam reforming to provide a fundamental underestanding on the reaction mechanisms.

3. This study shows that droplet size plays an important role in fuel conversion and product gas composition. Future work is required for conducting experiments under different atomisation conditions.

REFERENCES

1. Catoire, L., M. Yahyaoui, A. Osmont, I. Gökalp, M. Brothier, H. Lorcet, and D. Guénadou, Thermochemistry of compounds formed during fast pyrolysis of lignocellulosic biomass. *Energy & Fuels* **2008**, 22**,** (6), 4265-4273.

2. Demirbas, A., Progress and recent trends in biofuels. *Progress in Energy and Combustion Science* **2007**, 33**,** (1), 1-18.

3. Wu, H., Q. Fu, R. Giles, and J. Bartle, Production of Mallee Biomass in Western Australia: Energy Balance Analysis†. *Energy & Fuels* **2007**, 22**,** (1), 190-198.

4. Bartle, J., G. Olsen, D. Cooper, and T. Hobbs, Scale of biomass production from new woody crops for salinity control in dryland agriculture in Australia. *International journal of global energy issues* **2007**, 27**,** (2), 115-137.

5. Yu, Y., J. Bartle, C.-Z. Li, and H. Wu, Mallee Biomass as a Key Bioenergy Source in Western Australia: Importance of Biomass Supply Chain. *Energy & Fuels* **2009**, 23**,** (6), 3290-3299.

6. Yu, Y. and H. Wu, Bioslurry as a fuel. 2. Life-cycle energy and carbon footprints of bioslurry fuels from mallee biomass in western Australia. *Energy & Fuels* **2010**, 24**,** (10), 5660-5668.

7. Xu, Q., P. Lan, B. Zhang, Z. Ren, and Y. Yan, Hydrogen Production via Catalytic Steam Reforming of Fast Pyrolysis Bio-oil in a Fluidized-Bed Reactor. *Energy & Fuels* **2010**, 24**,** (12), 6456-6462.

8. Asadullah, M., M. Anisur Rahman, M. Mohsin Ali, M. Abdul Motin, M. Borhanus Sultan, M. Robiul Alam, and M. Sahedur Rahman, Jute stick pyrolysis for bio-oil production in fluidized bed reactor. *Bioresource technology* **2008**, 99**,** (1), 44-50.

9. Lind, T., T. Vaimari, E. Kauppinen, K. Nilsson, G. Sfiris, and W. Maenhaut, Ash formation mechanisms during combustion of wood in circulating fluidized beds. *Proceedings of the Combustion Institute* **2000**, 28**,** (2), 2287-2295.

10. Lind, T., T. Valmari, E.I. Kauppinen, G. Sfiris, K. Nilsson, and W. Maenhaut, Volatilization of the heavy metals during circulating fluidized bed combustion of forest residue. *Environmental science & technology* **1999**, 33**,** (3), 496-502.

11. Gao, X. and H. Wu, Effect of sampling temperature on the properties of inorganic particulate matter collected from biomass combustion in a drop-tube furnace. *Energy & Fuels* **2010**, 24**,** (8), 4571-4580.

12. Gao, X. and H. Wu, Biochar as a fuel: 4. Emission behavior and characteristics of PM1 and PM10 from the combustion of pulverized biochar in a drop-tube furnace. *Energy & Fuels* **2011**, 25**,** (6), 2702-2710.

13. Ni, M., D.Y. Leung, M.K. Leung, and K. Sumathy, An overview of hydrogen production from biomass. *Fuel processing technology* **2006**, 87**,** (5), 461-472.

14. Abdullah, H. and H. Wu, Biochar as a Fuel: 1. Properties and Grindability of Biochars Produced from the Pyrolysis of Mallee Wood under Slow-Heating Conditions. *Energy & Fuels* **2009**, 23**,** (8), 4174-4181.

15. Abdullah, H., K.A. Mediaswanti, and H. Wu, Biochar as a Fuel: 2. Significant Differences in Fuel Quality and Ash Properties of Biochars from Various Biomass Components of Mallee Trees. *Energy & Fuels* **2010**, 24**,** (3), 1972-1979.

16. Yip, K., M. Xu, C.-Z. Li, S.P. Jiang, and H. Wu, Biochar as a fuel: 3. Mechanistic understanding on biochar thermal annealing at mild temperatures and its effect on biochar reactivity. *Energy & Fuels* **2010**, 25**,** (1), 406-414.

17. Sakaguchi, M., A.P. Watkinson, and N. Ellis, Steam Gasification of Bio-Oil and Bio-Oil/Char Slurry in a Fluidized Bed Reactor. *Energy & Fuels* **2010**, 24**,** (9), 5181-5189.

18. Latifi, M., Gasification of Bio-oils to Syngas in Fluidized Bed Reactors, PhD Thesis, Department of Chemical and Biochemical Engineering, University of Western Ontario Canada, 2012.

19. Czernik, S. and A.V. Bridgwater, Overview of Applications of Biomass Fast Pyrolysis Oil. *Energy & Fuels* **2004**, 18**,** (2), 590-598.

20. Mohan, D., C.U. Pittman, and P.H. Steele, Pyrolysis of Wood/Biomass for Bio-oil: A Critical Review. *Energy & Fuels* **2006**, 20**,** (3), 848-889.

21. Al-Sabawi, M., J. Chen, and S. Ng, Fluid Catalytic Cracking of Biomass-Derived Oils and Their Blends with Petroleum Feedstocks: A Review. *Energy & Fuels* **2012**, 26**,** (9), 5355-5372.

22. Yip, K., F. Tian, J.-i. Hayashi, and H. Wu, Effect of Alkali and Alkaline Earth Metallic Species on Biochar Reactivity and Syngas Compositions during Steam Gasification†. *Energy & Fuels* **2009**, 24**,** (1), 173-181.

23. van Rossum, G., S.R.A. Kersten, and W.P.M. van Swaaij, Catalytic and Noncatalytic Gasification of Pyrolysis Oil. *Industrial & Engineering Chemistry Research* **2007**, 46**,** (12), 3959-3967.

24. Sirignano, W.A., Fluid dynamics and transport of droplets and sprays, Cambridge University Press, The United States of America, (2010).

25. Lefebvre, A.H., Atomization and Sprays, CRC Press, USA, (1988).

26. Lee Black, D., M.Q. McQuay, and M.P. Bonin, Laser-based techniques for particle-size measurement: A review of sizing methods and their industrial applications. *Progress in Energy and Combustion Science* **1996**, 22**,** (3), 267-306.

27. Blaisot, J.B. and J. Yon, Droplet size and morphology characterization for dense sprays by image processing: application to the Diesel spray. *Experiments in Fluids* **2005**, 39**,** (6), 977-994.

28. Tropea and Cameron, Optical Particle Characterization in Flows *Annual Review of Fluid Mechanics* **2011**, 43**,** (1), 399-426.

29. Crau, C., G. De Sercey, and M.R. Heikal, Dropsizing of Near-Nozzle Diesel and RME Sprays by Microscopic Imaging, *ICLASS 2012, 12th triennial international conference on liquid atomization and spray systems*, Heidelberg, Germany, 2012.

30. Dodge, L.G., Comparison of performance of drop-sizing instruments. *Appl. Opt.* **1987**, 26**,** (7), 1328-1341.

31. May, K., The measurement of airborne droplets by the magnesium oxide method. *Journal of Scientific Instruments* **1950**, 27**,** (5), 128.

32. Mugele, R.A. and H.D. Evans, Droplet Size Distribution in Sprays. *Industrial & Engineering Chemistry* **1951**, 43**,** (6), 1317-1324.

33. Ashgriz, N., Handbook of Atomization and Sprays : Theory and Applications, Springer, Boston, (2011).

34. Crowe, C., M. Sommerfeld, and Y. Tsuji, Multiphase flows with droplets and particles, CRC press, USA, (1998).

35. Sakaguchi, M., Gasification of bio-oil and bio-oil/char slurry, Department of Chemical and Biochemical Engineering, University of British Columbia, Canada, 2010.

36. Wang, D., S. Czernik, and E. Chornet, Production of Hydrogen from Biomass by Catalytic Steam Reforming of Fast Pyrolysis Oils. *Energy & Fuels* **1998**, 12**,** (1), 19-24.

37. Marda, J.R., J. DiBenedetto, S. McKibben, R.J. Evans, S. Czernik, R.J. French, and A.M. Dean, Non-catalytic partial oxidation of bio-oil to synthesis gas for distributed hydrogen production. *International Journal of Hydrogen Energy* **2009**, 34**,** (20), 8519-8534.

38. Garcia, L.a., R. French, S. Czernik, and E. Chornet, Catalytic steam reforming of bio-oils for the production of hydrogen: effects of catalyst composition. *Applied Catalysis A: General* **2000**, 201**,** (2), 225-239.

39. Czernik, S., R. French, C. Feik, and E. Chornet, Hydrogen by Catalytic Steam Reforming of Liquid Byproducts from Biomass Thermoconversion Processes. *Industrial & Engineering Chemistry Research* **2002**, 41**,** (17), 4209-4215.

40. Panigrahi, S., S.T. Chaudhari, N.N. Bakhshi, and A.K. Dalai, Production of Synthesis Gas/High-Btu Gaseous Fuel from Pyrolysis of Biomass-Derived Oil. *Energy & Fuels* **2002**, 16**,** (6), 1392-1397.

41. Panigrahi, S., A.K. Dalai, S.T. Chaudhari, and N.N. Bakhshi, Synthesis Gas Production from Steam Gasification of Biomass-Derived Oil. *Energy & Fuels* **2003**, 17**,** (3), 637-642.

42. Kechagiopoulos, P.N., S.S. Voutetakis, A.A. Lemonidou, and I.A. Vasalos, Hydrogen Production via Steam Reforming of the Aqueous Phase of Bio-Oil in a Fixed Bed Reactor. *Energy & Fuels* **2006**, 20**,** (5), 2155-2163.

43. Davidian, T., N. Guilhaume, E. Iojoiu, H. Provendier, and C. Mirodatos, Hydrogen production from crude pyrolysis oil by a sequential catalytic process. *Applied Catalysis B: Environmental* **2007**, 73**,** (1–2), 116-127.

44. Czernik, S., R. Evans, and R. French, Hydrogen from biomass-production by steam reforming of biomass pyrolysis oil. *Catalysis Today* **2007**, 129**,** (3–4), 265-268.

45. Basagiannis, A.C. and X.E. Verykios, Steam reforming of the aqueous fraction of bio-oil over structured Ru/MgO/Al2O3 catalysts. *Catalysis Today* **2007**, 127**,** (1–4), 256-264.

46. Wang, Z., Y. Pan, T. Dong, X. Zhu, T. Kan, L. Yuan, Y. Torimoto, M. Sadakata, and Q. Li, Production of hydrogen from catalytic steam reforming of bio-oil using C12A7-O⁻-based catalysts. *Applied Catalysis A: General* **2007**, 320**,** (0), 24-34.

47. van Rossum, G., S.R.A. Kersten, and W.P.M. van Swaaij, Staged Catalytic Gasification/Steam Reforming of Pyrolysis Oil. *Industrial & Engineering Chemistry Research* **2009**, 48**,** (12), 5857-5866.

48. Wu, C., Q. Huang, M. Sui, Y. Yan, and F. Wang, Hydrogen production via catalytic steam reforming of fast pyrolysis bio-oil in a two-stage fixed bed reactor system. *Fuel Processing Technology* **2008**, 89**,** (12), 1306-1316.

49. Lan, P., Q. Xu, M. Zhou, L. Lan, S. Zhang, and Y. Yan, Catalytic Steam Reforming of Fast Pyrolysis Bio-Oil in Fixed Bed and Fluidized Bed Reactors. *Chemical Engineering & Technology* **2010**, 33**,** (12), 2021-2028.

50. Medrano, J.A., M. Oliva, J. Ruiz, L. García, and J. Arauzo, Hydrogen from aqueous fraction of biomass pyrolysis liquids by catalytic steam reforming in fluidized bed. *Energy* **2011**, 36**,** (4), 2215-2224.

51. Seyedeyn-Azad, F., E. Salehi, J. Abedi, and T. Harding, Biomass to hydrogen via catalytic steam reforming of bio-oil over Ni-supported alumina catalysts. *Fuel Processing Technology* **2011**, 92**,** (3), 563-569.

52. Garcìa-Pérez, M., A. Chaala, H. Pakdel, D. Kretschmer, D. Rodrigue, and C. Roy, Multiphase Structure of Bio-oils. *Energy & Fuels* **2005**, 20**,** (1), 364-375.

53. Garcia-Perez, M., X.S. Wang, J. Shen, M.J. Rhodes, F. Tian, W.-J. Lee, H. Wu, and C.-Z. Li, Fast Pyrolysis of Oil Mallee Woody Biomass: Effect of Temperature on the Yield and Quality of Pyrolysis Products. *Industrial & Engineering Chemistry Research* **2008**, 47**,** (6), 1846-1854.

54. Mulligan, C.J., L. Strezov, and V. Strezov, Thermal Decomposition of Wheat Straw and Mallee Residue Under Pyrolysis Conditions†. *Energy & Fuels* **2009**, 24**,** (1), 46-52.

55. Carpenter, D., T.L. Westover, S. Czernik, and W. Jablonski, Biomass feedstocks for renewable fuel production: a review of the impacts of feedstock and pretreatment on the yield and product distribution of fast pyrolysis bio-oils and vapors. *Green Chemistry* **2014**, 16**,** (2), 384-406.

56. Bridgwater, A.V., S. Czernik, and J. Piskorz, An Overview of Fast Pyrolysis, Blackwell Science Ltd, 2008.

57. Quyn, D.M., H. Wu, and C.-Z. Li, Volatilisation and catalytic effects of alkali and alkaline earth metallic species during the pyrolysis and gasification of Victorian brown coal. Part I. Volatilisation of Na and Cl from a set of NaCl-loaded samples. *Fuel* **2002**, 81**,** (2), 143-149.

58. Quyn, D.M., H. Wu, S.P. Bhattacharya, and C.-Z. Li, Volatilisation and catalytic effects of alkali and alkaline earth metallic species during the pyrolysis and gasification of Victorian brown coal. Part II. Effects of chemical form and valence. *Fuel* **2002**, 81**,** (2), 151-158.

59. Wu, H., D.M. Quyn, and C.-Z. Li, Volatilisation and catalytic effects of alkali and alkaline earth metallic species during the pyrolysis and gasification of Victorian

brown coal. Part III. The importance of the interactions between volatiles and char at high temperature. *Fuel* **2002**, 81**,** (8), 1033-1039.

60. Li, C.-Z., Some recent advances in the understanding of the pyrolysis and gasification behaviour of Victorian brown coal. *Fuel* **2007**, 86**,** (12), 1664-1683.

61. Zhang, S., Z. Min, H.-L. Tay, M. Asadullah, and C.-Z. Li, Effects of volatile–char interactions on the evolution of char structure during the gasification of Victorian brown coal in steam. *Fuel* **2011**, 90**,** (4), 1529-1535.

62. Sathe, C., J.-i. Hayashi, C.-Z. Li, and T. Chiba, Release of alkali and alkaline earth metallic species during rapid pyrolysis of a Victorian brown coal at elevated pressures☆. *Fuel* **2003**, 82**,** (12), 1491-1497.

63. Bridgwater, A., An introduction to fast pyrolysis of biomass for fuels and chemicals. *Fast pyrolysis of biomass: a handbook* **1999**, 1**,** 1-13.

64. Wang, D., D. Montané, and E. Chornet, Catalytic steam reforming of biomass-derived oxygenates: acetic acid and hydroxyacetaldehyde. *Applied Catalysis A: General* **1996**, 143**,** (2), 245-270.

65. Wang, D., S. Czernik, D. Montané, M. Mann, and E. Chornet, Biomass to Hydrogen via Fast Pyrolysis and Catalytic Steam Reforming of the Pyrolysis Oil or Its Fractions. *Industrial & Engineering Chemistry Research* **1997**, 36**,** (5), 1507-1518.

66. Marquevich, M., S. Czernik, E. Chornet, and D. Montané, Hydrogen from Biomass: Steam Reforming of Model Compounds of Fast-Pyrolysis Oil. *Energy & Fuels* **1999**, 13**,** (6), 1160-1166.

67. Galdámez, J.R., L. García, and R. Bilbao, Hydrogen Production by Steam Reforming of Bio-Oil Using Coprecipitated Ni−Al Catalysts. Acetic Acid as a Model Compound. *Energy & Fuels* **2005**, 19**,** (3), 1133-1142.

68. Takanabe, K., K.-i. Aika, K. Seshan, and L. Lefferts, Sustainable hydrogen from bio-oil—Steam reforming of acetic acid as a model oxygenate. *Journal of Catalysis* **2004**, 227**,** (1), 101-108.

69. Gungor, A. and N. Eskin, Hydrodynamic modeling of a circulating fluidized bed. *Powder Technology* **2007**, 172**,** (1), 1-13.

70. Behjat, Y., S. Shahhosseini, and S.H. Hashemabadi, CFD modeling of hydrodynamic and heat transfer in fluidized bed reactors. *International Communications in Heat and Mass Transfer* **2008**, 35**,** (3), 357-368.

71. Davidian, T., N. Guilhaume, C. Daniel, and C. Mirodatos, Continuous hydrogen production by sequential catalytic cracking of acetic acid: Part I. Investigation of reaction conditions and application to two parallel reactors operated cyclically. *Applied Catalysis A: General* **2008**, 335**,** (1), 64-73.

72. Ramos, M.C., A.I. Navascués, L. García, and R. Bilbao, Hydrogen Production by Catalytic Steam Reforming of Acetol, a Model Compound of Bio-Oil. *Industrial & Engineering Chemistry Research* **2007**, 46**,** (8), 2399-2406.

73. Basagiannis, A.C. and X.E. Verykios, Reforming reactions of acetic acid on nickel catalysts over a wide temperature range. *Applied Catalysis A: General* **2006**, 308**,** (0), 182-193.

74. Vagia, E.C. and A.A. Lemonidou, Thermodynamic analysis of hydrogen production via steam reforming of selected components of aqueous bio-oil fraction. *International Journal of Hydrogen Energy* **2007**, 32**,** (2), 212-223.

75. Bahng, M.-K., C. Mukarakate, D.J. Robichaud, and M.R. Nimlos, Current technologies for analysis of biomass thermochemical processing: A review. *Analytica Chimica Acta* **2009**, 651**,** (2), 117-138.

76. Takanabe, K., K.-i. Aika, K. Seshan, and L. Lefferts, Catalyst deactivation during steam reforming of acetic acid over Pt/ZrO2. *Chemical Engineering Journal* **2006**, 120**,** (1–2), 133-137.

77. Rioche, C., S. Kulkarni, F.C. Meunier, J.P. Breen, and R. Burch, Steam reforming of model compounds and fast pyrolysis bio-oil on supported noble metal catalysts. *Applied Catalysis B: Environmental* **2005**, 61**,** (1–2), 130-139.

78. Vagia, E.C. and A.A. Lemonidou, Hydrogen production via steam reforming of bio-oil components over calcium aluminate supported nickel and noble metal catalysts. *Applied Catalysis A: General* **2008**, 351**,** (1), 111-121.

79. Watkinson, A.P., J.P. Lucas, and C.J. Lim, A prediction of performance of commercial coal gasifiers. *Fuel* **1991**, 70**,** (4), 519-527.

80. Vamvuka, D., E.T. Woodburn, and P.R. Senior, Modelling of an entrained flow coal gasifier. 1. Development of the model and general predictions. *Fuel* **1995**, 74**,** (10), 1452-1460.

81. Huang, J. and A.P. Watkinson, Coal gasification in a stirred bed reactor. *Fuel* **1996**, 75**,** (14), 1617-1624.

82. Lucas, J.P., C.J. Lim, and A.P. Watkinson, A nonisothermal model of a spouted bed gasifier. *Fuel* **1998**, 77**,** (7), 683-694.

83. Yan, H.-m., C. Heidenreich, and D.-k. Zhang, Mathematical modelling of a bubbling fluidised-bed coal gasifier and the significance of 'net flow'. *Fuel* **1998**, 77**,** (9–10), 1067-1079.

84. Li, X., J.R. Grace, A.P. Watkinson, C.J. Lim, and A. Ergüdenler, Equilibrium modeling of gasification: a free energy minimization approach and its application to a circulating fluidized bed coal gasifier. *Fuel* **2001**, 80**,** (2), 195-207.

85. Li, X.T., J.R. Grace, C.J. Lim, A.P. Watkinson, H.P. Chen, and J.R. Kim, Biomass gasification in a circulating fluidized bed. *Biomass and Bioenergy* **2004**, 26**,** (2), 171-193.

86. Smith, W.R. and R.W. Missen, Chemical reaction equilibrium analysis: theory and algorithms, Wiley New York, (1982).

87. White, W.B., S.M. Johnson, and G.B. Dantzig, Chemical Equilibrium in Complex Mixtures. *The Journal of Chemical Physics* **1958**, 28**,** (5), 751-755.

88. Zeleznik, F.J. and S. Gordon, CALCULATION OF COMPLEX CHEMICAL EQUILIBRIA. *Industrial & Engineering Chemistry* **1968**, 60**,** (6), 27-57.

89. Steynberg, A. and M. Dry, Fischer-Tropsch Technology, Elsevier, (2004).

90. Zhang, M., X. Gao, and H. Wu, A Method for the Quantification of Alkali and Alkaline Earth Metallic Species in Bioslurry Fuels. *Energy & Fuels* **2013**, 27**,** (11), 6823-6830.

91. Wang, X., B. Jin, and W. Zhong, Three-dimensional simulation of fluidized bed coal gasification. *Chemical Engineering and Processing: Process Intensification* **2009**, 48**,** (2), 695-705.

92. Gerber, S., F. Behrendt, and M. Oevermann, An Eulerian modeling approach of wood gasification in a bubbling fluidized bed reactor using char as bed material. *Fuel* **2010**, 89**,** (10), 2903-2917.

93. Novia, N., M. S Ray, and V. Pareek, Three-dimensional hydrodynamics and reaction kinetics analysis in FCC riser reactors. *Chemical product and process modeling* **2007**, 2**,** (2).

94. Huber, G.W., S. Iborra, and A. Corma, Synthesis of Transportation Fuels from Biomass: Chemistry, Catalysts, and Engineering. *Chemical Reviews* **2006**, 106**,** (9), 4044-4098.

95. Anitescu, G. and T.J. Bruno, Liquid Biofuels: Fluid Properties to Optimize Feedstock Selection, Processing, Refining/Blending, Storage/Transportation, and Combustion. *Energy & Fuels* **2011**, 26**,** (1), 324-348.

96. Balat, M. and H. Balat, Recent trends in global production and utilization of bio-ethanol fuel. *Applied Energy* **2009**, 86**,** (11), 2273-2282.

97. Ma, F. and M.A. Hanna, Biodiesel production: a review. *Bioresource Technology* **1999**, 70**,** (1), 1-15.

98. Mata, T.M., A.A. Martins, and N.S. Caetano, Microalgae for biodiesel production and other applications: A review. *Renewable and Sustainable Energy Reviews* **2010**, 14**,** (1), 217-232.

99. Pinzi, S., I.L. Garcia, F.J. Lopez-Gimenez, M.D. Luque de Castro, G. Dorado, and M.P. Dorado, The Ideal Vegetable Oil-based Biodiesel Composition: A Review of Social, Economical and Technical Implications. *Energy & Fuels* **2009**, 23**,** (5), 2325-2341.

100. Rienstra, S.W., The shape of a sessile drop for small and large surface tension. *Journal of Engineering Mathematics* **1990**, 24**,** (3), 193-202.

101. Allen, J.S., An analytical solution for determination of small contact angles from sessile drops of arbitrary size. *J Colloid Interface Sci* **2003**, 261**,** (2), 481-9.

102. Amirfazli, A., J. Graham-Eagle, S. Pennell, and A.W. Neumann, Implementation and examination of a new drop shape analysis algorithm to measure contact angle and surface tension from the diameters of two sessile drops. *Colloids and Surfaces A: Physicochemical and Engineering Aspects* **2000**, 161**,** (1), 63-74.

103. Shanahan, M.E.R., An approximate theory describing the profile of a sessile drop. *Journal of the Chemical Society, Faraday Transactions 1: Physical Chemistry in Condensed Phases* **1982**, 78**,** (9), 2701-2710.

104. Ranz, W. and W. Marshall, Evaporation from drops. *Chem. Eng. Prog* **1952**, 48**,** (3), 141-146.

105. Skelland, A.H.P., Diffusional mass transfer, John Wiley and Sons, New York, (1974).

106. *CAMEO Chemicals* (accessed September 2013).]; Available from: http://cameochemicals.noaa.gov/chemical/11452.

107. Yuan, W., A. Hansen, and Q. Zhang, Predicting the physical properties of biodiesel for combustion modeling. *Transactions of the ASAE* **2003**, 46**,** (6), 1487-1493.

108. Goodrum, J.W., Volatility and boiling points of biodiesel from vegetable oils and tallow. *Biomass and Bioenergy* **2002**, 22**,** (3), 205-211.

109. Lefebvre, A.H. and X.F. Wang, Mean drop sizes from pressure-swirl nozzles. *Journal of Propulsion and Power* **1987**, 3**,** (1), 11-18.

110. Lefebvre, A.H. and M. Suyari, Film thickness measurements in a simplex swirl atomizer. *Journal of Propulsion and Power* **1986**, 2**,** (6), 528-533.

111. Sakaguchi, M., A.P. Watkinson, and N. Ellis, Steam gasification reactivity of char from rapid pyrolysis of bio-oil/char slurry. *Fuel* **2010**, 89**,** (10), 3078-3084.

112. Oasmaa, A., D. Meier, and A. Bridgwater, Fast Pyrolysis of Biomass: A Handbook, CPL Press, Newbury, UK, (2002).

113. Abdullah, H. and H. Wu, Bioslurry as a Fuel. 4. Preparation of Bioslurry Fuels from Biochar and the Bio-oil-Rich Fractions after Bio-oil/Biodiesel Extraction. *Energy & Fuels* **2011**, 25**,** (4), 1759-1771.

114. Latifi, M., Gasification of Bio-oils to Syngas in Fluidized Bed Reactors, University of Western Ontario 2012.

115. Ghezelchi, M.H., M. Garcia-Perez, and H. Wu, Bioslurry as a Fuel. 7: Spray Characteristics of Bio-Oil and Bioslurry via Impact and Twin-Fluid Atomizers. *Energy & Fuels* **2015**, 29**,** (12), 8058-8065.

116. Wang, X., B. Jin, W. Zhong, and R. Xiao, Modeling on the Hydrodynamics of a High-Flux Circulating Fluidized Bed with Geldart Group A Particles by Kinetic Theory of Granular Flow. *Energy & Fuels* **2009**, 24**,** (2), 1242-1259.

117. Dallavalle, J.M., Micromeritics the technology of fine particles, Pitman Publishing Corp., New York; Toronto; London, (1948).

118. Guide, A.F.U.s., Ansys. *Inc. Release* **2013**, 15.

119. Saboni, A. and S. Alexandrova, Numerical study of the drag on a fluid sphere. *AIChE Journal* **2002**, 48**,** (12), 2992-2994.

120. Hallett, W.L.H. and N.A. Clark, A model for the evaporation of biomass pyrolysis oil droplets. *Fuel* **2006**, 85**,** (4), 532-544.

121. Tamim, J. and W.L.H. Hallett, A continuous thermodynamics model for multicomponent droplet vaporization. *Chemical Engineering Science* **1995**, 50**,** (18), 2933-2942.

122. Zhang, L. and S.-C. Kong, Multicomponent vaporization modeling of bio-oil and its mixtures with other fuels. *Fuel* **2012**, 95**,** 471-480.

123. Poling, B.E., J.M. Prausnitz, O.C. John Paul, and R.C. Reid, The properties of gases and liquids, McGraw-Hill New York, (2001).

124. Pitzer, K.S., D.Z. Lippmann, R. Curl Jr, C.M. Huggins, and D.E. Petersen, The volumetric and thermodynamic properties of fluids. II. Compressibility factor, vapor pressure and entropy of vaporization1. *Journal of the American Chemical Society* **1955**, 77**,** (13), 3433-3440.

125. Kalyon, D.M. and J. Schweikart, Perry's Chemical Engineers' Handbook. *Chemical Engineering* **1997**, 104**,** (12), 12.

126. Sazhin, S.S., Advanced models of fuel droplet heating and evaporation. *Progress in Energy and Combustion Science* **2006**, 32**,** (2), 162-214.

127. Pimenidou, P. and V. Dupont, Characterisation of palm empty fruit bunch (PEFB) and pinewood bio-oils and kinetics of their thermal degradation. *Bioresource Technology* **2012**, 109**,** 198-205.

128. Wang, Y., X. Li, D. Mourant, R. Gunawan, S. Zhang, and C.-Z. Li, Formation of Aromatic Structures during the Pyrolysis of Bio-oil. *Energy & Fuels* **2012**, 26**,** (1), 241-247.

129. Jess, A., Mechanisms and kinetics of thermal reactions of aromatic hydrocarbons from pyrolysis of solid fuels. *Fuel* **1996**, 75**,** (12), 1441-1448.

130. Laosiripojana, N., W. Sangtongkitcharoen, and S. Assabumrungrat, Catalytic steam reforming of ethane and propane over CeO2-doped Ni/Al2O3 at SOFC temperature: Improvement of resistance toward carbon formation by the redox property of doping CeO2. *Fuel* **2006**, 85**,** (3), 323-332.

131. Ranjan, P., P. Kannan, A. Al Shoaibi, and C. Srinivasakannan, Modeling of ethane thermal cracking kinetics in a pyrocracker. *Chemical Engineering & Technology* **2012**, 35**,** (6), 1093-1097.

132. Veranitisagul, C., N. Koonsaeng, N. Laosiripojana, and A. Laobuthee, Preparation of gadolinia doped ceria via metal complex decomposition method: Its application as catalyst for the steam reforming of ethane. *journal of industrial and Engineering Chemistry* **2012**, 18**,** (3), 898-903.

133. Schädel, B.T., M. Duisberg, and O. Deutschmann, Steam reforming of methane, ethane, propane, butane, and natural gas over a rhodium-based catalyst. *Catalysis Today* **2009**, 142**,** (1–2), 42-51.

134. Sundaram, K.M. and G.F. Froment, Modeling of thermal cracking kinetics—I. *Chemical Engineering Science* **1977**, 32**,** (6), 601-608.

135. Watanabe, H., M. Ashizawa, M. Otaka, S. Hara, and A. Inumaru, Development on numerical simulation technology of heavy oil gasifier. *CRIEPI reports W* **2002**, 1023.

136. Watanabe, H., M. Otaka, S. Hara, M. Ashizawa, K. Kidoguchi, and J. Inumaru, Modelling and Simulation for Extra Heavy Oil Gasification on Entrained Flow Gasifier. **2002**, (36177), 667-674.

137. Yehesket, J., R. Rubin, A. Berman, and J. Karni. *Chemical kinetics of high temperature hydrocarbons reforming using a solar reactor*. in *Proceedings of Eurosun*. 2000.

138. Tinaut, F.V., A. Melgar, J.F. Perez, and A. Horrillo, Effect of biomass particle size and air superficial velocity on the gasification process in a downdraft fixed bed gasifier. An experimental and modelling study. *Fuel Processing Technology* **2008**, 89**,** (11), 1076-1089.

139. Prosperetti, A. and G. Tryggvason, Computational methods for multiphase flow, Cambridge university press, (2009).

140. *The Pawsey Supercomputing Centre* Available from: http://www.pawsey.org.au/.

141. Yaman, S., Pyrolysis of biomass to produce fuels and chemical feedstocks. *Energy conversion and management* **2004**, 45**,** (5), 651-671.

142. Ra, Y. and R.D. Reitz, A vaporization model for discrete multi-component fuel sprays. *International Journal of Multiphase Flow* **2009**, 35**,** (2), 101-117.

143. Zhang, L. and S.-C. Kong, Modeling of multi-component fuel vaporization and combustion for gasoline and diesel spray. *Chemical Engineering Science* **2009**, 64**,** (16), 3688-3696.

APPENDICES

APPENDIX A: PARTICLE STREAMS VELOCITY WITH TWIN-FLUID ATOMIZER

The velocity magnitude of the particle streams that will be oriented along the spray cone angle have been considered by a simulation study of the internal flow field of a twin-fluid atomizer, using three-dimensional computational fluid dynamics (CFD). In this model the geometry of injection port for twin-fluid atomizer, shown schematically in Figure A-1, was meshed by ANSYS DesignModeler. The constructed numerical grid consisted of 81061 tetrahedral cells including the nozzle itself and outlet domain bounded by an atmospheric pressure conditions. As can be seen from Figure A-1 the nozzle consists of six halves a circle gas jets, arranged in an annular fashion to provide outer gas flow in assisting the disintegration of fuel jet or sheet which provided by inner tube.

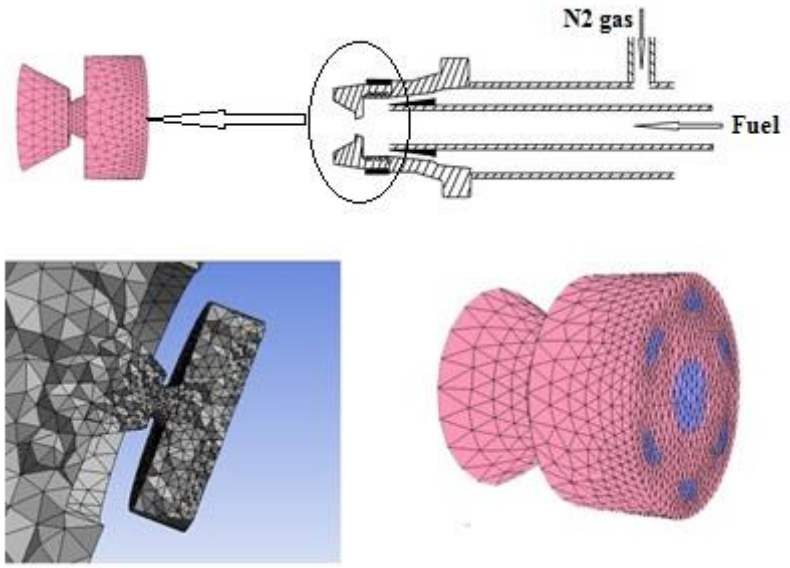

Figure A- 1: Twin-fluid atomizer and its flow ports, created geometries and mesh for FLUENT using DesignModeler

For a steady spray system, the three-dimensional turbulent fluid flow model in ANSYS FLUENT was employed to compute flow velocity at specified intervals (nozzle cone angle before interring in fluidized bed reactor) during the fluid phase calculation. The realizable $k-\varepsilon$ turbulence model has been chosen in this study with additional equations, solved for the conservation of parameters of k and ε. The Pressure-based solver with coupled algorithm has been used and least squares cell based, standard, second order upwind and first order upwind discretization has been chosen for gradient, pressure, momentum, and turbulent parameters respectively. In addition the second order upwindscheme also has been used for discretization of the species transport equation.

Figure A-2 display the clip plane of flow field at the midpoint of the atomizer section by examining contours of velocity magnitude in which the nitrogen gas and bio-oil moves into ports of twin-fluid atomizer. The hybrid initialization was considered to provide better initial velocity and pressure fields for flows complex topologies in case of improving the convergence behaviour of the solver. The approximate convergence has been reached after 400 iterations appropriately and the average velocities magnitude estimated in different position along the spray cone angle at different operating conditions is reported in Table A-1.

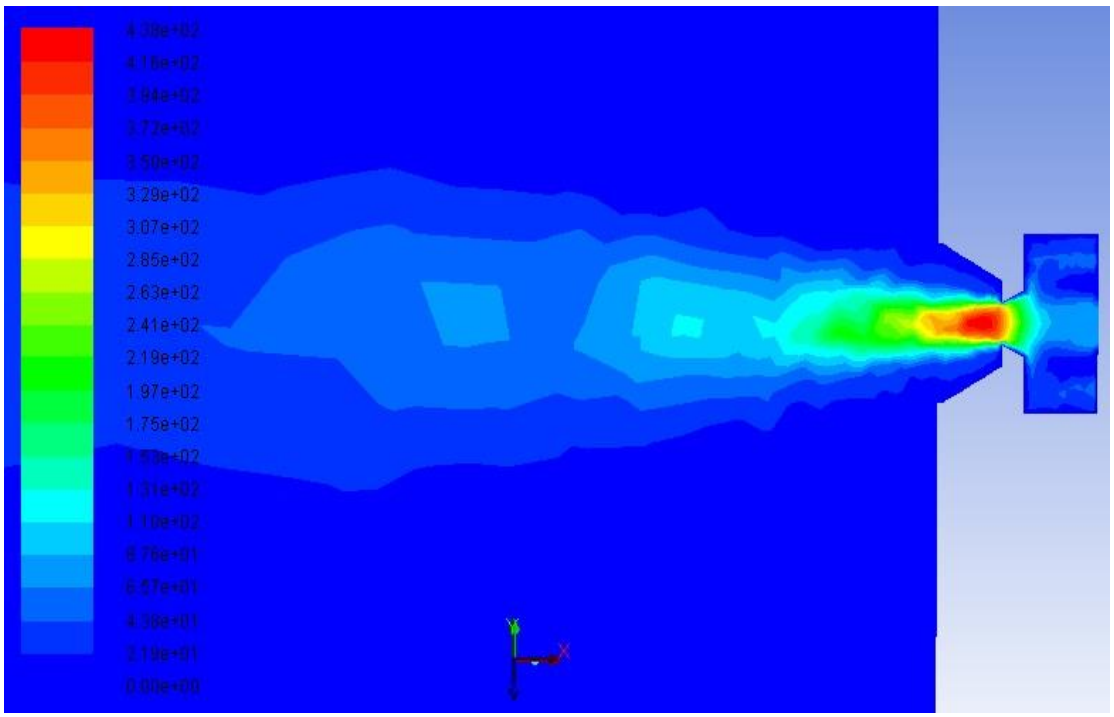

Figure A- 2: Velocity magnitude estimated in different position along the spraycone

angle at different gas to liquid mass ratio ($\dot{m}_A/\dot{m}_L$)

Table A- 1:Velocity magnitude estimated in different position along the spray cone angle at different gas to liquid mass ratio ($\dot{m}_A/\dot{m}_L$)

Continuous phase mass source ($\dot{m}_A$) kg/s	Discrete phase mass source ($\dot{m}_L$) kg/s	$\dot{m}_A/\dot{m}_L$	Average velocity m/s
2.39E-04	8.90E-05	2.68	94.5
2.39E-04	7.10E-05	3.37	85.7
2.39E-04	4.52E-05	5.28	75.4

APPENDIX B: THE DETAILS OF CFD SOFTWARE USED IN THIS PhD STUDY (ANSYS FLUENT 15.0)

Appendix B incorporates the details of CFD code employed in this thesis for modelling of bio-oil and bioslurry in fluidized bed reactor. This appendix summarizes the solution setup, solver and post processing

B1: Solution Setup

The General set up includes: 3D simulation, Pressure-Based solver, Absolute Velocity Formulation, Transient, and Gravitational Acceleration.

B2: Models

Models used:

- Multiphase - Eulerian
- Energy-on

- Viscous: Standard $k-epsilon$ (2 eqn) with standard wall functions and Dispersed as turbulence multiphase model

- Species transport with volumetric reactions. The properties of gas phase for density, specific heat, thermal conductivity, viscosity and mass diffusivity were incompressible-ideal-gas, mixing law, mass-weighted-mixing law, mass-weighted-mixing law, and kinetic-theory respectively.

- Discrete Phase Model with continues phase interaction. The DPM sources is updated every flow iteration. Particle treatment has been done with unsteady particle tracking and track with fluid flow time step. The continues phase mass source was considered with a UDF written and hooked in the UDF source section. For particles tracking the high order runge-kutta and low order implicit scheme have been used. In addition, injection created for different operating condition (see Chapter 6 and 7 for more details)

B3: Boundary conditions

Table B3- 1:Boundary conditions of flow field, specified for injection bio-oil and bioslurry in a fluidized bed reactor

Name	Phase			Type
	Bio-oil-steam	Solid	Mixture	
Inlet	• Thermal: Temperature (K) • Momentum: 1-Velocity Magnitude (m/s Normal to Boundary) 2-Turbulent Intensity = 10% and Hydraulic Diameter = 0.077 m • Species (mole fraction): specified for water vapour and nitrogen gas inlet	• Thermal: Temperature (K) • Multiphase: Volume Fraction=0	• DPM: Discrete phase BC Type = reflect	Velocity-inlet
Outlet	• Thermal: Temperature (K) • Species (mole fraction): specified for water vapour and nitrogen gas inlet	• Thermal: Temperature (K)	• DPM: Discrete phase BC Type = escape	Pressure-outlet

Hot surface	• Momentum: Shear Condition: Specified Shear and Shear Stress for X,Y, and Z = 0	• Momentum: Shear Condition: Specified Shear and Shear Stress for X,Y, and Z = 0	• Momentum: 1-Wall Motion = Stationary wall, • Thermal 1- Thermal Conditions = Temperature (Specified reactor temperature)	Wall
Default-interior				Interior

B4: Solution

Table B4 - 1: The various parameters associated with the solution

Solution control The under –relaxation factors		Solution Method	
Pressure	0.8	Pressure-velocity coupling	Phase –Coupled SIMPLE
Density	0.8	Gradient	Green-gauss node based
Body Forces	1	Momentum	Second order upwind
Momentum	0.8	Volume fraction	Second order upwind
Volume Fraction	0.8	Turbulent kinetic energy	Second order upwind
Granular Temperature	0.8	Turbulent dissipation rate	Second order upwind
Turbulent kinetic energy	0.8	Energy	Second order upwind
Turbulent dissipation rate	0.8	Bio-oil steam species	Second order upwind
Turbulent viscosity	1	Solids species	Second order upwind
Energy	0.8	Transient formulation	Second order implicit
Discrete phase source	1	High order term relaxation	
Bio-steam species	1		
Solid species	1		

APPENDIX C: PERMISSION CERTIFICATE FROM THE ACS FOR CHAPTERS 4, 5 AND 6

Permission certificate from ACS for Chapters 5 which include Chapter 4 as supporting documents as well

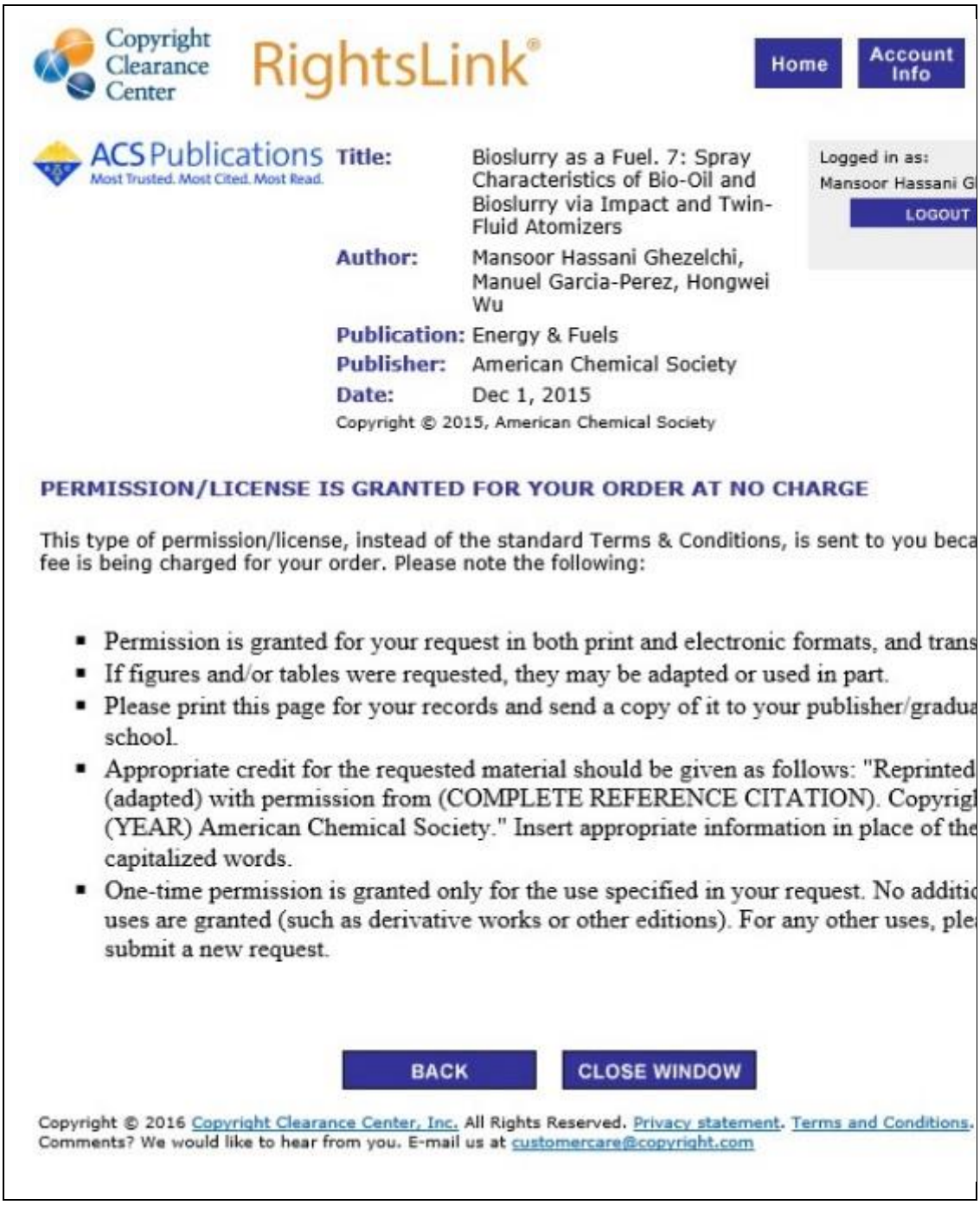

Copyright Clearance Center RightsLink®

Home | Account Info

ACS Publications
Most Trusted. Most Cited. Most Read.

Title: Bioslurry as a Fuel. 7: Spray Characteristics of Bio-Oil and Bioslurry via Impact and Twin-Fluid Atomizers

Logged in as: Mansoor Hassani G
LOGOUT

Author: Mansoor Hassani Ghezelchi, Manuel Garcia-Perez, Hongwei Wu

Publication: Energy & Fuels

Publisher: American Chemical Society

Date: Dec 1, 2015

Copyright © 2015, American Chemical Society

PERMISSION/LICENSE IS GRANTED FOR YOUR ORDER AT NO CHARGE

This type of permission/license, instead of the standard Terms & Conditions, is sent to you beca
fee is being charged for your order. Please note the following:

- Permission is granted for your request in both print and electronic formats, and trans
- If figures and/or tables were requested, they may be adapted or used in part.
- Please print this page for your records and send a copy of it to your publisher/gradua school.
- Appropriate credit for the requested material should be given as follows: "Reprinted (adapted) with permission from (COMPLETE REFERENCE CITATION). Copyrigh (YEAR) American Chemical Society." Insert appropriate information in place of the capitalized words.
- One-time permission is granted only for the use specified in your request. No additio uses are granted (such as derivative works or other editions). For any other uses, ple submit a new request.

BACK | CLOSE WINDOW

Copyright © 2016 Copyright Clearance Center, Inc. All Rights Reserved. Privacy statement. Terms and Conditions.
Comments? We would like to hear from you. E-mail us at customercare@copyright.com